CMS Draft Analysis Note

2012/03/21
Head Id: 111581
Archive Id: 111833M
Archive Date: 2012/03/20
Archive Tag: trunk

Measurement of the top dilepton cross section using b-tagging at $\sqrt{s}$ = 7 TeV with 2.2 fb^{-}1 in pp collisions

J. Andrea[2], A. Calderón[1], M. Cardaci[2], E. Chabert[2], C. Collard[2], J. Cuevas[3], J. Fernández[3], D. Gelé[2], C. Jordá[1], P. Lobelle[1], A.Y. Rodríguez[1], L. Scodellaro[1], and R. Vilar[1]

[1] IFCA, CSIC-Universidad de Cantabria, Spain
[2] IPHC, Strasbourg, France
[3] University of Oviedo, Spain

Abstract

This note presents a measurement of the top quark pair cross section using the dilepton final state ($e-e$, $e-\mu$ and $\mu-\mu$) in pp collisions at $\sqrt{s}$ = 7 TeV. To extract the signal out of the background, a robust event selection, partially based on b-tagging, was defined. The backgrounds coming from Drell-Yan events or from mis-identified leptons are estimated using data-driven methods. The event selection efficiencies are estimated from simulated events and controlled or corrected using data. The cross section measurement is preformed using two very different and complementary methods, a counting experiment and a likelihood fit method. With an integrated luminosity of 2.3 fb^{-1} , we found a ttbar cross section for the channels $e-e$, $e-\mu$ and $\mu-\mu$.

Contents

1 Introduction

The study of $t\bar{t}$ production at the LHC is one of the key of the LHC physics program. Given its large cross section, the LHC is a true top factory, which allows for a deep understanding of top productions and decays. Top events become a very powerful tool for the understanding of the detectors [1] and its rediscovery have, which happened at the very beginning of the CMS data taking, shown the great performance of the CMS detectors [2]. With the high luminosity of the

LHC, a large amount of data was (and will be) collected, which opens new perspectives for precisions measurements related to tops ([3–7]), allowing for search of deviations with respect to the the Standard Model predictions. Precisions measurement of the $t\bar{t}$ cross sections allows also to improve our understanding of one of the major background of various search for new physics.

This analysis note presents a measurement of the cross-section of the $t\bar{t}$ process in dilepton final state using $t\bar{t}$ event candidates using b-tagging. The $t\bar{t}$ production cross-section: $\sigma_{NNLO}(t\bar{t}; 7\text{ TeV}) = 163$ pb [8–11], dominated by the gluon-gluon fusion mechanism is considered in the dileptonic final states (ee, $\mu\mu$, and $e\mu$ including leptons from τ decays).

Two different and very complementary approaches are followed. A simple and robust cut&count analysis,and a more elaborate Profile Likelihood Ratio (PLR) method. These two measurements are following very different techniques, and provide very valuable cross checks.

The presented analyses corresponds to an update of the already approved preliminary results [12].

A summary of the data and Monte Carlo samples used in the analysis is presented in Sec. 2. The triggers used, the selection of leptons and jets and all other kinematics observables are described in Sec. 3. Selection efficiencies from data are discussed in Sec. 4. Section 5 describes the determination of the Drell-Yan background using data-driven methods, the estimation from data of the QCD and W+jets backgrounds being presented in Sec. 6. Cutflow tables and data/MC comparisons are presented in Sec. 7 with the inclusion of the different scale factors described in Sec. 4 to 6. Systematic sources are discussed in Sec. 8. Finally, the cross-section measurement is presented in Sec. 9. Some conclusions follow in Sec. 10.

2 Data and Monte Carlo samples

The analyses presented here have been carried out using the CMS event data model and the official software framework of CMS for event generation, simulation and reconstruction (Data and Summer11 MC in version CMSSW_4_2_5 analysed with CMSSW_4_2_8_patch7).

Signal and background events come from the CMS Monte Carlo production performed with the full simulation of the realistic detector conditions (miscalibration and misalignment effects resulting of the start-up conditions are taken into account). The Physics Analysis Tool (PAT) [13–15] along with PF2PAT [16, 17] framework are used in the analysis.

Dataset Description	Primary Dataset Name	Version	x-section (pb)
$t\bar{t}$	/TTJets_TuneZ2T_7TeV-madgraph-tauola/	S4	164
tbarW	/Tbar_TuneZ2_tW-channel-DR_7TeV-powheg-tauola/	S4	7.87
tW	/T_TuneZ2_tW-channel-DR_7TeV-powheg-tauola/	S4	7.87
WW	/WW_TuneZ2_7TeV_pythia6_tauola/	S4	47.04
WZ	/WZ_TuneZ2_7TeV_pythia6_tauola/	S4	18.20
ZZ	/ZZ_TuneZ2_7TeV_pythia6_tauola/	S4	7.67
W Jets	/WJetsToLNu_TuneZ2_7TeV-madgraph-tauola/	S4	31314
Drell-Yan samples:			
$Z/gamma^*[10\text{-}50] \to ll$	/DYJetsToLL_M-10To50_TuneZ2_7TeV-madgraph/	S6	11908.83
$Z/gamma^*[50\text{-inf}] \to ll$	/DYJetsToLL_TuneZ2_M-50_7TeV-madgraph-tauola/	S4	3048

Table 1: Summary of Monte Carlo datasets used. All MC samples processed with PU /Summer11-PU_S4_START42_V11-v1/AODSIM but the $Z/gamma^*[10\text{-}50] \to ll$ that is Fall11-PU_S6_START42_V14B-v1/AODSIM.

The generation of signal events ($t\bar{t}$) and major background events (Z+jets, W+jets) was performed using mainly the Madgraph [18] generators. Additional backgrounds are produced with PYTHIA(VV, where the boson $V = Z, W^{\pm}$ is decaying into leptons) ad the Powheg (single top (tW channel)) generators. For each MonteCarlo process, the corresponding cross-sections and the dataset path are given in Tab.1.

The Monte Carlo samples used for systematic studies are presented in the Tab.2. The systematics related to the signal events selection efficiencies is estimated by using samples generated with different MadGraph to Pythia matching threshold, with different Q^2 scales, with different top masses or produced with a different top generator. For the uncertainty related to single top, samples generated with different matching thresholds and with different Q^2 scales are also used.

Dataset Description	Primary Dataset Name	Version	x-section (pb)
$t\bar{t}$	TTTo2L2Nu2B_7TeV-powheg-pythia6	S4	164
$t\bar{t}$	TTjets_TuneZ2_matchingup_7TeV-madgraph-tauola	S4	164
$t\bar{t}$	TTjets_TuneZ2_matchingdown_7TeV-madgraph-tauola	S4	164
$t\bar{t}$	TTjets_TuneZ2_scaledown_7TeV-madgraph-tauola	S4	164
$t\bar{t}$	TTjets_TuneZ2_scaleup_7TeV-madgraph-tauola	S4	164
$t\bar{t}$	TTJets_TuneZ2_mass161_5_7TeV-madgraph-tauola	S4	164
$t\bar{t}$	TTJets_TuneZ2_mass163_5_7TeV-madgraph-tauola	S4	164
$t\bar{t}$	TTJets_TuneZ2_mass166_5_7TeV-madgraph-tauola	S4	164
$t\bar{t}$	TTJets_TuneZ2_mass169_5_7TeV-madgraph-tauola	S4	164
$t\bar{t}$	TTJets_TuneZ2_mass175_5_7TeV-madgraph-tauola	S4	164
$t\bar{t}$	TTJets_TuneZ2_mass178_5_7TeV-madgraph-tauola	S4	164
$t\bar{t}$	TTJets_TuneZ2_mass181_5_7TeV-madgraph-tauola	S4	164
$t\bar{t}$	TTJets_TuneZ2_mass184_5_7TeV-madgraph-tauola	S4	164
t	T_TuneZ2_scaleup_tW-channel-DR_7TeV-powheg-tauola	S4	7.8
$\bar{t}$	Tbar_TuneZ2_scaleup_tW-channel-DR_7TeV-powheg-tauola	S4	7.8
t	T_TuneZ2_scaledown_tW-channel-DR_7TeV-powheg-tauola	S4	7.8
$t\bar{t}$	Tbar_TuneZ2_scaledown_tW-channel-DR_7TeV-powheg-tauola	S4	7.8

Table 2: Summary of Monte Carlo samples used for systematic studies. All MC samples processed with PU /Summer11-PU_S4_START42_V11-v1/AODSIM.

The datasets used for this analysis are summarised in Tab. 3 for data. As the cross section measurement is dominated by systematic uncertainties, we used only the 2011A runs, to lower the PU effects which are more important in run 2011B. The total integrated luminosity is 2.3 fb^{-1} . The JSON files used as well as the corresponding luminosity are summarised in Tab. 4.

They corresponds to data collected in 2011 by CMS at the centre of mass energy of 7 TeV. They are provided by the DoubleMuon, DoubleElectron and MuEG Primary Dataset based on HLT trigger conditions. Datasets based on MET triggers are also used to estimate the dilepton trigger efficiencies. These samples are cleaned by requiring that luminosity section were validated by the DQM and PVT groups according to the validation criteria applied for each sub-detector. The good luminosity sections are provided in JSON files applied at the beginning of the analysis chain. The JSON files used as well as the corresponding luminosity are summarised in Tab. 4. The corresponding integrated luminosity is given by the convolution of these JSON files with the analysed samples (depending of reprocessing). Overlap between data samples are excluded.
Beam scrapping events are vetoed by selecting a significant fraction of high purity tracks w.r.t. the total number of tracks ($> 25\%$) when the event has at least 10 tracks. Events with anomalous HCAL noise are also rejected. Finally, primary vertices selection requires at least one non-fake primary vertex, with more than 4 effective degrees of freedom, $|vertex.z| < 24$ cm

Dataset Description	Dataset Name
Run2011A Muon 05Aug ReReco	DoubleMu/Run2011A-05Aug2011-v1
Run2011A Muon May10 ReReco	DoubleMu/Run2011A-May10ReReco-v1
Run2011A Muon Prompt Reco v4	DoubleMu/Run2011A-PromptReco-v4
Run2011A Muon Prompt Reco v6	DoubleMu/Run2011A-PromptReco-v6
Run2011A Electron 05Aug ReReco	DoubleElectron/Run2011A-05Aug2011-v1
Run2011A Electron May10 ReReco	DoubleElectron/Run2011A-May10ReReco-v1
Run2011A Electron Prompt Reco v4	DoubleElectron/Run2011A-PromptReco-v4
Run2011A Electron Prompt Reco v6	DoubleElectron/Run2011A-PromptReco-v6
Run2011A Muon-Electron 05Aug ReReco	MuEG/Run2011A-05Aug2011-v1
Run2011A Muon-Electron May10 ReReco	MuEG/Run2011A-May10ReReco-v1
Run2011A Muon-Electron Prompt Reco v4	MuEG/Run2011A-PromptReco-v4
Run2011A Muon-Electron Prompt Reco v6	MuEG/Run2011A-PromptReco-v6
Run2011A MET 05Aug ReReco	MET/Run2011A-05Aug2011-v1
Run2011A METBTag May10 ReReco	METBTag/Run2011A-May10ReReco-v1
Run2011A MET Prompt Reco v4	MET/Run2011A-PromptReco-v4
Run2011A MET Prompt Reco v6	MET/Run2011A-PromptReco-v6

Table 3: Summary of data datasets used.

Datasets	JSON file	Luminosity
May10	Cert_160404-163869_7TeV_May10ReReco_Collisions11_JSON_v3.txt	216.20 pb^{-1}
05Aug	Cert_170249-172619_7TeV_ReReco5Aug_Collisions11_JSON_v3.txt	368.04 pb^{-1}
PromptReco v4	Cert_160404-173692_7TeV_PromptReco_Collisions11_JSON.txt	929.75 pb^{-1}
PromptReco v6	Cert_160404-173692_7TeV_PromptReco_Collisions11_JSON.txt	658.89 pb^{-1}

Table 4: Summary of JSON files used and the corresponding luminosities.

and $|vertex.position.rho| < 2$ cm.

On MC events, an additional (official) filter called "*totalKinematicsFilter*" is applied at generator level to remove events affected by a bug found in implementation of Pythia, conducting to the presence of events with non conservation of the momentum.

Because muons and electrons have different reconstruction and selection efficiencies and because backgrounds are final state dependent, exclusive cross section measurements have been studied. The analysis is based on the robust selection of events by means of successive simple and discriminative criteria. The b-tagging is either used to finalised the events selection (cut&count method) or in a Profile Likelihood Fit (PLR method).

3 Description of the event selection

3.1 Trigger selection

In the CMS design, the real time selection of events is achieved in two physical steps, namely the fast Level-1 Trigger and the High-Level Trigger (HLT) operating on longer timescales. The Level-1 trigger is built of mostly hardware level information of the detectors while the HLT selection is implemented as a sequence of reconstruction and filter steps of increasing complexity. Several High Level inclusive triggers have been considered according to the dilepton channel

studied:

- di-electron:
  HLT_Ele17_CaloIdL_CaloIsoVL_Ele8_CaloIdL_CaloIsoVL_v* for run <= 170901
  HLT_Ele17_CaloIdT_CaloIsoVL_TrkIdVL_TrkIsoVL_Ele8_CaloIdT_CaloIsoVL_TrkIdVL_TrkIsoVL_v* for run >= 170902
- di-muon:
  HLT_DoubleMu7_v* for run <= 165208
  HLT_Mu13_Mu8_v* for run >= 165209 and run <= 178419
  HLT_Mu17_Mu8_v* OR HLT_Mu17_TkMu8_v* for run <= 178420
- electron-muon:
  HLT_Mu8_Ele17_CaloIdL_v* for run <=167913
  HLT_Mu8_Ele17_CaloIdT_CaloIsoVL_v* for run >=167914
  HLT_Mu17_Ele8_CaloIdL_v* for run <= 175972
  HLT_Mu17_Ele8_CaloIdT_CaloIsoVL_v*for run >= 175973

For MC studies the trigger selection relies on:

- di-electron: HLT_Ele17_CaloIdL_CaloIsoVL_Ele8_CaloIdL_CaloIsoVL_v2
- di-muon: HLT_DoubleMu6_v1
- electron-muon: HLT_Mu8_Ele17_CaloIdL_v2 OR
  HLT_Mu10_Ele10_CaloIdL_v3

3.2 Reconstruction of signal and background events

The e/μ final states for the $t\bar{t}$ signal are characterised by the presence of two highest-p_T isolated leptons (coming from W boson decays) associated with a large missing transverse energy $\not{E}_T$ and 2 b-jets. The reconstruction of the different objects is based on the Particle-Flow (PF) algorithm [19]. The selection is based on the following requirements [20]:

3.2.1 Selection of electrons

The selection criteria for PF electron candidates are:

- $p_T > 20$ GeV/c and $|\eta| < 2.5$;
- Transverse impact parameter w.r.t. the beam spot < 0.04 cm, applied on the gsf-Track;
- Photon conversion rejection: number of lost hits in the tracker < 2 and minimal distance between the electron and its closest opposite sign track ($|\Delta \cos\theta| > 0.02$ and distance > 0.02 in the $r-\phi$ plane [21]);
- $\Delta R > 0.1$ ($R = \sqrt{\Delta\eta^2 + \Delta\phi^2}$) between the electron and any global or tracker muon in the event whose number of hits in the inner tracker is greater than 10;
- Relative Electron Isolation (REI) < 0.17, based on particle flow candidates, with REI defined as :

$$REI = \frac{(ChargedHadronIso + NeutralHadronIso + PhotonIso)}{p_T(e)}$$

Each components is computed from PF Isodeposits in a cone of 0.3 around the electron direction, with charged PF candidates coming from PU events are removed (PF charged subtraction). $p_T(e)$ represents the transverse momentum of the electron.

3.2.2 Selection of muons

The selection criteria for PF muon candidates are:

- $p_T > 20$ GeV/c and $|\eta| < 2.4$;
- is a GlobalMuon and TrackerMuon;
- Identification as GlobalMuonPromptTight [22];
- Number of valid hits in the inner tracker > 10;
- $\chi^2/ndof < 10$ for the global muon fit;
- Transverse impact parameter w.r.t. the beam spot < 0.02 cm, applied on the track from the inner tracker;
- Relative Muon Isolation (RMI) < 0.20, based on particle flow candidates, with RMI defined as

$$REI = \frac{(ChargedHadronIso + NeutralHadronIso + PhotonIso)}{p_T(\mu)}$$

Each components is computed from PF Isodeposits in a cone of 0.3 around the muon direction, with charged PF candidates coming from PU events are removed (PF charged subtraction). $p_T(\mu)$ represents the transverse momentum of the muon.

In addition, the selected leptons have to be close to the goodPV: the difference between the muon track at its vertex and the PV along the Z position is less than 1 cm.

3.2.3 Selection of jets

The jets are reconstructed using PF candidates (without considering the charged PF particles coming from PU) with the anti-kT algorithm witn an opening angle of 0.5.

The selection criteria for jet candidates are:

- L1Fastjet corrections compatible with PFnoPU, Level 2 and Level 3 jet energy corrections and L2L3Residual corrections for data;
- $p_T > 30$ GeV/c and $|\eta| < 2.5$;

- Loose Jet Identification, which corresponds to a fraction of charged hadronic energy ≥ 0, a fraction of charged electromagnetic energy ≤ 0.99, a fraction of neutral hadronic energy < 0.99 and a fraction of neutral electromagnetic fraction < 0.99;

- As the PF top projection was disable for leptons removal, we apply a Jet Lepton Cleaning: exclusion of jets overlapping with fully selected leptons (electron/muon) used in the analysis if $\Delta R(jet, lepton) < 0.4$);

3.2.4 Selection in Transverse Missing Energy

The missing transverse energy ($\not\!\!E_T$) was reconstructed using the PF candidates, as the transverse vectorial sum of all PF candidates. No corrections are applied to the $\not\!\!E_T$ calculation (no Jet Energy Scale nor Jet Energy Resolution), this is the so called "raw" $\not\!\!E_T$. Instead, the $\not\!\!E_T$ selection efficiencies will be directly measured from data, as explained in Sec. 4.4.

In the previous analyses, a $\not\!\!E_T$ cut of 30 GeV was applied for the ee and $\mu\mu$ channels. Since then, the $\not\!\!E_T$ selection efficiency was studied using MC events in order to do optimisation. The Fig 1 shows the figure of merit $S/(S+B)$ (with S the number of signal events and B the number of backgrounds) as a function of the $\not\!\!E_T$ selection. Compared to a cut of 30 GeV, it was found that a cut of 40 GeV was rejecting more than 65% MC DY events with a loss of signal efficiency of about 10%. As the $\not\!\!E_T$ selection efficiency is determined from data, no significant increase of systematics is expected.

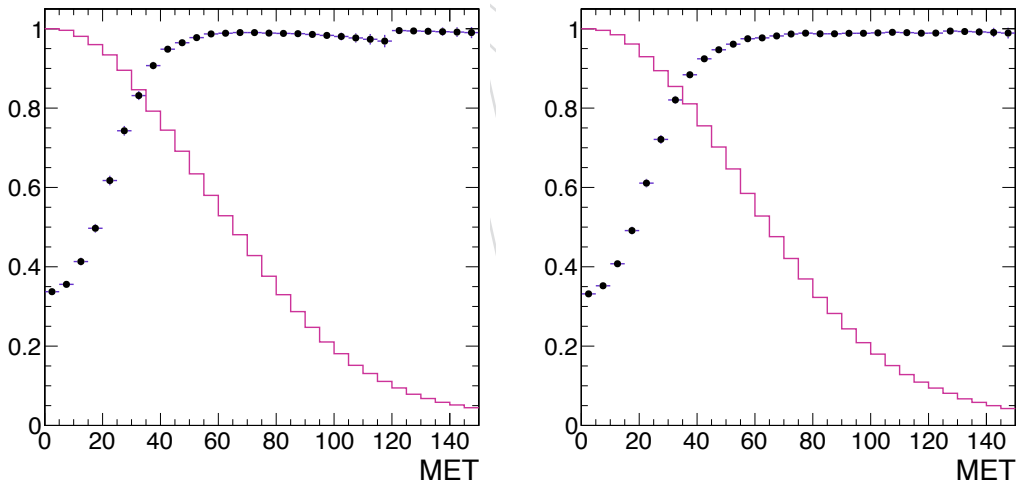

Figure 1: Signal efficiency (histogram) and S/(S+B) (dots) for the ee (left) and $\mu\mu$ (right) channels, as a function of the $\not\!\!E_T$cut

In the presented analyses, it was then decided to apply a $\not\!\!E_T$ selection cut of 40 GeV.

3.2.5 Modelisation of the b-tagging efficiency in MC

As the $t\bar{t}$ signal is enriched in jets originating from a b quark, the b-tagging is used in the selection to improve the background rejection and therefore clean the signal in the data for the cut&count analysis, or in a likelihood fit for the PLR analysis. In previous analyses, for the first data, the simple and robust Track Counting b-tagging algorithm [23, 24] has been chosen, using the Loose working point for High Efficiency conditions (TCHEL) [2, 12].

As some more elaborate taggers are successfully commissioned within CMS, for the presented analyses the Combined Secondary Vertex algorithms with the Loose (CSVL) working point is used. For a given mistag rate, the CSV tagger gives the best b-tagging efficiency. It was also shown that this tagger has very similar performance in data and MC [25] efficiency scale factor close to 1.

The cases with at least 1 b-tag jet (i.e. jet with a Discriminant value higher than 0.244) or at least 2 b-tag jets will be considered in the following of the analysis.

As the MC do not reproduce completely the b-tagging performance, some scale factors (SF) have to be applied [26]. They are directly taken from the Data-Base [27], with

- RecoBTag.PerformanceDB.PoolBTagPerformanceDB1107,
- RecoBTag.PerformanceDB.BTagPerformanceDB1107.

Concerning the b-quark, the scale factor SF_b for TCHEL is equal to 0.95 ± 0.095 (for jets with $20 < p_T < 240$ GeV/c and $|\eta| < 2.4$). For the CSVL, the scale factor SF_b is equal to 1.00 ± 0.03 in $t\bar{t}$ events [25]. To avoid correlations, the SF_b estimated from $t\bar{t}$ are not used, instead the estimations from muon in jets are considered in this analysis, according to the recommendations of the BTV group.

For the light jets (u,d,s and gluons), as an example, the scale factor SF_l is presented in Fig. 2 for the TCHEL as a function of p_T and $|\eta|$, as well as its associated error. In the case of the c-quark, SF_c is taken the same as SF_b.

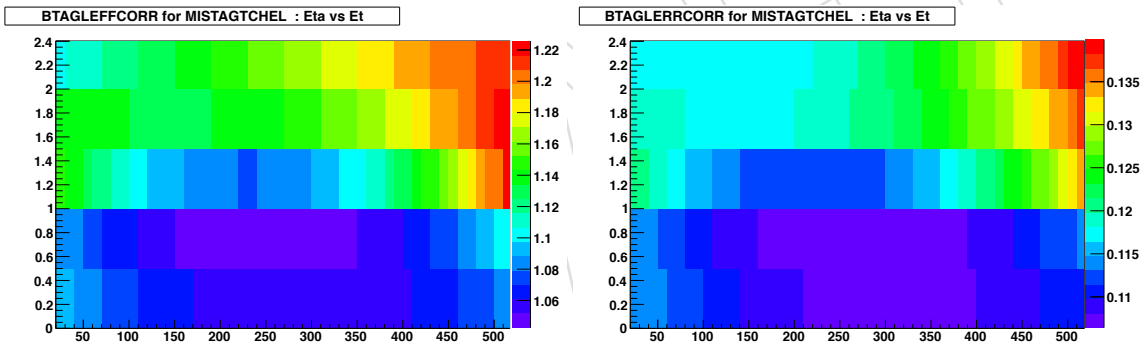

Figure 2: Scale factor SF_l for light quarks on the left and its error on the right, as a function of $|\eta|$ and p_T for TCHEL.

In the MC, in order to describe correctly the data, the probability to tag a jet i as originated from a b-quark should then be computed as:

$$P_i = SF_i \cdot Eff_i^{MC} \tag{1}$$

where SF_i is the scale factor with the quark flavour associated to the jet and Eff_i^{MC} is the b-tagging efficiency computed in $|\eta|$ and p_T bins on $t\bar{t}$ MC samples with a preselection of at least two (one) isolated leptons and two jets for b quarks (for c and light quarks). The efficiencies and their errors are given in Fig. 3 and Fig. 4 respectively for b, c and light quarks. Note that the probability P_i is not allowed to exceed 1.

As the event contains in general more than one reconstructed jet, the probability to tag at least 1 jet is given by:

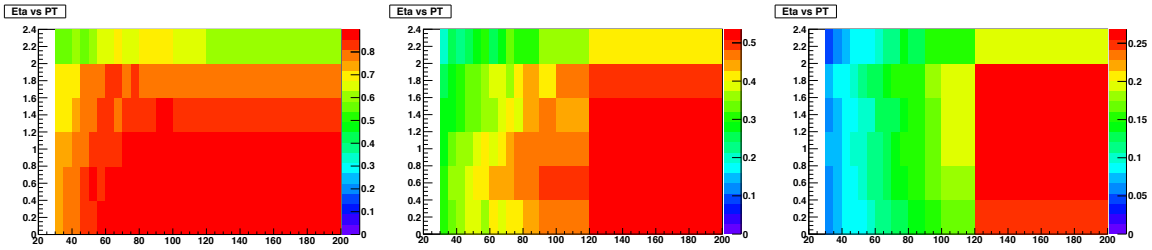

Figure 3: b-tagging efficiencies extracted on $t\bar{t}$ MC samples, as a function of $|\eta|$ and p_T, for b, c and light quarks respectively for TCHEL.

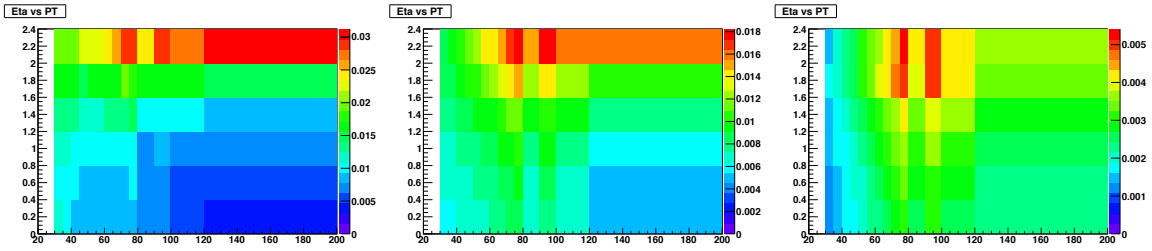

Figure 4: Errors on the b-tagging efficiencies extracted on $t\bar{t}$ MC samples, as a function of $|\eta|$ and p_T, for b, c and light quarks respectively for TCHEL.

$$P(\geq 1b\text{tag jet}) = 1 - P(0\ tag) \tag{2}$$

with

$$P(0\ tag) = \Pi_i(1 - P_i), \tag{3}$$

where the product Π_i is done on the different reconstructed jets i of the event. In order to be able to plot the distribution of the b-tag jet multiplicity, three other probabilities have to be defined:

$$P(1\ tag) = \sum_i [P_i \cdot \Pi_j(1 - P_j)] \text{ with } j \neq i, \tag{4}$$

$$P(2\ tag) = \sum_i \sum_j [P_i \cdot P_j \cdot \Pi_k(1 - P_k)] \text{ with } j > i \text{ and } k \neq i, j, \tag{5}$$

$$P(\geq 3b\text{tag jets}) = 1 - P(0\ tag) - P(1\ tag) - P(2\ tag). \tag{6}$$

Knowing that, the probability to tag at least 2 jets in the event can easily be computed as:

$$P(\geq 2b\text{tag jets}) = 1 - P(0\ tag) - P(1\ tag). \tag{7}$$

As a closure test, the probability approach is compared in Fig. 5 to the result of the discriminant cut, when all SF are taken equal to 1. The agreement between the two approaches is very good. Comparing directly the number of events with at least 1 b-jet, the difference between the two approaches is 0.26%.

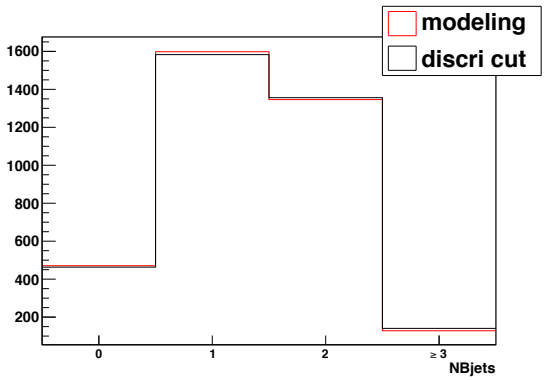

Figure 5: Multiplicity of b-jets in $t\bar{t}$ MC events (ee, $e\mu$ and $\mu\mu$ merged together), after the $\not\!\!E_T$ selection. The last bin is inclusive ($N_{bjets} \geq 3$). The discriminant value is used to select the tag jets for the black histogram. The red crosses are obtained with the probability approach described in the text.

3.3 Event selection

Events having more than 2 selected leptons are classified in ee, $\mu\mu$ or $e\mu$ channel according to a mutual excluding assignment: the lepton pair of opposite charge maximising the sum of the transverse momenta is kept.
In addition, at this step at cut on invariant mass > 20 GeV$/c^2$ is applied to remove DY events with low invariant masses. Also a trigger fiducial requirement is applied to channels with muon(s), asking that the muon in the eμ final state and at least one muon in $\mu\mu$ final states has to be in $|\eta| < 2.1$. In order to remove various background while keeping a good signal efficiency, the following sequential cuts are applied:

- Presence of a selected lepton pair with opposite charges;
- Dileptonic invariant mass $\notin [76;106]$ GeV$/c^2$ for the ee and $\mu\mu$ channels ($Z + jets$ events rejection);
- Jet multiplicity ≥ 2;
- Transverse missing energy $\not\!\!E_T > 40$ GeV for ee and $\mu\mu$ channels (no $\not\!\!E_T$ cut is applied for the $e\mu$ channel);
- Number of loose b-tagged jets ≥ 1 for the $cut\&count$ analysis.

3.4 Pileup Reweighting procedure

The Monte Carlo events have been re-weighted according to the pileup in data. The procedure describes at [28] has been followed and the official 3D pileup reweighting was used. Two pileup distributions, produced assuming a minimum bias cross section of 68 mb (pythia) and 73.5 mb (from TOTEM [29]), were tested. As shown in the Figure 6, a better agreement between data and MC was observed when taking a minimum bias cross section of 73.5 mb. Therefore, the corresponding pileup distribution will be used to re-weight the MC pileup distribution.

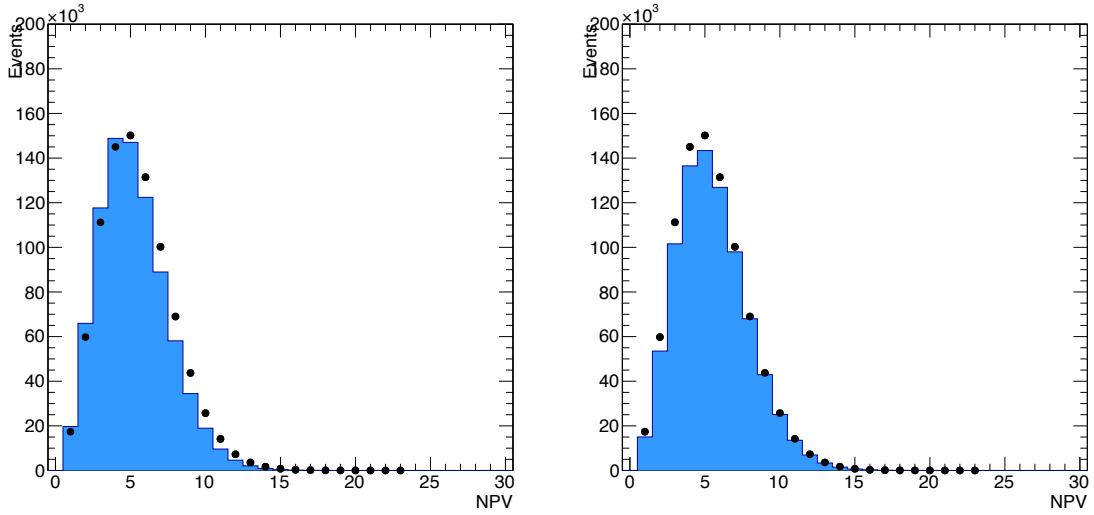

Figure 6: Pileup distribution in data for a luminosity of 2.3 fb^{-1} after the dilepton selection, for a minimum bians cross section of 68 mb (left) and 73.5 mb (right).

4 Selection efficiencies from data

Section 4.1 presents the Trigger efficiencies, section 4.2 the Lepton selection (identification and isolation) efficiencies, and section 4.3 gives a summary of the scale factors used in the analysis. Finally, in section 4.4 the estimate of $\not\!\!E_T$ cut efficiency is estimated from data.

4.1 Trigger efficiencies

The method use events selected by a trigger selection weakly correlated with dilepton triggers (cross triggers) and count the number of such events passing and failing the dilepton trigger selection.

The method can be described as follow :

- Determine a set of triggers (cross triggers) weakly correlated with the dilepton triggers used in the analysis,
- Count the number of events N_{Xtrig} passing the cross triggers and the $t\bar{t}$ dilepton events selection,
- Count the number of events $N_{Xtrig+DILtrig}$ which pass the cross triggers selection, the $t\bar{t}$ dilepton events selection and the dilepton trigger selection.

Then, the dilepton trigger efficiency is simply given by the ratio $\varepsilon_{trigg} = N_{Xtrig+DILtrig}/N_{Xtrig}$. The main difficulty of this method is to find cross triggers weakly correlated with dilepton trigger which allows to select enough dilepton events to have a small statistical uncertainty.

In addition, in some sense the requirement to have weakly correlated cross triggers is equivalent to use $t\bar{t}$ signal events to estimate the dilepton trigger efficiency. Trigger efficiency is then much less biased by kinematic differences between Z and $t\bar{t}$ events as for the tag&probe method.

Relevant cross triggers could then be di-jet triggers, b-tag based trigger or missing E_T based trigger. To define cross triggers, different datasets were tested : Jet, $MultiJet$, $BTag$, $BTagMET$ and MET. The datasets Jet and $MultiJet$ were found to either have small statistic because of

high prescaled and/or to be strongly correlated to electrons triggers. While *BTag* should be weakly correlated to dilepton triggers, it suffers from lack of statistic. The *MET* based datasets were found to be weakly correlated with dilepton and to have a large enough number of events to keep a statistic uncertainty below 1%. The correlations of *MET* datasets with dilepton triggers is estimated from $t\bar{t}$ MC events. The chosen datasets to defined N_{Xtrig} are presented in Tab.5.

Dataset Description	Dataset Name
Run2011A METBTag May10 ReReco	/METBTag/Run2011A-May10ReReco-v1/
Run2011A MET Prompt Reco	/MET/Run2011A-PromptReco-v4/
Run2011A MET Aug10 ReReco	/MET/Run2011A-05Aug2011-v1/
Run2011A MET Prompt Reco	/MET/Run2011A-PromptReco-v6/

Table 5: Dataset used to defined N_{Xtrig}. See the text for more details.

The systematic uncertainties are related to the correlations between *MET* trigger and dilepton triggers. They are estimated from $t\bar{t}$ MC events by counting the number of events passing the *MET* triggers only, the dilepton triggers only, passing or failing both trigger selections. The *MET* trigger considered for this MC based study are $HLT\_CentralJet80\_MET65\_v1$, $HLT\_CentralJet80\_MET80\_v1$, $HLT\_CentralJet80\_MET100\_v1$, $HLT\_CentralJet80\_MET160\_v1$, $HLT\_DiJet60\_MET45\_v1$, $HLT\_PFMHT150\_v2$, HLT_MET100_v1 , HLT_MET120_v1 and HLT_MET200_v1.

In the case where the dilepton and missing E_T trigger are independent, the efficiency to pass both trigger selection can be factorised and expanded as the product of the dilepton and missing E_T trigger efficiencies such that :

$$\varepsilon_{trgLL,trgMissE_T} = \varepsilon_{trgLL} \times \varepsilon_{trgMissE_T}, \tag{8}$$

with ε_{trgLL} and $\varepsilon_{trgMissE_T}$ the efficiencies to pass the dilepton and the missing E_T trigger selections and $\varepsilon_{trgLL,trgMissE_T}$ the efficiency to pass both trigger selections.

If these two trigger selections are correlated, one can then have an idea of the correlations by looking at the ratio :

$$\alpha = \frac{\varepsilon^{MC}_{trgLL} \times \varepsilon^{MC}_{trgMissE_T}}{\varepsilon^{MC}_{trgLL,trgMissE_T}} \tag{9}$$

The fraction α are determined for each channel using $t\bar{t}$ MC events (sping 11 studies). They were found to be 1.003, 1.000 and 0.997 for the ee, $e\mu$ and $\mu\mu$ channels respectively. The corresponding systematic uncertainty on the measured trigger dilepton efficiencies is conservatively estimated to be 0.005.

Another bias could come from the presence of BTag triggers (based on muons in jets) in the METBTag May10 ReReco dataset. However, in this dataset, the fraction of events which fired the BTag triggers was found to be negligible compared to the fraction of events which fired MET triggers.

As the $\not\!\!E_T$ trigger thresholds and pre-scales have changed during the data taking, two different run period are considered. The first one corresponds to the May10ReReco and PromptRecov4 datasets (with a integrated luminosity $L_1 = 1.146$ fb^{-1}), the second one corresponds to August05ReReco and Promptv6 datasets (with an integrated luminosity $L_2 = 1.027$ fb^{-1}). For

each period, the trigger efficiencies are estimated separately (ε^1_{trg},ε^2_{trg}) and the total trigger efficiency is determined as follow :

$$SF_{trig} = \frac{\varepsilon^1_{trg} L_1 + \varepsilon^2_{trg} L_2}{L_1 + L_2} \tag{10}$$

The summary of trigger scale factors, as well as their uncertainties, are summarised in Tab.6 for the different selection steps. The scale factors are found to not depend significantly on the selection step.

channel	$\mu\mu$	ee	$e\mu$
dilepton	0.972 ± 0.007	0.970 ± 0.008	1.013 ± 0.008
Mll	0.966 ± 0.008	0.948 ± 0.011	-
≥ 2 jets	0.969 ± 0.010	0.957 ± 0.013	1.011 ± 0.008
$\not{E}_T$>40GeV	0.975 ± 0.013	0.958 ± 0.016	-
≥ 1 btag	0.977 ± 0.015	0.962 ± 0.016	1.008 ± 0.009
≥ 2 btag	0.968 ± 0.021	0.959 ± 0.023	1.003 ± 0.010

Table 6: Summery of trigger efficiencies and scale factor for different selection steps. Selections are cumulative.

To stay consistent with the event selection used for the cut&count analysis, the trigger scale factors measured at the selection step "$N_{btag} \geq 1$" will be used.

4.2 Lepton identification and isolation efficiencies

For the estimation of muon efficiencies the tag and probe method is used in both data and MC. The followed approach is a simple cut&count base tag&probe method.

In this study, the di-lepton candidates compatible with the Z mass ($76 < m_{ll} < 106$ GeV/c^2) are assumed to come from the Z bosons and used to estimate the efficiency.

The measured efficiencies are compared to the efficiencies in MC DY, where the pileup correction is applied, following the recipe presented in Sec.3.4. This allows to define scale factors ($SF_l = \epsilon_l^{data}/\epsilon_l^{MC}$) which are used to correct the MC predictions.

The lepton isolation and identification efficiencies are estimated separately. The isolation efficiency is defined as the rate of prompt isolated leptons passing the isolation requirements presented in Sec.3. The identification efficiency corresponds to the complete lepton selection efficiency, except for the isolation cuts. The tag&probe estimate is applied after the trigger selection. This way, correlations between lepton selection and trigger selection are automatically taken into account.

The definition of "tag" lepton selection corresponds to the complete lepton selection, including acceptance, isolation and identification. The "probe" leptons are defined as:

- leptons passing the acceptance and isolation selections (for identification efficiency measurement),
- or leptons passing the acceptance and identification selections (for isolation efficiency measurement).

The event selection for the efficiency measurements is the following:

- the di-lepton triggers have to be fired,

- at least one "tag" lepton,
- at least one "probe" lepton which does not match with the tag lepton,
- the tag and probe leptons have opposite charges and an invariant mass compatible with the Z mass ($76 < m_{\ell\ell} < 106\,\mathrm{GeV/c^2}$).

The lepton selection efficiency is then given by the number of selected events with the probe lepton passing the studied selection, divided by the total number of selected events. As the kinematics of leptons in Z events and $t\bar{t}$ are different, the efficiencies and scale factors will be given as function of p_T of the probe leptons, for different η ranges.

The isolation and identification efficiencies and scale factors for muons are presented in Fig. 7, Fig. 8 and Fig. 9. respectively. The isolation and identification efficiencies and scale factors for electrons are presented in Fig. 10, Fig. 11 and Fig. 12. respectively. An overall excellent agreement between data and MC is found.

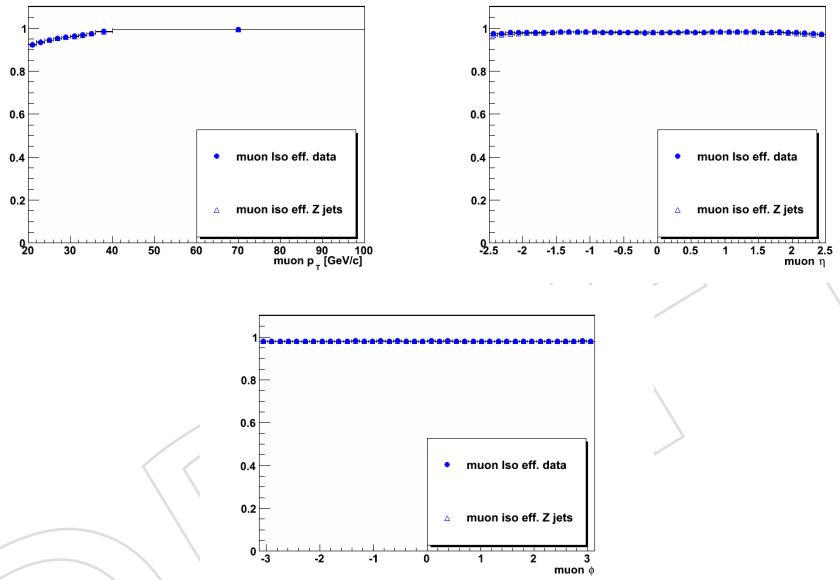

Figure 7: Muon isolation efficiency as a function of p_T, η and ϕ of the probe muon. The circles are obtained from the Tag&Probe method applied on data, the triangles are efficiencies from DY MC.

The systematic uncertainties are estimated by moving the invariant mass window cut by ± 5 GeV/c^2 and re-applying the tag&probe method. The largest variation of the efficiencies and scale factors with respect to their nominal value is taken as a systematic uncertainty.

All the corresponding values for data efficiencies and scale factors are given in tables 7 to 16. The various scale factors for electrons and muons are found to be very close to 1.

Global lepton scale factors are determined using $t\bar{t}$ MC events. From the p_T and η spectra of selected leptons in signal events, a per event SF factor is determined and combined for all selected events in order to calculate inclusive scale factors, which corresponds to the p_T and η spectra of leptons observed in $t\bar{t}$ MC. The inclusive scale factors are found to be $SF_{\mu\mu}^{lept} = 0.997 \pm 0.005$, $SF_{ee}^{lept} = 0.994 \pm 0.005$ and $SF_{\mu\mu}^{lept} = 0.995 \pm 0.003$.

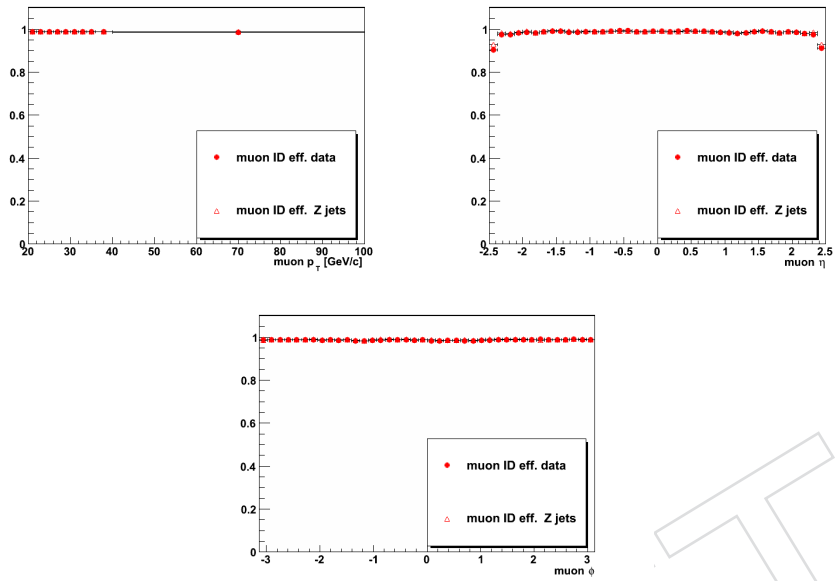

Figure 8: Muon identification efficiency as a function of p_T, η and ϕ a of the probe muon. The circles are obtained from the Tag&Probe method applied on data, the triangles are efficiencies from DY MC.

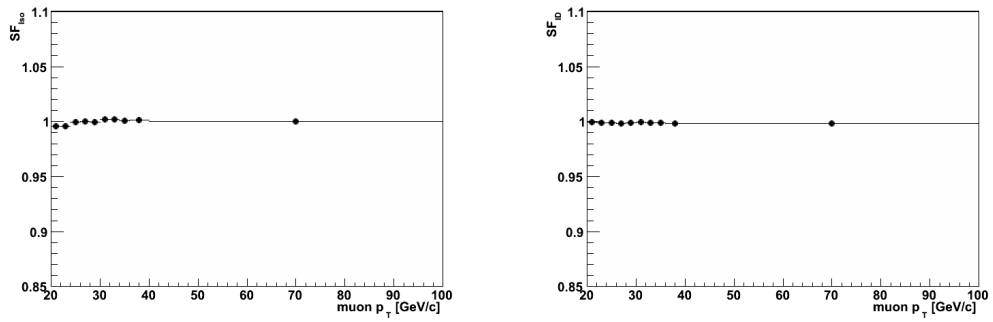

Figure 9: Muon isolation (left) and identification (right) scale factor as a function of p_T of the probe muon.

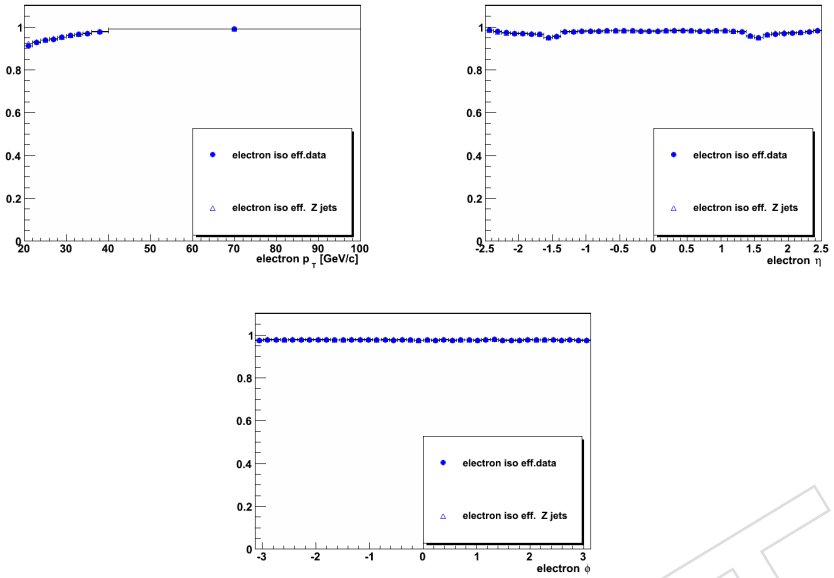

Figure 10: Electron isolation efficiency as a function of p_T, η and ϕ of the probe electron. The circles are obtained from the Tag&Probe method, the triangles are coming from MC.

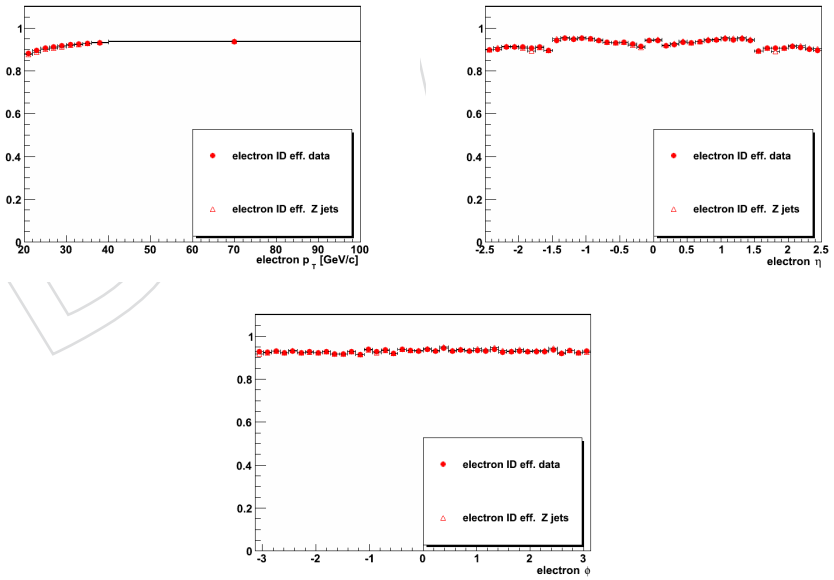

Figure 11: Electron identification efficiency as a function of p_T, η and ϕ of the probe electron. The circles are obtained from the Tag&Probe method, the triangles are coming from MC.

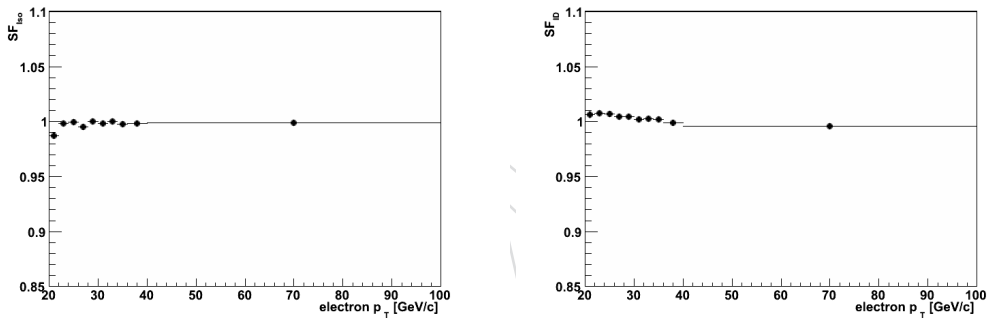

Figure 12: Electron isolation (left) and identification (right) scale factor as a function of p_T of the probe electron.

pt ranges	20-22	22-24	24-26	26-28	28-30
$\|\eta\| < 1.5$	$0.919 \pm 0.002 \pm 0.006$	$0.934 \pm 0.002 \pm 0.005$	$0.943 \pm 0.001 \pm 0.006$	$0.948 \pm 0.001 \pm 0.006$	$0.956 \pm 0.001 \pm 0.005$
$\|\eta\| > 1.5$	$0.895 \pm 0.004 \pm 0.010$	$0.918 \pm 0.003 \pm 0.009$	$0.930 \pm 0.002 \pm 0.011$	$0.931 \pm 0.002 \pm 0.009$	$0.945 \pm 0.002 \pm 0.007$
pt ranges	30-32	32-34	34-36	36-40	40-100
$\|\eta\| < 1.5$	$0.963 \pm 0.001 \pm 0.004$	$0.969 \pm 0.001 \pm 0.003$	$0.972 \pm 0.001 \pm 0.002$	$0.980 \pm 0.000 \pm 0.001$	$0.991 \pm 0.000 \pm 0.000$
$\|\eta\| > 1.5$	$0.949 \pm 0.002 \pm 0.006$	$0.953 \pm 0.002 \pm 0.006$	$0.959 \pm 0.001 \pm 0.005$	$0.967 \pm 0.001 \pm 0.002$	$0.986 \pm 0.000 \pm 0.001$

Table 7: Electron isolation efficiency as function of electrons p_T [GeV/c] and η.

pt ranges	20-22	22-24	24-26	26-28	28-30
$\|\eta\| < 1.5$	$0.899 \pm 0.003 \pm 0.004$	$0.908 \pm 0.002 \pm 0.004$	$0.921 \pm 0.002 \pm 0.004$	$0.922 \pm 0.002 \pm 0.004$	$0.926 \pm 0.001 \pm 0.004$
$\|\eta\| > 1.5$	$0.847 \pm 0.004 \pm 0.005$	$0.866 \pm 0.004 \pm 0.004$	$0.874 \pm 0.003 \pm 0.003$	$0.884 \pm 0.003 \pm 0.004$	$0.893 \pm 0.002 \pm 0.003$
pt ranges	30-32	32-34	34-36	36-40	40-100
$\|\eta\| < 1.5$	$0.932 \pm 0.001 \pm 0.004$	$0.935 \pm 0.001 \pm 0.002$	$0.936 \pm 0.001 \pm 0.001$	$0.939 \pm 0.001 \pm 0.001$	$0.942 \pm 0.000 \pm 0.000$
$\|\eta\| > 1.5$	$0.896 \pm 0.002 \pm 0.002$	$0.899 \pm 0.002 \pm 0.003$	$0.905 \pm 0.002 \pm 0.002$	$0.906 \pm 0.001 \pm 0.002$	$0.917 \pm 0.001 \pm 0.000$

Table 8: Electron identification efficiency as function of electrons p_T [GeV/c] and η.

pt ranges	20-22	22-24	24-26	26-28	28-30
$\|\eta\| < 1.5$	$0.917 \pm 0.002 \pm 0.011$	$0.931 \pm 0.002 \pm 0.010$	$0.941 \pm 0.001 \pm 0.009$	$0.950 \pm 0.001 \pm 0.008$	$0.956 \pm 0.001 \pm 0.009$
$\|\eta\| > 1.5$	$0.932 \pm 0.002 \pm 0.005$	$0.940 \pm 0.002 \pm 0.007$	$0.952 \pm 0.002 \pm 0.005$	$0.957 \pm 0.002 \pm 0.005$	$0.963 \pm 0.001 \pm 0.006$
pt ranges	30-32	32-34	34-36	36-40	40-100
$\|\eta\| < 1.5$	$0.963 \pm 0.001 \pm 0.008$	$0.968 \pm 0.001 \pm 0.006$	$0.975 \pm 0.001 \pm 0.004$	$0.985 \pm 0.000 \pm 0.001$	$0.993 \pm 0.000 \pm 0.001$
$\|\eta\| > 1.5$	$0.965 \pm 0.001 \pm 0.007$	$0.970 \pm 0.001 \pm 0.005$	$0.974 \pm 0.001 \pm 0.004$	$0.983 \pm 0.000 \pm 0.001$	$0.992 \pm 0.000 \pm 0.001$

Table 9: Muon isolation efficiency as function of muons p_T [GeV/c] and η.

pt ranges	20-22	22-24	24-26	26-28	28-30
$\|\eta\| < 1.5$	$0.991 \pm 0.001 \pm 0.000$	$0.990 \pm 0.001 \pm 0.000$	$0.990 \pm 0.001 \pm 0.000$	$0.990 \pm 0.001 \pm 0.000$	$0.990 \pm 0.000 \pm 0.000$
$\|\eta\| > 1.5$	$0.985 \pm 0.001 \pm 0.000$	$0.984 \pm 0.001 \pm 0.000$	$0.985 \pm 0.001 \pm 0.000$	$0.983 \pm 0.001 \pm 0.000$	$0.982 \pm 0.001 \pm 0.001$
pt ranges	30-32	32-34	34-36	36-40	40-100
$\|\eta\| < 1.5$	$0.990 \pm 0.000 \pm 0.000$	$0.989 \pm 0.000 \pm 0.000$	$0.989 \pm 0.000 \pm 0.000$	$0.988 \pm 0.000 \pm 0.000$	$0.988 \pm 0.000 \pm 0.000$
$\|\eta\| > 1.5$	$0.983 \pm 0.001 \pm 0.001$	$0.983 \pm 0.001 \pm 0.001$	$0.982 \pm 0.001 \pm 0.000$	$0.982 \pm 0.001 \pm 0.000$	$0.982 \pm 0.000 \pm 0.000$

Table 10: Muon identification efficiency as function of muons p_T [GeV/c] and η.

pt ranges	20-22	22-24	24-26	26-28	28-30
$\|\eta\| < 1.5$	0.987 ± 0.003±0.001	0.996 ± 0.002±0.001	0.997 ± 0.002±0.001	0.995 ± 0.001±0.002	0.998 ± 0.001±0.001
$\|\eta\| > 1.5$	0.989 ± 0.004±0.001	1.002 ± 0.003±0.003	1.003 ± 0.003±0.005	0.995 ± 0.003±0.002	1.004 ± 0.002±0.001
pt ranges	30-32	32-34	34-36	36-40	40-100
$\|\eta\| < 1.5$	0.998 ± 0.001±0.001	1.000 ± 0.001±0.000	0.998 ± 0.001±0.000	0.998 ± 0.000±0.000	0.999 ± 0.000±0.000
$\|\eta\| > 1.5$	0.999 ± 0.002±0.001	1.000 ± 0.002±0.001	0.999 ± 0.002±0.001	0.999 ± 0.001±0.001	0.998 ± 0.000±0.000

Table 11: Electron isolation SF as function of electrons p_T [GeV/c] and η.

pt ranges	20-22	22-24	24-26	26-28	28-30
$\|\eta\| < 1.5$	1.003 ± 0.003±0.001	1.003 ± 0.003±0.000	1.006 ± 0.002±0.001	1.002 ± 0.002±0.001	1.003 ± 0.002±0.001
$\|\eta\| > 1.5$	1.013 ± 0.005±0.004	1.016 ± 0.005±0.001	1.008 ± 0.004±0.001	1.011 ± 0.003±0.001	1.009 ± 0.003±0.000
pt ranges	30-32	32-34	34-36	36-40	40-100
$\|\eta\| < 1.5$	1.001 ± 0.001±0.001	1.002 ± 0.001±0.001	1.000 ± 0.001±0.000	0.998 ± 0.001±0.000	0.995 ± 0.000±0.000
$\|\eta\| > 1.5$	1.004 ± 0.003±0.001	1.005 ± 0.003±0.002	1.007 ± 0.002±0.002	1.001 ± 0.002±0.001	0.998 ± 0.001±0.000

Table 12: Electron identification SF as function of electrons p_T [GeV/c] and η.

pt ranges	20-22	22-24	24-26	26-28	28-30
$\|\eta\| < 1.5$	0.992 ± 0.002±0.001	0.993 ± 0.002±0.001	0.997 ± 0.001±0.001	0.998 ± 0.001±0.001	0.997 ± 0.001±0.001
$\|\eta\| > 1.5$	1.002 ± 0.003±0.003	1.001 ± 0.002±0.004	1.005 ± 0.002±0.004	1.004 ± 0.002±0.005	1.006 ± 0.002±0.004
pt ranges	30-32	32-34	34-36	36-40	40-100
$\|\eta\| < 1.5$	1.000 ± 0.001±0.001	0.999 ± 0.001±0.001	1.000 ± 0.001±0.000	1.000 ± 0.000±0.000	0.999 ± 0.000±0.000
$\|\eta\| > 1.5$	1.007 ± 0.001±0.004	1.008 ± 0.001±0.003	1.005 ± 0.001±0.002	1.005 ± 0.001±0.001	1.003 ± 0.000±0.000

Table 13: Muon isolation SF as function of muons p_T [GeV/c] and η.

pt ranges	20-22	22-24	24-26	26-28	28-30
$\|\eta\| < 1.5$	1.000 ± 0.001±0.000	0.999 ± 0.001±0.000	0.999 ± 0.001±0.000	0.999 ± 0.001±0.000	1.000 ± 0.000±0.000
$\|\eta\| > 1.5$	0.999 ± 0.001±0.000	0.998 ± 0.001±0.000	0.999 ± 0.001±0.000	0.997 ± 0.001±0.000	0.996 ± 0.001±0.001
pt ranges	30-32	32-34	34-36	36-40	40-100
$\|\eta\| < 1.5$	1.000 ± 0.000±0.000	1.000 ± 0.000±0.000	0.999 ± 0.000±0.000	0.999 ± 0.000±0.000	0.999 ± 0.000±0.000
$\|\eta\| > 1.5$	0.998 ± 0.001±0.001	0.997 ± 0.001±0.000	0.997 ± 0.001±0.000	0.997 ± 0.001±0.000	0.997 ± 0.000±0.000

Table 14: Muon identification SF as function of muons p_T [GeV/c] and η.

pt ranges	20-22	22-24	24-26	26-28	28-30
$\|\eta\| < 1.5$	$0.993 \pm 0.002 \pm 0.001$	$0.992 \pm 0.002 \pm 0.001$	$0.996 \pm 0.002 \pm 0.001$	$0.997 \pm 0.001 \pm 0.001$	$0.997 \pm 0.001 \pm 0.001$
$\|\eta\| > 1.5$	$1.001 \pm 0.003 \pm 0.003$	$0.999 \pm 0.003 \pm 0.004$	$1.004 \pm 0.002 \pm 0.004$	$1.001 \pm 0.002 \pm 0.005$	$1.001 \pm 0.002 \pm 0.004$
pt ranges	30-32	32-34	34-36	36-40	40-100
$\|\eta\| < 1.5$	$1.000 \pm 0.001 \pm 0.000$	$0.999 \pm 0.001 \pm 0.001$	$0.999 \pm 0.001 \pm 0.000$	$0.999 \pm 0.000 \pm 0.000$	$0.998 \pm 0.000 \pm 0.000$
$\|\eta\| > 1.5$	$1.004 \pm 0.002 \pm 0.004$	$1.005 \pm 0.002 \pm 0.003$	$1.002 \pm 0.001 \pm 0.002$	$1.002 \pm 0.001 \pm 0.001$	$1.000 \pm 0.000 \pm 0.000$

Table 15: Muon overall SF as function of muon p_T [GeV/c] and η.

pt ranges	20-22	22-24	24-26	26-28	28-30
$\|\eta\| < 1.5$	$0.990 \pm 0.004 \pm 0.001$	$0.999 \pm 0.003 \pm 0.001$	$1.003 \pm 0.003 \pm 0.002$	$0.997 \pm 0.002 \pm 0.002$	$1.001 \pm 0.002 \pm 0.000$
$\|\eta\| > 1.5$	$1.002 \pm 0.007 \pm 0.005$	$1.018 \pm 0.006 \pm 0.005$	$1.012 \pm 0.005 \pm 0.006$	$1.006 \pm 0.004 \pm 0.002$	$1.013 \pm 0.004 \pm 0.001$
pt ranges	30-32	32-34	34-36	36-40	40-100
$\|\eta\| < 1.5$	$0.999 \pm 0.002 \pm 0.001$	$1.001 \pm 0.001 \pm 0.000$	$0.998 \pm 0.001 \pm 0.000$	$0.996 \pm 0.001 \pm 0.000$	$0.993 \pm 0.000 \pm 0.000$
$\|\eta\| > 1.5$	$1.003 \pm 0.003 \pm 0.002$	$1.005 \pm 0.003 \pm 0.002$	$1.005 \pm 0.003 \pm 0.002$	$1.000 \pm 0.002 \pm 0.001$	$0.997 \pm 0.001 \pm 0.000$

Table 16: Electron overall SF as function of electron p_T [GeV/c] and η.

4.2.1 Isolation difference between $t\bar{t}$ and Z events.

Because of kinematic and topological differences between $t\bar{t}$ and Z events, mainly coming from the differences in jet multiplicity, the lepton selection efficiency can be different between $t\bar{t}$ and Z events. The $t\bar{t}$ and Z+jets identification and isolation efficiencies are shown on Fig 13 for events passing the trigger and the lepton p_T and η selection, with at least 2 jets. At this selection step, the identification efficiencies are very similar between $t\bar{t}$ and Z events, then the differences are neglected.

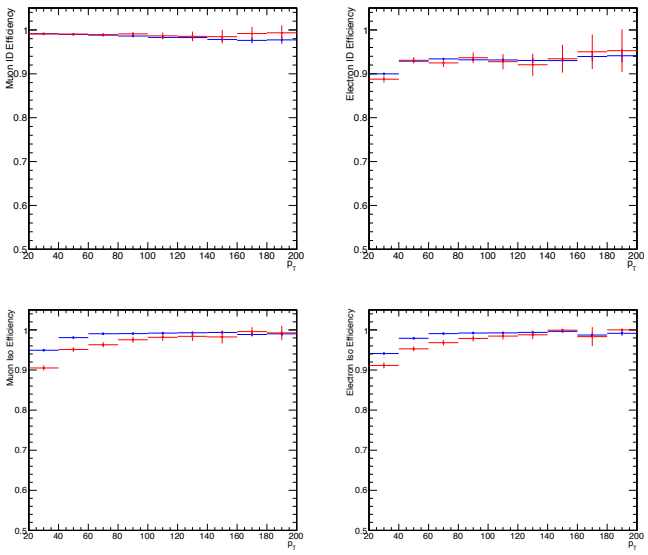

Figure 13: From MC truth, identification (upper plots) and isolation (bottom plot) efficiencies as function of the lepton p_T for muons (left) and electrons (right) for events passing the trigger and the p_T and η selection, and with at least 2 jets.

The $t\bar{t}$ and $Zjet$ isolation efficiencies are shown on Fig 14 after the trigger and the lepton p_T and η selections, asking for the presence of 2 selected jets in the events and with $\not{E}_T > 40$ GeV.

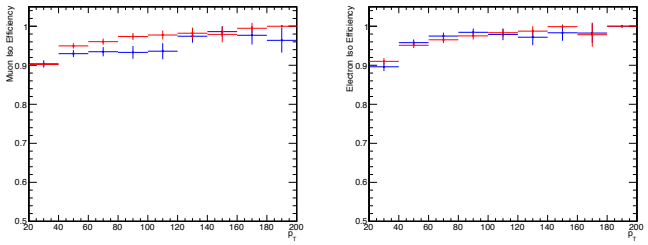

Figure 14: From MC truth, isolation for muons (left) and electrons (right) as function of the lepton p_T for events passing the trigger, the p_T and η selection, asking for at least 2 selected jets in the events and $\not{E}_T > 40$ GeV.

Using the information from previous distributions (13, 14), a bin per bin difference for efficiencies in $t\bar{t}$ and Z events is done and the largest differences are summarised in the Table 17 for event passing the trigger selection, the lepton p_T and η selection, at least 2 jets and with or without the $\not{E}_T$requirements.

The mean of the $t\bar{t}$-Z differences between the *electron* and *muon* isolation efficiencies is found

selection	electron	muon	mean
trigger+dilepton+Njet$\geq$ 2	2.0%	2.8%	2.4%
trigger+dilepton+Njet$\geq$ 2 + $\not\!\!E_T > 40$	0.3%	1.1%	0.6%

Table 17: From MC truth, the largest isolation efficiencies differences between $t\bar{t}$ and Z events observed using p_T spectra.

to be $< 1\%$ once that $\not\!\!E_T$ is required in the event, so for the moment no additional systematic uncertainty is assigned to the lepton selection modelling.

4.3 Summary on trigger and lepton efficiencies

The final trigger efficiencies and SF used for the analysis are presented in the Tab 6. To be consistent with the cut& count analysis, and since the triggers SF are stable with the level of selection, the scale factors for at least 1 b-tagged jets is used in both analyses.

- ee **channel :** SF^{ee}_{trig} =0.962 $\pm$ 0.016
- $e\mu$ **channel :** $SF^{e\mu}_{trig}$ =1.008 $\pm$ 0.009
- $\mu\mu$ **channel :** $SF^{\mu\mu}_{trig}$ =0.977 $\pm$ 0.015

The mean scale factor for lepton isolation and identification for $t\bar{t}$ event is obtained by applying the scale factors from the tables 15 and 16 to MC events and by calculating the mean SF and their uncertainties. Finally, the uncertainty coming from the lepton energy scale (LES) is estimated by comparing the dilepton invariant mass in Z+jets events and data after the trigger and the dilepton selections. The LES uncertainties are discussed in the [12] and the corresponding analysis note. They are estimated to be of 0.3%, 0.2% and 0.2% for the $\mu\mu$, $e\mu$ and ee channels respectively for 2.3 fb^{-1} validated data.

The isolation and identification SF used in the analysis are then :

- ee **channel :** $SF^{ee}_{Iso,ID} = 0.995 \pm 0.003$
- $e\mu$ **channel :** $SF^{e\mu}_{Iso,ID} = 0.994 \pm 0.005$
- $\mu\mu$ **channel :** $SF^{\mu\mu}_{Iso,ID} = 0.997 \pm 0.005$

Accounting for trigger, isolation, identification efficiencies, the final scale factors became :

- ee **channel :** $SF^{ee}_{Tri,Iso,ID} = 0.957 \pm 0.016$
- $e\mu$ **channel :** $SF^{e\mu}_{Tri,Iso,ID} = 1.002 \pm 0.010$
- $\mu\mu$ **channel :** $SF^{\mu\mu}_{Tri,Iso,ID} = 0.974 \pm 0.016$

4.4 $\not\!\!E_T$ selection efficiency from data

After the di-jets selection, the $e\mu$ channel is already highly enriched in $t\bar{t}$ events. Estimated from MC, the signal over backgrounds ratio after requiring at least one b-tagged jet is higher than 10. Given this high level of purity, and since no $\not\!\!E_T$ selection is applied for the $e\mu$ channel, one can estimate the selection efficiency of the $\not\!\!E_T$ cut from the $e\mu$ channels by simply counting the fraction of events passing a $\not\!\!E_T$ cut of 40 GeV.

As an illustration, the $\not\!\!E_T$ distribution in the $e\mu$ channel is presented in Fig 15 after the jet selection. The MC is found to be in very good agreement with the data. The data to MC ratio of $\not\!\!E_T$ efficiencies ε_{met} (SF_{met}) is then expected to be close to 1.

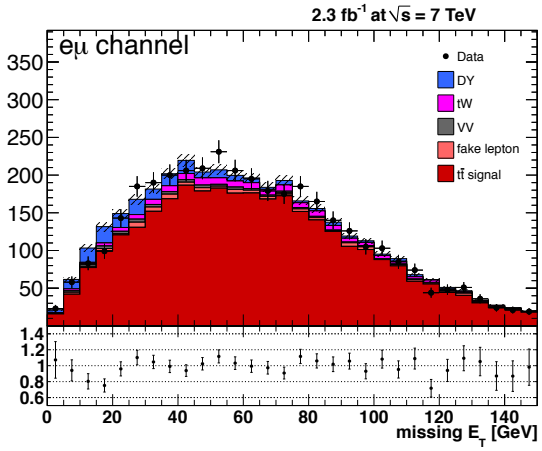

Figure 15: $\not\!\!E_T$ in the $e\mu$ channels distributions after the jet selection.

channel	$\mu\mu$	ee	$e\mu$
$\not\!\!E_T$ > 40GeV	1.003 ± 0.013	1.003 ± 0.017	1.003 ± 0.013
$\geq$ 1 btag	1.008 ± 0.012	1.008 ± 0.016	1.008 ± 0.011
$\geq$ 2 btag	1.015 ± 0.018	1.015 ± 0.017	1.015 ± 0.013

Table 18: $\not\!\!E_T$ selection efficiencies Scale Factors as function of the selection step. Central values corresponds to the observed efficiency in the $e\mu$ channel, only the uncertainties change from a channel to the other.

The $\not\!\!E_T$ selection efficiency is the estimated by

- constructing the $e\mu$ $\not\!\!E_T$ distribution in data with the substraction of residual backgrounds contamination, using MC estimates for single top and dibosons, and using the data driven estimate for DY events (as described in 5).
- in this distribution, counting the fraction of events passing a $\not\!\!E_T$ cut of 40 GeV.

Two different sources of systematics are considered :

- The background contamination : ε_{met} is estimated by changing the backgrounds normalization before substraction by $\pm$30%. The observed variations with respect to the true nominal $\not\!\!E_T$ efficiency are taken as systematics.
- The effect of lepton resolution into the $\not\!\!E_T$: as the resolution of electrons and muons are different, and since the leptons are used in the $\not\!\!E_T$ reconstruction, the $\not\!\!E_T$ selection efficiencies could be different between the three channels. To account for this effect, difference of the true $t\bar{t}$ MC efficiency between the three channels are accounted as an additional systematics.

The measured $\not\!\!E_T$ selection efficiencies Scale Factors are presented in Tab 18. The scale factors are found to be very close to 1 with uncertainties of few percent. To stay consistent with the events selection applied for the cut&count measurement, the scale factors estimated after the requiring at least one b-tagged jet are used in the following ($SF^{\mu\mu}_{met}$=1.008 $\pm$ 0.012 for the $\mu\mu$ channel and SF^{ee}_{met}=1.008 $\pm$ 0.016 for the ee channel).

5 Determination of the DY background from data-driven methods

As it is the main remaining background after the events selection, it is important to measure the background contamination from data and to compare it to the MC predictions. This is specially crucial for the ee and $\mu\mu$ channels, but also for the remaining lower order contamination in $e\mu$ channel, in the case of the the process $Z/\gamma^* \to \tau\tau \to e\mu$.

In precedent measurements [12] it was observed that the DY background contamination was not well described by the MC samples. At that time, a combination of a MadGraph sample ($M_{ll} > 50$ GeV) and Powheg sample ($10 < M_{ll} < 50$ GeV) was used. As it can be seen in Fig 16, after the jet selection, the low invariant mass region was not well described by the Powheg samples.

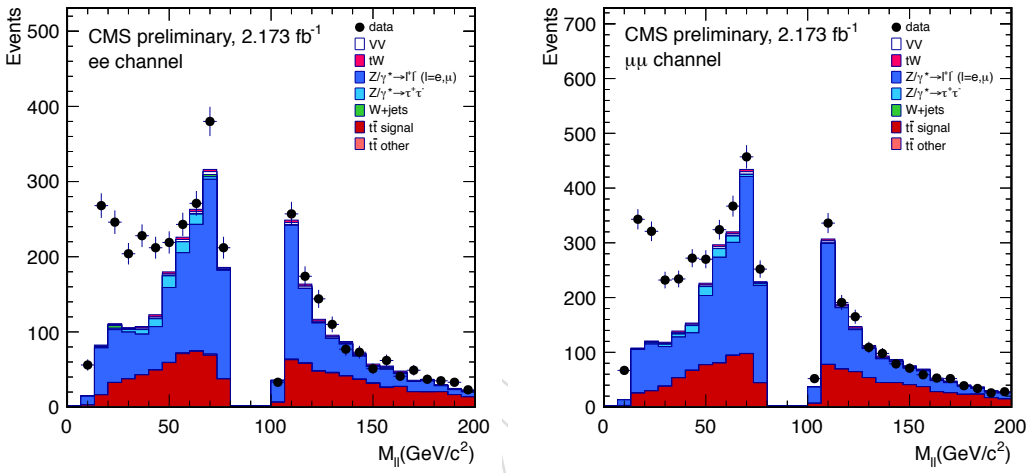

Figure 16: Dilepton invariant mass after the jet selection in the ee (left) and $\mu\mu$ (right) channels. A combination of Powheg and MadGraph sample is used to described the DY contamination.

In Fig 17, the Powheg samples was substituted with the MadGraph samples for ($10 < M_{ll} < 50$ GeV), see Sec 3). A much better agreement between data and MC is observed. For this reason, the MadGraph sample will be used to described all the DY, for the complete M_{ll} range ($10 < M_{ll} < 50$ GeV + $M_{ll} > 50$ GeV).

Description of the strategy for DY estimation

Three different methods are used to described estimate the DY contamination :

- the $\mathbf{R}_{out/in}$ method is used as the reference method for the ee and $\mu\mu$ channels. It will be used to estimate the data to MC scale factors.
- the **Fitting Function** method is used as a cross check method for the ee and $\mu\mu$ channels. It helps also to determine the systematic uncertainties.
- the **Template Fit** method is used to estimate the DY contamination in the $e\mu$ channel. It is also used an another cross check for the ee and $\mu\mu$ channels.

The results of these three methods are compared and combined to determine the number of DY events in data and its ratio with the MC prediction SF_{DY}. In sections 5.1, 5.2 and 5.3 the different methods are presented. In section 5.4, the combination of the three methods is presented and the final DY SFs are given.

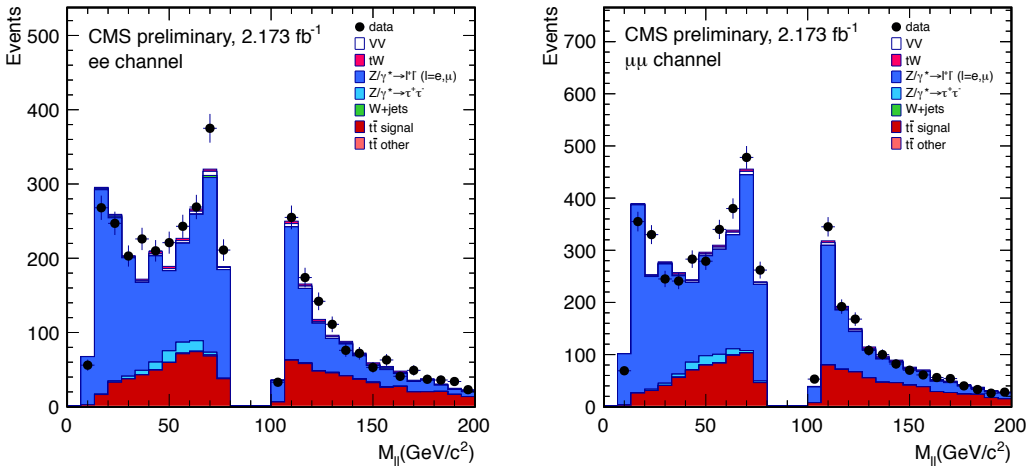

Figure 17: Dilepton invariant mass after the jet selection in the ee (left) and $\mu\mu$ (right) channels. MadGraph samples are used to described the DY contamination.

5.1 Description of the "$R_{out/in}$ method"

The analysis makes use of the Drell-Yan estimation method described in reference [30], extracting the events outside the Z-veto region from the events inside. As contamination from Non-DY backgrounds can still be present in the control region, this contribution is subtracted from the emu channel and then scaled according to the event yields in ee and $\mu\mu$ channels.

Then the number of events outside the Z-veto can be measured from data as:

$$N_{out}^{l^+l^-,obs} = R_{out/in}^{l^+l-}(N_{in}^{l^+l^-} - 0.5N_{in}^{e\mu}k_{ll}) \tag{11}$$

where $ll = \mu\mu$ or ee and $R_{out/in}$ is the ratio of the number of events outside/inside the Zveto region taken from a DY MC sample:

$$R_{out/in} = \frac{N_{DYMC}^{out}}{N_{DYMC}^{in}}$$

k is a corrector factor that must be applied to take into account the differences between electron and muon reconstruction, it is calculated using the events in the Z peak region passing the standard dilepton and jet selections but without any $\not\!\!E_T$ cut, and can be expressed as:

$$k_{ee} = \sqrt{\frac{N^{e^+e^-_{in},loose}}{N^{\mu^+\mu^-_{in},loose}}}$$

$$k_{\mu\mu} = \sqrt{\frac{N^{\mu^+\mu^-_{in},loose}}{N^{e^+e^-_{in},loose}}}$$

5.1.1 Results using MC based $R_{out/in}$

In these first round of estimate, the $R_{out/in}$ is extracted directly from MadGraph DY events. Results are summarised in Tab. 19. The differences between simulation and data driven estimates are coming from the discrepancies already observed in the $\not\!\!E_T$ and jet distributions between data and MC.

channel	$R_{out/in}$	DY MC	DY pred.	SF
ee, NJets >=2	0.120±0.003	2151.5±47.4	2125.2±51.1	0.988±0.024
ee, MET $\geq$ 40	0.194±0.025	73.4±8.8	119.6±27.5	1.629±0.374
ee, NBjets $\geq$1	0.183±0.036	30.3±5.6	54.2±14.8	1.790±0.489
ee, NBjets $\geq$2	0.175±0.076	6.2±2.6	11.2±6.0	1.801±0.967
$\mu\mu$, NJets >=2	0.119±0.002	2722.1±53.3	2718.9±58.1	0.999±0.021
$\mu\mu$, MET $\geq$ 40	0.250±0.025	124.2±11.4	179.9±42.4	1.448±0.341
$\mu\mu$, NBjets $\geq$1	0.234±0.037	49.3±7.2	67.8±19.5	1.375±0.394
$\mu\mu$, NBjets $\geq$2	0.229±0.080	10.1±3.2	6.5±5.7	0.651±0.571

Table 19: $R_{out/in}$, DY predicted by the MC and estimated from data as well as the corresponding scale factor. The uncertainty is statistical only.

5.1.2 Comparisons of $R_{out/in}$ in data and MC

In this data driven method, most of the uncertainty is coming from the $R^{MC}_{out/in}$ ratio which is taken from MC. A conservative 50% uncertainty was used up to know. By defining control regions enriched in DY events, $R^{Data}_{out/in}$ can be estimated from data directly, in order to decrease the uncertainty.

The $R_{out/in}$ dependency was studied as function of the number of vertices and the jet multiplicity. For this purpose, it was tried to select a pure sample of DY events. The selections are:

1. **for pileup studies :** dilepton invariant mass cut,
2. **for NJet studies :** dilepton invariant mass cut and $\not\!\!E_T <$ 10 GeV.

For each selection, the $R_{out/in}$ factor is calculated as function of the number of vertices and the jet multiplicity respectively. The purity of DY events is estimated using MC by the fraction N_{DY}/N_{allMC}. Out of these control regions, $R_{out/in}$ in MC is compared to the same quantity in data and a correction factor $CF_{R_{out/in}} = R^{data}_{out/in}/R^{MC}_{out/in}$ is deduced.

The plot in Fig. 18 show $R_{out/in}$ as function of the number of reconstructed vertices after the dilepton pair selection. The purity of DY events is expected to be almost 100%. One can see no dependence of $R_{out/in}$ for both the ee and $\mu\mu$ channels, while there is an overall underestimate of $R_{out/in}$ in MC. The scaling factors $CF_{R_{out/in}}$ are extracted by fitting $R_{out/in}$ with constants. They are found to be $CF_{R_{out/in}}(ee) = 1.050\pm < 0.001$ and $CF_{R_{out/in}}(\mu\mu) = 1.076\pm < 0.001$.

These corrections are applied the plots and numbers above.

The plots in Fig.19 show $R_{out/in}$ as function of the number of selected jets after the dilepton pair selection and for $\not\!\!E_T <$ 10 GeV. The purity of DY events is expected to be very high for low jet multiplicity, but can be significant at large jet multiplicity ($\geq$ 4). The Table 20 shows the $R_{out/in}$ for the different jet multiplicity bins.

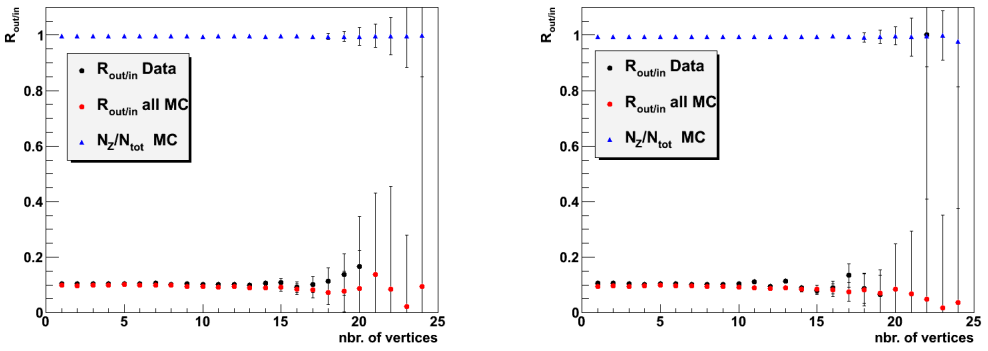

Figure 18: For the $\mu\mu$ (left) and ee (right), $R_{out/in}$ as function of the number of reconstructed vertices for data (black dots), MC prediction (red dots), after the dilepton pair selection. The fraction of DY events is also shown (blue triangles).

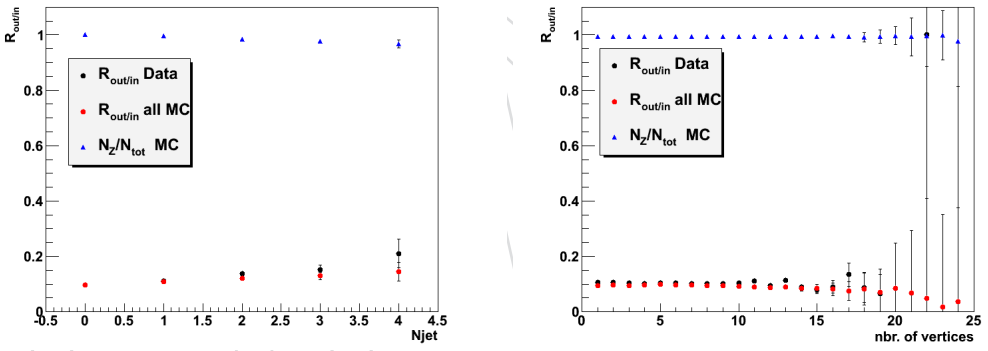

Figure 19: For the $\mu\mu$ (left) and ee (right), $R_{out/in}$ as function of the number of the jet multiplicity for data (black dots), MC prediction(red dots), after the dilepton pair selection and for $\not\!\!E_T < 10$ GeV. The fraction of DY events is also shown (blue triangles).

njet	0	1	2	3	4
$CF_{out/in}(\mu\mu)$	0.987±0.009	1.017 ±0.025	1.148±0.0655	1.179± 0.167	1.452±0.494
$CF_{out/in}(ee)$	1.008±0.010	1.015 ±0.028	1.053±0.0680	1.119± 0.167	0.988±0.388

Table 20: $CR_{out/in}$ as function of jet multiplicity for data and MC.

channel	$R_{out/in}$	DY MC	DY pred.	SF
ee, NJets >=2	0.136±0.009	2151.5±47.4	2409.1±158.7	1.120±0.074
ee, MET $\geq$ 40	0.220±0.028	73.5±8.8	135.6±28.9	1.847±0.394
ee, NBjets $\geq$1	0.208±0.038	30.3±5.6	61.5±15.5	2.029±0.512
ee, NBjets $\geq$2	0.198±0.077	6.2±2.5	12.7±6.3	2.042±1.008
$\mu\mu$, NJets >=2	0.143±0.009	2722.1±53.3	3278.2±203.0	1.204±0.075
$\mu\mu$, MET $\geq$ 40	0.302±0.031	124.2±11.4	216.9±44.7	1.745±0.360
$\mu\mu$, NBjets $\geq$1	0.282±0.041	49.3±7.2	81.7±20.5	1.658±0.417
$\mu\mu$, NBjets $\geq$2	0.276±0.082	10.1±3.2	7.9±6.5	0.785±0.642

Table 21: $R_{out/in}$, DY predicted by the MC and estimated from data as well as the corresponding scale factor. The uncertainty is statistical and systematics, as described in section 5.4.

5.1.3 Results using corrected MC $R_{out/in}$

In this section the $R_{out/in}$ method is used with the $R_{out/in}$ calculated from MC but corrected using data, as described in Sec 5.1.2. The DY estimate for different selection steps are summarised in the Tab. 21. The error is statistical only, where the error on the correction factors CR are taken into account. No clear dependence on $R_{out/in}$ as a function of the $\not\!\!E_T$ is observed with the DY MC. Additional systematic uncertainties are deduced from the comparisons with the "Fit Function" method, see section 5.4 for more details. **These results are used in the final cross-section measurement.**

5.2 Description of the "Fitting Function" method

This section presents the estimate of the DY contamination from data in the ee and $\mu\mu$ channels. The method is based on the definition of a control region highly enriched in DY events and on the comparisons of the dilepton invariant mass inside and outside the Z-mass veto region. The DY background is estimated inclusively before any b-tagging selection.

5.2.1 Description of the method

This method to estimate the DY contamination starts by defining two different regions:

- the Signal Region "SR", in which the final selection is applied, but without cuts on the dilepton invariant mass nor on b-tagging,
- the Control Region "CR", which is characterised by a low jet multiplicity ($N_{jets} \leq 1$) in addition to the two well identified and isolated leptons with opposite charge and the default missing transverse energy cut ($\not\!\!E_T > 40$ GeV/c).

The CR region is assumed to be dominated by the presence of DY events, with a low contamination from other processes. It is also assumed that the shape of the dilepton invariant mass is the same for the SR and CR. Small differences between the two shapes are found and are treated as systematic uncertainties.

As the ratio of DY events inside and outside the Z mass window is assumed to be the same in the control and signal regions, the expected number of DY events after the final selection, outside the Z mass window, can be expressed as:

$$N_{SR}^{out} = N_{CR}^{out} \cdot \frac{N_{SR}^{in}}{N_{CR}^{in}} \tag{12}$$

where

- N_{CR}^{out} is the number of DY events outside the Z mass window in CR region,
- N_{CR}^{in} is the number of DY events inside the Z mass window in CR region,
- N_{SR}^{in} is the number of DY events inside the Z mass window in SR region.

N_{CR}^{out}, N_{CR}^{in} and N_{SR}^{in} can be estimated by fitting the dilepton invariant mass in the data.

The DY contribution is modelized by an asymmetric Breit-Wigner distribution (depending on the sign of $(m_{\ell\ell} - p_7)$) convoluted with a Gaussian and added to a special function which describes the effect of the p_T lepton cut for the low part of the dilepton invariant mass (a trough appears around $M_{ll} \sim 50\ GeV$):

$$f(m_{\ell\ell}) = p_4 + p_5(1 + Erf(p_8 m_{\ell\ell} - p_6) - p_7(1 + (1 + \frac{p_4}{p_7})) * Erf(m_{\ell\ell} - p_7) + \frac{p_0}{p_1 \pi[1 + (\frac{(m_{\ell\ell} - p_3)}{p_1})^2]} \times exp(\frac{(m_{\ell\ell} - p_1)^2}{2p_9^2}) \quad (13)$$

with p_i being floating parameters.

The non DY contamination is described using a continuum distribution which is a combination of an exponential function and a polynomial function:

$$g(m_{\ell\ell}) = p_4((p_5 m_{\ell\ell})^{p_0} \cdot e^{p_1(p_5 m_{\ell\ell})^{p_3}} + p_2) \quad (14)$$

with p_0 to p_5 being the floating parameters. After the fits, the number of DY events is estimated by integrating the fit functions $f(m_{\ell\ell})$ and $g(m_{\ell\ell})$ inside or outside the Z mass region.

To test the behaviour of the continuum fit and to get a first set of parameters which will be used as starting values for other fits, the continuum function is fitted on the $e\mu$ invariant mass distribution which is free from DY events. An example of such fit is presented in the Fig. 20 for MC events. The shape of this distribution is taken as background representing non DY events in the fit with data (its normalisation being a free parameter).In principle, this $e\mu$ mass distribution could be inferred from data but the MC is used in the method.

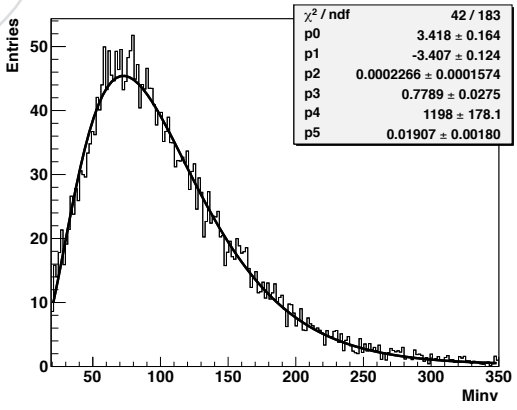

Figure 20: $e\mu$ invariant mass fitted with the function $g(m_{\ell\ell})$, given in eq. (14).

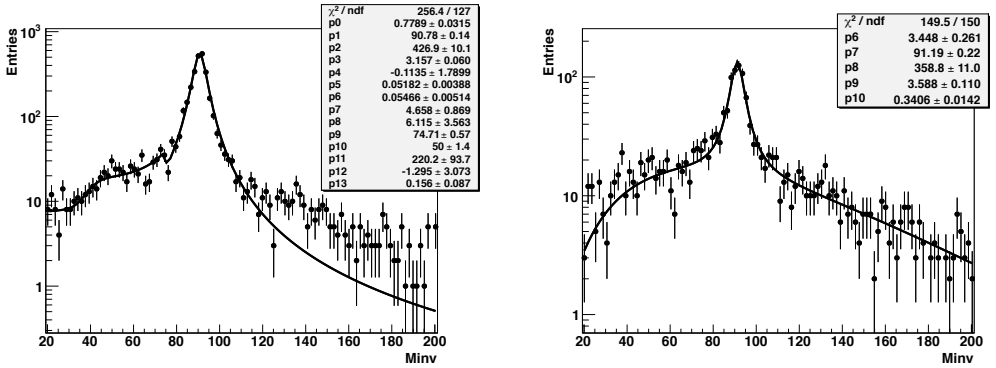

Figure 21: Results of the fit on the $m_{\ell\ell}$ distribution for the *ee* channel in the control region (left) and in the signal region (right).

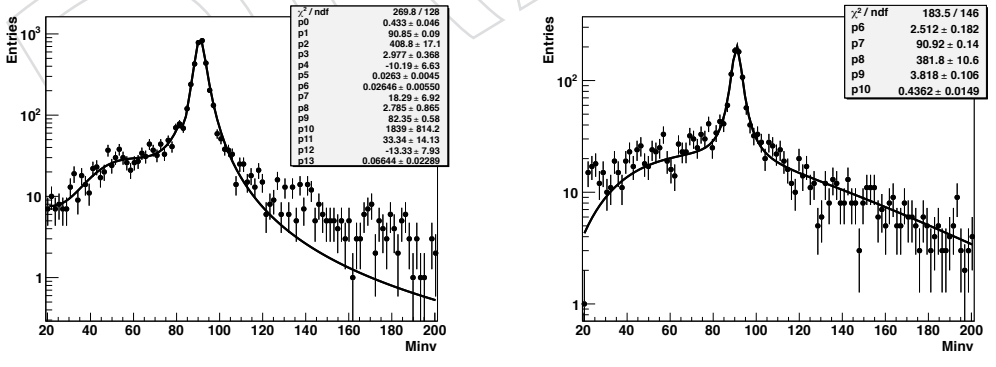

Figure 22: Results of the fit on the $m_{\ell\ell}$ distribution for the $\mu\mu$ channel in the control region (left)and in the signal region (right).

The method is tested on Data with a luminosity of 2.3 fb^{-1} . The results of the fits are shown in the Fig. 21 for the ee channel and in Fig. 22 for the $\mu\mu$ channel.

After the fits, the $g(m_{\ell\ell})$ is integrated inside and outside the Z mass window, and the DY background estimate is done using the equation (13). In order to verify the validity of the method, the DY estimate has also been extracted by means of a closure test. The estimated yield provided by the method for $\mu\mu$ channel and ee channel are found to be consistent with the expected yields (6% and 7% of difference respectively).
The derived scale factor defined as the ratio of the number of fitted DY events outside the Z mass peak to the corresponding number of expected MC DY events is $1.40 \pm 0.08(stat)$ and $1.66 \pm 0.10(stat)$ for $\mu\mu$ and ee channels respectively.

The systematic uncertainties are coming from 3 main contributions which are, by decreasing order: the presence of residual non-DY events in the CR and its uncertainty the SR regions(30-40%), the fitting model which appears to not describe well the tail of the invariant mass distribution at high value (15-25%), the validity of the hypothesis defined by equation12 (<4%). Combining statistical and systematical uncertainties, one gets an inclusive DY scale factor before any B-tagging cut of 1.39 ± 0.55 and 1.65 ± 0.75 for $\mu\mu$ and ee channels respectively. The Data/MC comparison before and after DY rescaling is illustrated by the Fig. 23 for the $\mu\mu$ and for the ee channel.

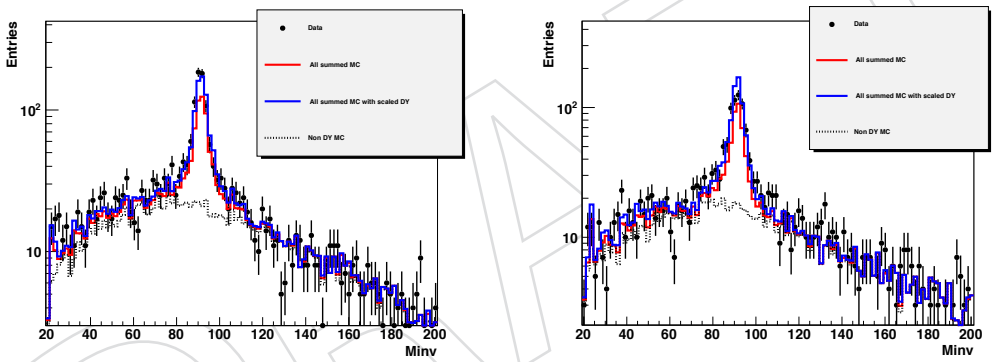

Figure 23: Data/MC comparisons for the $m_{\ell\ell}$ distribution for the $\mu\mu$ channel before (red curve) and after (blue curve) DY rescaling .

5.3 Description of the "Template fit method" (Drell-Yan in $e\mu$ channel)

In the $e\mu$ channel, most of the DY contribution is coming from the process $Z/\gamma^* \rightarrow \tau\tau \rightarrow e^{\nu}_{e}\nu_{\tau}\ \mu\nu_{e}\nu_{\tau}$. As the cross section of this process is much lower than inclusive $Drell - Yan$ cross section, its background contamination is expected to be small.

In addition, because of the presence of neutrinos coming from tau decays, the dilepton invariant mass is not compatible with the known Z mass and the Z mass peak is shifted to the low masses.

For these reasons, it is rather difficult to estimate the Drell-Yan contamination from data. We try here to estimate the overall scale of Drell-Yan contamination in the $e\mu$ channel by using a binned "template" likelihood of the dilepton invariant mass distribution using the RooFit package. The templates are extracted from MC from both signal and background events.

The fit is performed after the jet multiplicity selection. The results of the fits are presented

in the Fig. 24. As a cross check, similar fits are performed for the ee (Figure 25) and the $\mu\mu$ channels (Figure 26) after the jet and $\not\!\!E_T$ selections. Because of lake of statistic, the template fits are not performing well after requiring at least 1 b-tagged jet. The results of the fits and the corresponding data/MC scale factors are presented in Tab. 22.

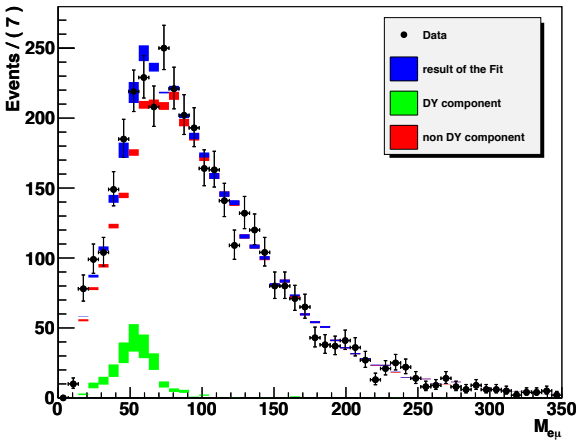

Figure 24: For the $e\mu$ channel. Results of the DY fit of the dilepton invariant mass, after the jet multiplicity selections. Black dots correspond to data, blue area corresponds to the output of the fit, green area to the DY component after the fit and red area the contributions from other processes after the fit. Width of the area corresponds to statistical uncertainty.

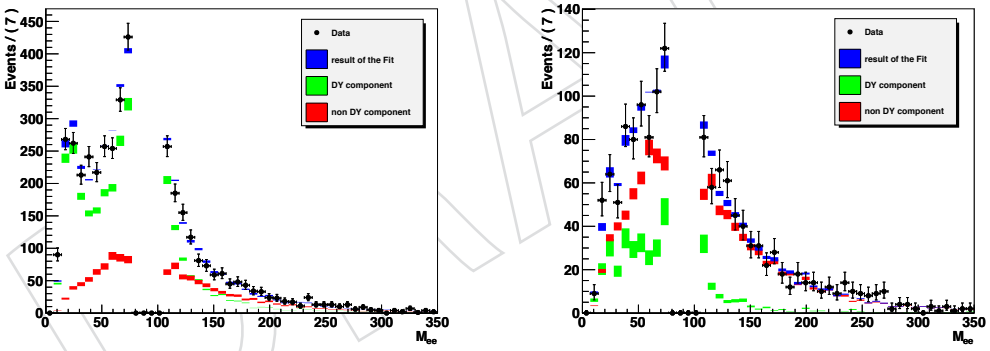

Figure 25: For the ee channel. Results of the DY fit after the jet multiplicity (left) and the $\not\!\!E_T$(right) selections.Black dots correspond to data, blue area corresponds to the output of the fit, green area to the DY component after the fit and red area the contributions from other processes after the fit. Width of the area corresponds to statistical uncertainty.

The fitting procedure is found to give reasonable and meaningful results. However, we can not necessarily rely on the DY shape from the MC and there is large statistical uncertainty.

5.4 Summary of DY estimate

Three different methods are presented and gives compatibles results within uncertainties (Tables 23, 24). Small discrepancies are observed for template fit method in the $\mu\mu$ channels, most likely coming from a bad description of the $\mu\mu$ invariant mass by DY in the MC.

For the ee and $\mu\mu$ channels, the DY scale factor values are taken from the $R_{out/in}$ method. The SF values are compared to the estimates of the Fit Function method and the absolute difference

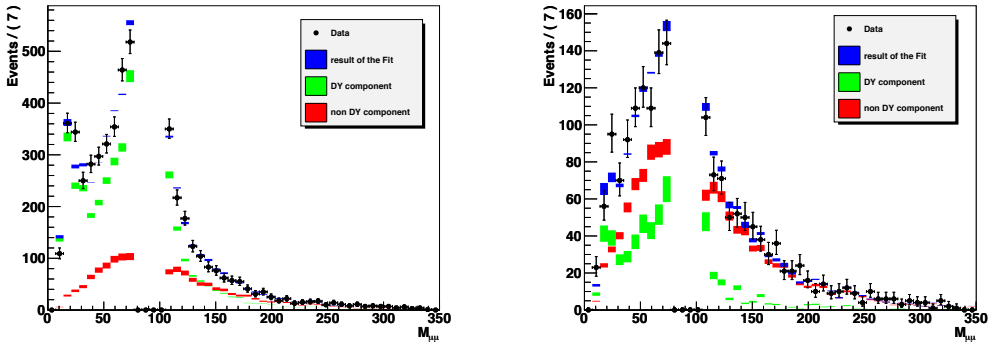

Figure 26: For the $\mu\mu$ channel. Results of the DY fit after the jet multiplicity (left) and the $\not\!\!E_T$(right) selections.Black dots correspond to data, blue area corresponds to the output of the fit, green area to the DY component after the fit and red area the contributions from other processes after the fit. Width of the area corresponds to statistical uncertainty.

selection	$e\mu$	ee	$\mu\mu$
jet sel	1.33±0.28	1.11±0.04	1.19±0.03
met sel	-	1.32±0.48	2.14±0.37

Table 22: Data to MC scale factors from the template fit method.

between the two measurements are found to be around 0.25. We conservatively account for an additional absolute 0.30 systematic uncertainty added in quadrature to the $R_{out/in}$ uncertainty.

method	$R_{out/in}$	Fitting function	Template fit
jet sel	1.120±0.074	-	1.11±0.04
met sel	1.857±0.394	1.65±0.75	1.32±0.48
$\geq$ 1 b-tag	2.029±0.512	-	
$\geq$ 2 b-tag	2.042±1.008	-	

Table 23: Data to MC SF for DY events in the ee channel.

6 QCD and W+jets backgrounds from data-driven methods

6.1 Matrix Method for same sign leptons channels

On the aim to estimate backgrounds to a dileptonic signal with two well isolated leptons, three sets of selections can be defined: loose, medium and tight. Typically, the tight selection set corresponds to ask both leptons to satisfy the isolation criteria, medium selection corresponds to the case where at least one lepton passes the isolation condition and the loose selection corresponds to the case where the lepton isolations are relaxed on both selected leptons. Thus, we have:

$$N^t = N^t_S + N^t_W + N^t_{QCD}, \quad (15)$$
$$N^m = N^m_S + N^m_W + N^m_{QCD}, \quad (16)$$
$$N^l = N^l_S + N^l_W + N^l_{QCD}. \quad (17)$$

method	$R_{out/in}$	Fitting function	Template fit
jet sel	1.204±0.074	-	1.19±0.03
met sel	1.745±0.360	1.39±0.55	2.14±0.37
≥ 1 b-tag	1.658±0.417	-	
≥ 2 b-tag	0.785±0.642	-	

Table 24: Data to MC SF for DY events in the $\mu\mu$ channel.

where N_S, N_{QCD} et N_W are respectively the number of "Signal"-like, "QCD"-like and "W+jets"-like events. The upper indexes l, m and t refer to the loose, medium and tight selections.

One can introduce the efficiencies $\epsilon_S^{l\to m}$, $\epsilon_W^{l\to m}$ and $\epsilon_{QCD}^{l\to m}$, which represent the probability that an event satysfing the loose selection will also satisfy the medium selection. Analougsly, the efficiencies $\epsilon_S^{l\to t}$, $\epsilon_W^{l\to t}$ and $\epsilon_{QCD}^{l\to t}$ will represent the probability that an event satysfies the tight selection being in a preselected sample of events passing the loose selection. Thanks to these definitions we can rewrite the equations (15) to (17) in the form:

$$N^t = \epsilon_S^{l\to t} N_S^l + \epsilon_W^{l\to t} N_W^l + \epsilon_{QCD}^{l\to t} N_{QCD}^l, \quad (18)$$
$$N^m = \epsilon_S^{l\to m} N_S^l + \epsilon_W^{l\to m} N_W^l + \epsilon_{QCD}^{l\to m} N_{QCD}^l, \quad (19)$$
$$N^l = N_S^l + N_W^l + N_{QCD}^l. \quad (20)$$

Given the fact that the efficiencies can be evaluated from data, equations (18) to (20) form a system of three equations and three unknowns, namely N_S^l, N_W^l and N_{QCD}^l. It can be solved and yields the number of events passing the loose cuts: N_S^l, N_W^l and N_{QCD}^l. The expected number of selected signal and background events for the tight set of cuts (corresponding to the standard selection) are then simply given by:

$$N_S^t = \epsilon_S^{l\to t} N_S^l, \quad (21)$$
$$N_W^t = \epsilon_W^{l\to t} N_W^l, \quad (22)$$
$$N_{QCD}^t = \epsilon_{QCD}^{l\to t} N_{QCD}^l. \quad (23)$$

These efficiencies have to be evaluated as a function of event features, for example jet multiplicity.

Some assumptions and definitions have to be done in order to solve the system formed by eq. (18) to (20).

Firstly, the loose to medium efficiencies can be factorized:

$$\epsilon_S^{l\to m} = 2\epsilon_s - \epsilon_s^2, \quad (24)$$
$$\epsilon_W^{l\to m} = \epsilon_s + \epsilon_{fake} - \epsilon_s \epsilon_{fake}, \quad (25)$$
$$\epsilon_{QCD}^{l\to m} = 2\epsilon_{fake} - \epsilon_{fake}^2. \quad (26)$$

where ϵ_s (ϵ_{fake}) represents the probability for a real (fake) lepton to pass isolation cuts.

Secondly, the loose to tight efficiencies are given by:

$$\epsilon_S^{l\to t} = \epsilon_s^2, \quad (27)$$
$$\epsilon_W^{l\to t} = \epsilon_s\epsilon_{fake}, \quad (28)$$
$$\epsilon_{QCD}^{l\to t} = \epsilon_{fake}^2. \quad (29)$$

Doing these assumptions, the equation system becomes:

$$N^t = \epsilon_s^2 N_S^l + \epsilon_s\epsilon_f N_W^l + \epsilon_{fake}^2 N_{QCD}^l, \quad (30)$$
$$N^m = (2\epsilon_s - \epsilon_s^2)N_S^l + (\epsilon_s + \epsilon_{fake} - \epsilon_s\epsilon_{fake})N_W^l + (2\epsilon_{fake} - \epsilon_{fake}^2)N_{QCD}^l, \quad (31)$$
$$N^l = N_S^l + N_W^l + N_{QCD}^l, \quad (32)$$

which can be solved analitically:

$$N_S^l = \frac{N^t - \epsilon_{fake}(N^m + N^t - \epsilon_{fake}N^l)}{(\epsilon_s - \epsilon_{fake})^2}, \quad (33)$$
$$N_W^l = \frac{(\epsilon_s + \epsilon_{fake})(N^m + N^t) - 2(N^t + \epsilon_s\epsilon_{fake}N^l)}{(\epsilon_s - \epsilon_{fake})^2}, \quad (34)$$
$$N_{QCD}^l = \frac{N^t - \epsilon_s(N^m + N^t - \epsilon_s N^l)}{(\epsilon_s - \epsilon_{fake})^2}. \quad (35)$$

6.1.1 Matrix method for different flavor final state leptons

Among the various conditions allowing the factorization in eq. (24) to (26), there is the assumption that the two leptons are of the same flavor. A different approach can be used in order to write a system of equations for the case of different flavor final state leptons. In such an approach the number of events containing an electron loosly/tightly selected and a muon loosly/tightly selected $N^{e_{l/t}\mu_{l/t}}$ can be expressed in terms of the number of events containing a real/fake electron and a real/fake muon $N^{e_{T/F}\mu_{T/F}}$:

$$N^{e_l\mu_l} = N^{e_F\mu_F} + N^{e_T\mu_F} + N^{e_F\mu_T} + N^{e_T\mu_T}, \quad (36)$$
$$N^{e_l\mu_t} = \epsilon_f^\mu N^{e_F\mu_F} + \epsilon_f^\mu N^{e_T\mu_F} + \epsilon_s^\mu N^{e_F\mu_T} + \epsilon_s^\mu N^{e_T\mu_T}, \quad (37)$$
$$N^{e_t\mu_l} = \epsilon_f^e N^{e_F\mu_F} + \epsilon_s^e N^{e_T\mu_F} + \epsilon_f^e N^{e_F\mu_T} + \epsilon_s^e N^{e_T\mu_T}, \quad (38)$$
$$N^{e_t\mu_t} = \epsilon_f^e\epsilon_f^\mu N^{e_F\mu_F} + \epsilon_s^e\epsilon_f^\mu N^{e_T\mu_F} + \epsilon_f^e\epsilon_s^\mu N^{e_F\mu_T} + \epsilon_s^e\epsilon_s^\mu N^{e_T\mu_T}. \quad (39)$$

where $\epsilon_s^{e/\mu}$ and $\epsilon_f^{e/\mu}$ are respectively the loose-to-tight signal efficiency and fake rate for an/a electron/muon. This system of equations can be solved analitically leading to the different components of the background. Namely: $N^{e_F\mu_F}$ is the number of events with two fake leptons, therefore the number of "QCD"-'like events, $N^{e_{T/F}\mu_{T/F}} + N^{e_{T/F}\mu_{T/F}}$ is the number of events with a real and a fake leptons (alternatevely an electron and a muon and viceversa), therefore the "W"-like component of the background, and finally $N^{e_T\mu_T}$ is the number of "Signal"-like events.

6.1.2 Contaminations

The fact that a loosly isolated lepton can possibly not pass the tight isolation selection, enables the possibility of contaminations among the various background estimates. A simple example which can help to understand how this can happen, is the one of a "Signal"-like event in which one of the two loosly isolated leptons is not passing the tight isolation criteria and a fake lepton is instead passing the tight isolation criteria. This kind of event will belong to the "W+jets"-like category even if it was produced thanks to a process meant to be in the "Signal"-like category.

In order to correct for this kind of contamination we need to estimate the probability for a certain background to contaminate another category. First of all we define the probability that a lepton passing the criteria of loose isolation does not pass the tight isolation one. This is simply given by:

$$\overline{\epsilon_s} = 1 - \epsilon_s. \tag{40}$$

Analogously, the probability that a fake lepton passing the criteria of loose isolation does not pass the tight isolation one, is given by:

$$\overline{\epsilon_f} = 1 - \epsilon_f. \tag{41}$$

Let us now split the sample of loose "Signal"-like events in its various components:

$$N_S^l = N_{TT}^{tt} + N_{TTF}^{t\bar{t}t} + N_{TTF}^{t\bar{t}\bar{t}} + N_{TTFF}^{\bar{t}tt} + N_{TTFF}^{\bar{t}t\bar{t}} + N_{TTFF}^{\bar{t}\bar{t}\bar{t}}. \tag{42}$$

where the index t ($\bar{t}$) indicates a lepton passing (not-passing) the tight isolation and T (F) indicates that the lepton is True (False). It is straightforward to prove that all the components of the loose "Signal"-like sample have been written down, by summing up their expression:

$$\begin{aligned}
N_{TT}^{tt} &= N_S^l \epsilon_s^2 = N_S^t & (43)\\
N_{TTF}^{t\bar{t}t} &= N_S^l (2\overline{\epsilon_s} - 2\overline{\epsilon_s}^2)\epsilon_f & (44)\\
N_{TTF}^{t\bar{t}\bar{t}} &= N_S^l (2\overline{\epsilon_s} - 2\overline{\epsilon_s}^2)\overline{\epsilon_f} & (45)\\
N_{TTFF}^{\bar{t}tt} &= N_S^l \overline{\epsilon_s}^2 \epsilon_f^2 & (46)\\
N_{TTFF}^{\bar{t}t\bar{t}} &= N_S^l \overline{\epsilon_s}^2 (2\overline{\epsilon_f} - 2\overline{\epsilon_f}^2) & (47)\\
N_{TTFF}^{\bar{t}\bar{t}\bar{t}} &= N_S^l \overline{\epsilon_s}^2 \overline{\epsilon_f}^2 & (48)
\end{aligned}$$

Among these various components, the number of events selected by the tight isolation cuts are those having two leptons (True or False) passing the tight selection. In particular, $N_{TTF}^{t\bar{t}t}$ is the number of events assigned by the Matrix Method to the "W+jets"-like category (having two leptons among three passing the tight selection, one of which being False and the other being True) and $N_{TTFF}^{\bar{t}tt}$ is the number of events assigned to the "QCD"-like category (having two leptons among four passing the tight selection, both being False). These events must be re-assigned to the "Signal"-like category:

$$N_S^{t,COR} = N_S^t + N_{TTF}^{t\bar{t}tt} + N_{TTFF}^{\bar{t}ttt}. \quad (49)$$

Let us now split the sample of loose "W+jets"-like events in its various components:

$$N_W^l \epsilon_f = N_{TF}^{tt} + N_{TFF}^{\bar{t}tt} + N_{TFF}^{t\bar{t}\bar{t}}. \quad (50)$$

It is easy to prove that all the components of the loose "W+jets"-like sample have been written down, by summing up their expression:

$$N_{TF}^{tt} = (N_W^l \epsilon_f)\epsilon_s = N_W^t \quad (51)$$
$$N_{TFF}^{\bar{t}tt} = (N_W^l \epsilon_f)\overline{\epsilon_s}\epsilon_f \quad (52)$$
$$N_{TFF}^{\bar{t}t\bar{t}} = (N_W^l \epsilon_f)\overline{\epsilon_s \epsilon_f} \quad (53)$$
$$(54)$$

Among these various components, the events being selected by the analysis selection, are those having two leptons (True or False) passing the tight selection.

In particular, $N_{TFF}^{\bar{t}tt}$ is the number of events assigned by the Matrix Method to the "QCD"-like category. These events must be re-assigned to the "W+jets"-like category:

$$N_W^{t,COR} = N_W^t + N_{TFF}^{\bar{t}tt} - N_{TTF}^{t\bar{t}tt}. \quad (55)$$

As you can notice, the events previously re-assigned to the "Signal"-like category have been subtracted from the "W+jets"-like category in order to keep the total number of events the same as before corrections.

Finally, let us correct the "QCD"-like sample:

$$N_{QCD}^{t,COR} = N_{QCD}^t - N_{TFF}^{\bar{t}tt} - N_{TTFF}^{\bar{t}\bar{t}tt}. \quad (56)$$

Alsoe in this case, the events re-assigned to the "W+jets"-like and "Signal"-like categories have been finally subtracted form the "QCD"-like category.

These corrections are applied at the level of the tight selection.

For the sake of compliteness, we give here also the formulas related to the generalization to the different flavor lepton channel:

$$\begin{aligned} N_S^l &= N_{T(e)T(\mu)}^{tt} + N_{T(e)T(\mu)F(\mu)}^{t\bar{t}tt} + N_{T(\mu)T(e)F(e)}^{t\bar{t}tt} + N_{T(e)T(\mu)F(\mu)}^{t\bar{t}\bar{t}t} + N_{T(\mu)T(e)F(e)}^{t\bar{t}\bar{t}t} \quad (57)\\ &+ N_{T(e)T(\mu)F(e)F(\mu)}^{\bar{t}\bar{t}tt} + N_{T(e)T(\mu)F(e)F(\mu)}^{\bar{t}t\bar{t}t} + N_{T(e)T(\mu)F(\mu)F(e)}^{\bar{t}\bar{t}t\bar{t}} + N_{T(e)T(\mu)F(e)F(\mu)}^{\bar{t}\bar{t}\bar{t}t} \\ N_{W_{e\mu}^{TF}}^l \epsilon_f^\mu &= N_{T(e)F(\mu)}^{tt} + N_{T(e)F(\mu)F(e)}^{\bar{t}tt} + N_{T(e)F(\mu)F(e)}^{\bar{t}t\bar{t}} \quad (58)\\ N_{W_{e\mu}^{FT}}^l \epsilon_f^e &= N_{T(\mu)F(e)}^{tt} + N_{T(\mu)F(e)F(\mu)}^{\bar{t}tt} + N_{T(\mu)F(e)F(\mu)}^{\bar{t}t\bar{t}} \quad (59) \end{aligned}$$

The expression of the various components are given by:

$$N^{tt}_{T(e)T(\mu)} = N^{l}_{S}\epsilon^{e}_{s}\epsilon^{\mu}_{s} \quad (60)$$

$$N^{t\bar{t}t}_{T(e)T(\mu)F(\mu)} = N^{l}_{S}\epsilon^{e}_{s}\overline{\epsilon^{\mu}_{s}}\epsilon^{\mu}_{f} \quad (61)$$

$$N^{t\bar{t}t}_{T(\mu)T(e)F(e)} = N^{l}_{S}\epsilon^{\mu}_{s}\overline{\epsilon^{e}_{s}}\epsilon^{e}_{f} \quad (62)$$

$$N^{t\bar{t}\bar{t}}_{T(e)T(\mu)F(\mu)} = N^{l}_{S}\epsilon^{e}_{s}\overline{\epsilon^{\mu}_{s}}\overline{\epsilon^{\mu}_{f}} \quad (63)$$

$$N^{t\bar{t}\bar{t}}_{T(\mu)T(e)F(e)} = N^{l}_{S}\epsilon^{\mu}_{s}\overline{\epsilon^{e}_{s}}\overline{\epsilon^{e}_{f}} \quad (64)$$

$$N^{\bar{t}\bar{t}tt}_{T(e)T(\mu)F(e)F(\mu)} = N^{l}_{S}\overline{\epsilon^{e}_{s}}\overline{\epsilon^{\mu}_{s}}\epsilon^{e}_{f}\epsilon^{\mu}_{f} \quad (65)$$

$$N^{\bar{t}\bar{t}t\bar{t}}_{T(e)T(\mu)F(e)F(\mu)} = N^{l}_{S}\overline{\epsilon^{e}_{s}}\overline{\epsilon^{\mu}_{s}}\epsilon^{e}_{f}\overline{\epsilon^{\mu}_{f}} \quad (66)$$

$$N^{\bar{t}\bar{t}t\bar{t}}_{T(e)T(\mu)F(\mu)F(e)} = N^{l}_{S}\overline{\epsilon^{e}_{s}}\overline{\epsilon^{\mu}_{s}}\epsilon^{\mu}_{f}\overline{\epsilon^{e}_{f}} \quad (67)$$

$$N^{\bar{t}\bar{t}\bar{t}\bar{t}}_{T(e)T(\mu)F(e)F(\mu)} = N^{l}_{S}\overline{\epsilon^{e}_{s}}\overline{\epsilon^{\mu}_{s}}\overline{\epsilon^{e}_{f}}\overline{\epsilon^{\mu}_{f}} \quad (68)$$

$$N^{tt}_{T(e)F(\mu)} = (N^{l}_{W^{TF}_{e\mu}}\epsilon^{\mu}_{f})\epsilon^{e}_{s} \quad (69)$$

$$N^{\bar{t}tt}_{T(e)F(\mu)F(e)} = (N^{l}_{W^{TF}_{e\mu}}\epsilon^{\mu}_{f})\overline{\epsilon^{e}_{s}}\epsilon^{e}_{f} \quad (70)$$

$$N^{\bar{t}t\bar{t}}_{T(e)F(\mu)F(e)} = (N^{l}_{W^{TF}_{e\mu}}\epsilon^{\mu}_{f})\overline{\epsilon^{e}_{s}}\overline{\epsilon^{e}_{f}} \quad (71)$$

$$N^{tt}_{T(\mu)F(e)} = (N^{l}_{W^{FT}_{e\mu}}\epsilon^{e}_{f})\epsilon^{\mu}_{s} \quad (72)$$

$$N^{\bar{t}tt}_{T(\mu)F(e)F(\mu)} = (N^{l}_{W^{FT}_{e\mu}}\epsilon^{e}_{f})\overline{\epsilon^{\mu}_{s}}\epsilon^{\mu}_{f} \quad (73)$$

$$N^{\bar{t}t\bar{t}}_{T(\mu)F(e)F(\mu)} = (N^{l}_{W^{FT}_{e\mu}}\epsilon^{e}_{f})\overline{\epsilon^{\mu}_{s}}\overline{\epsilon^{\mu}_{f}} \quad (74)$$

Therefore the formulas for corrections are the followings:

$$N^{t,COR}_{S} = N^{t}_{S} + N^{t\bar{t}t}_{T(e)T(\mu)F(\mu)} + N^{t\bar{t}t}_{T(\mu)T(e)F(e)} + N^{\bar{t}\bar{t}tt}_{T(e)T(\mu)F(e)F(\mu)} \quad (75)$$

$$N^{t,COR}_{W^{TF}_{e\mu}} = N^{t}_{W^{TF}_{e\mu}} - N^{t\bar{t}t}_{T(e)T(\mu)F(\mu)} + N^{\bar{t}tt}_{T(e)F(\mu)F(e)} \quad (76)$$

$$N^{t,COR}_{W^{FT}_{e\mu}} = N^{t}_{W^{FT}_{e\mu}} - N^{t\bar{t}t}_{T(\mu)T(e)F(e)} + N^{\bar{t}tt}_{T(\mu)F(e)F(\mu)} \quad (77)$$

$$N^{t,COR}_{QCD} = N^{t}_{QCD} - N^{\bar{t}\bar{t}tt}_{T(e)T(\mu)F(e)F(\mu)} - N^{\bar{t}tt}_{T(e)F(\mu)F(e)} - N^{\bar{t}tt}_{T(\mu)F(e)F(\mu)} \quad (78)$$

6.1.3 MC-driven and DATA-driven isolation efficiencies and fake rates

The MC-driven isolation efficiencies and fake rates are estimated using all available MC samples by requiring at generator level the presence of two real leptons or one real and one fake lepton. Both, signal efficiencies and fake rates, are computed taking into account the number of events corresponding to the loose and tight isolation selections.

In the first case we obtain the $\epsilon^{l\to t}_{S}$ which is the square of ϵ_s. In the second case we obtain $\epsilon^{l\to t}_{W}$ which can be devide by ϵ_s to obtain ϵ_{fake}.

Values of efficiencies and fake rates are used to feed the Matrix Method solution of the system for the closure test (see next section) as function of jet multiplicty.

The DATA-driven Signal Efficiencies are estimated using a Tag and Probe approach on the "DataEG" and "DataMu" samples, while the fake rates are estimated by enanching the QCD contribution in "Jet"-triggered sample. The selection used to enanch the presence of the QCD events are: MET $<$ 20 GeV, MT(lepton and MET) $<$ 20 GeV and presence of only one lepton. The systematic error on the DATA-driven efficiencies is taken conservatively as 50% of the difference between DATA and MC.

Both, signal efficiencies and fake rates, are computed taking into account the number of leptons corresponding to the loose and tight isolation selections.

Values of isolation efficiencies and fake rates are used to feed the Matrix Method solution of the system to perform the estimate of backgrounds on DATA, as function of jet multiplicty.

6.1.4 Results on Data

In these section the number of estimated fake lepton backgrounds from DATA are given. This estimation was made of an integated luminosity of 2.3 fb^{-1} . **These results are used in the final cross-section measurement.**

The data-driven isolation efficiencies and fake rates are used for the data-driven background estimation, making these estimates entirely data-driven. The integral of values over the jet multiplicity bins together with uncertainty added in quadrature over all the bins is as follows: $N_W = 7.8 \pm 5.9$ and $N_{QCD} = 0.74 \pm 0.56$ for the ee channel, $N_W = 14.9 \pm 7.1$ and $N_{QCD} = 0.41 \pm 0.29$ for the $\mu\mu$ channel and $N_W = 63.8 \pm 16.8$ and $N_{QCD} = 21.1 \pm 10.0$ for the eμ channel.

Similarly, for the 1 b-tag event selection we have: $N_W = 1.8 \pm 4.8$ and $N_{QCD} = 0.58 \pm 0.50$ for the ee channel, $N_W = 9.8 \pm 5.6$ and $N_{QCD} = 0.16 \pm 0.15$ for the $\mu\mu$ channel and $N_W = 42.4 \pm 14.6$ and $N_{QCD} = 7.5 \pm 3.9$ for the eμ channel.

The results are summarized in Table 25 and Table 26.

selection	$e\mu$	ee	$\mu\mu$
met sel	63.8 ± 16.8	7.8 ± 5.9	14.9 ± 7.1
≥ 1 bjet	42.4 ± 14.6	1.8 ± 4.8	9.8 ± 5.6

Table 25: Estimate of the W+jet like background for the three channels at different selection steps.

selection	$e\mu$	ee	$\mu\mu$
met sel	21.1 ± 10.0	0.74 ± 0.56	0.41 ± 0.29
≥ 1 bjet	7.5 ± 3.9	0.58 ± 0.50	0.16 ± 0.15

Table 26: Estimate f the QCD like background for the three channels at different selection steps.

7 Cutflow and data/MC comparisons using scale factors

This section contains the cut flow results of the selection for $\mu\mu$, ee, and $e\mu$ applied to Monte-Carlo and to real data samples, modelling the btagging in the MC, including reweighting for trigger and lepton selection scale factors and by rescaling backgrounds using data driven estimates.

The data/MC comparisons plots are presented in Figs. 27 to 34.

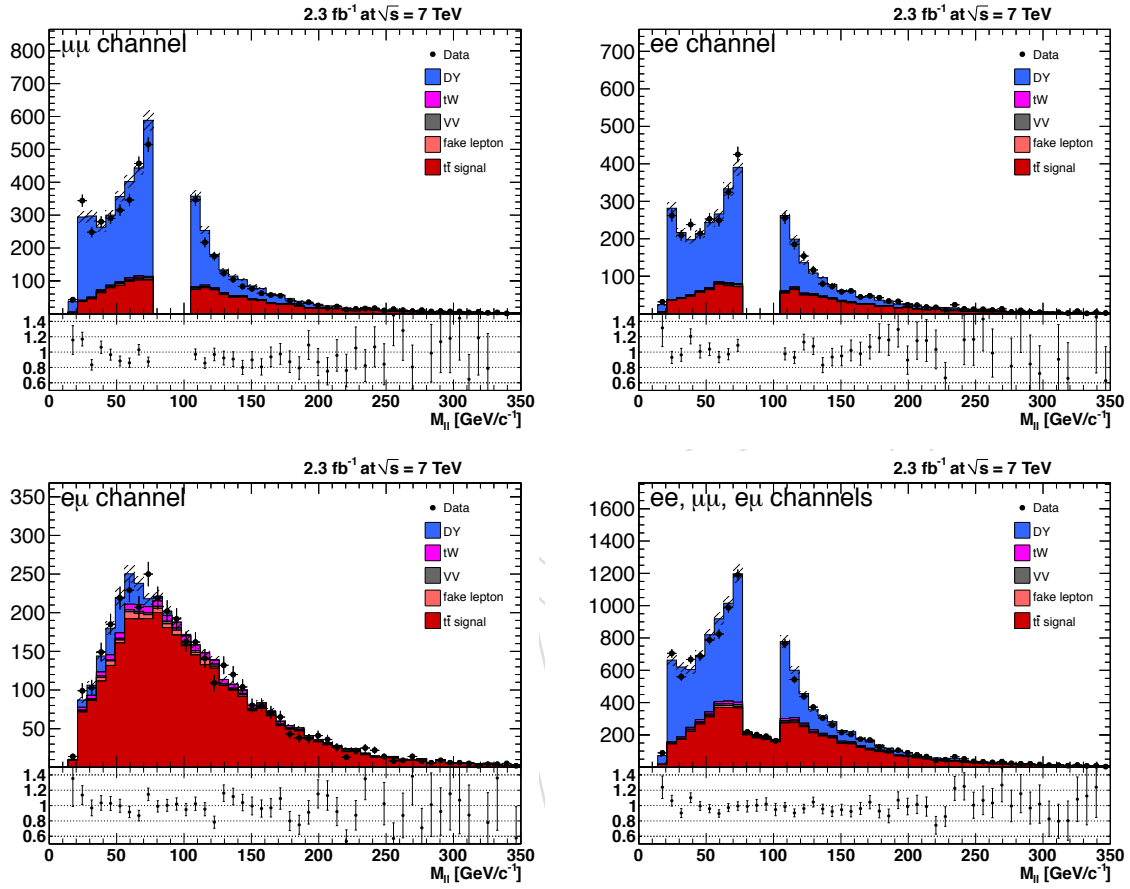

Figure 27: Distribution of the dilepton invariant mass in the three lepton-lepton channels, and for the overall combination after the jet multiplicity cut. Scale factors for trigger, lepton selection and data driven background estimate are used. The hatched area corresponds to the SF uncertainties summer with an uncertainty of 4.5% on the luminosity.

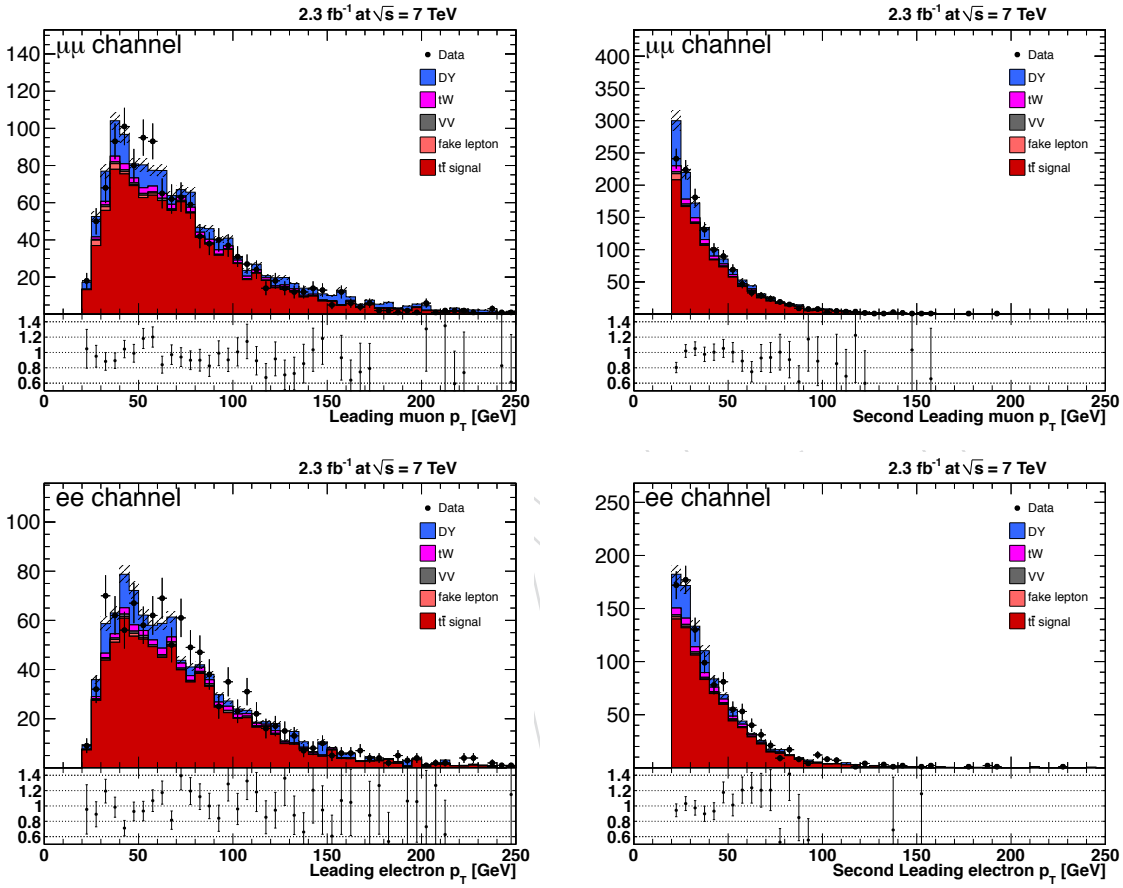

Figure 28: Distributions of the muon (upper plots) and electron (lower plots) p_T after cutting in the $\not\!\!E_T$ cut. Scale factors for trigger, lepton selection and data driven background estimate are used. The hatched area corresponds to the SF uncertainties summer with an uncertainty of 4.5% on the luminosity.

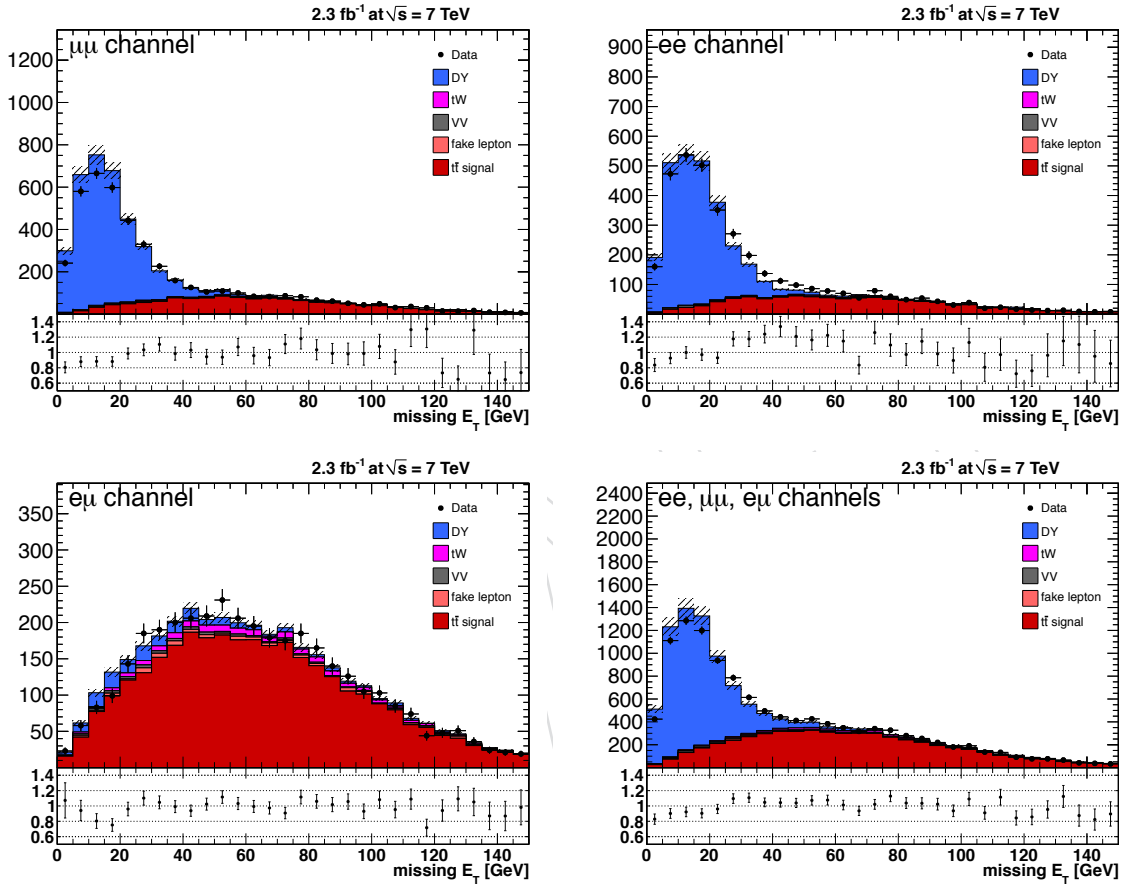

Figure 29: Missing E_T distributions in the three lepton-lepton channels, and for the overall combination after the jet multiplicity cut. Scale factors for trigger, lepton selection and data driven background estimate are used. The hatched area corresponds to the SF uncertainties summer with an uncertainty of 4.5% on the luminosity.

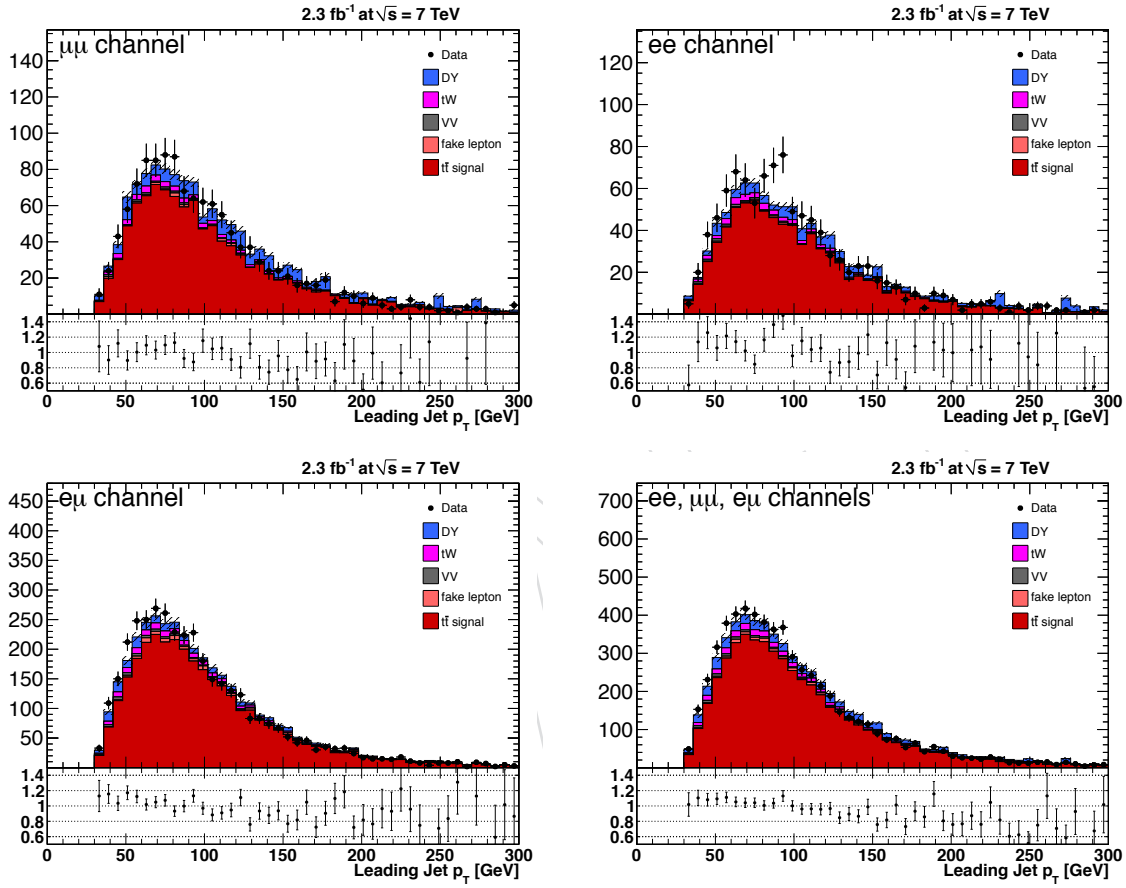

Figure 30: Jet p_T of the leading p_T jets in the three lepPtJet1ton-lepton channels, and for the overall combination after cutting on the missing E_T. Scale factors for trigger, lepton selection, $\not{E}_T$ and data driven background estimate are used. The hatched area corresponds to the SF uncertainties summer with an uncertainty of 4.5% on the luminosity.

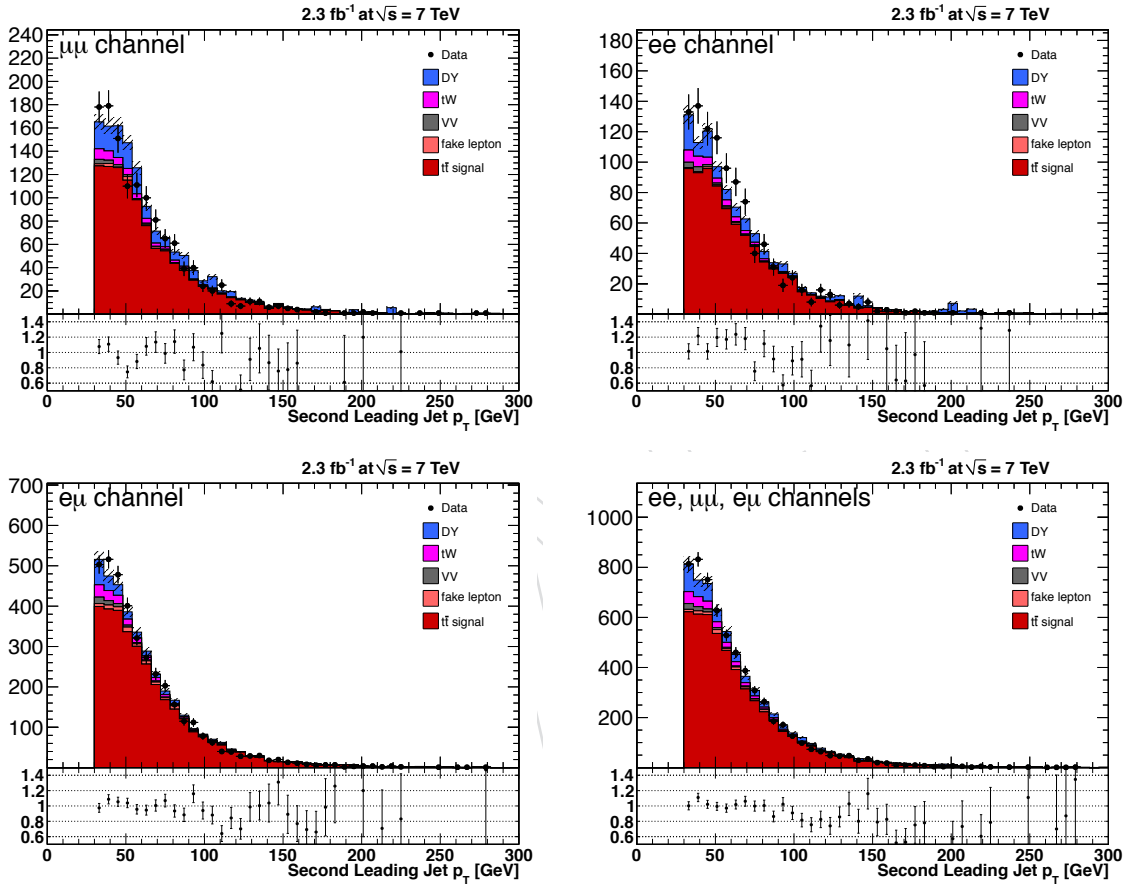

Figure 31: Jet p_T of the second leading p_T jets in the three lepPtJet1ton-lepton channels, and for the overall combination after cutting on the missing E_T. Scale factors for trigger, lepton selection, $\not{E}_T$ and data driven background estimate are used. The hatched area corresponds to the SF uncertainties summer with an uncertainty of 4.5% on the luminosity.

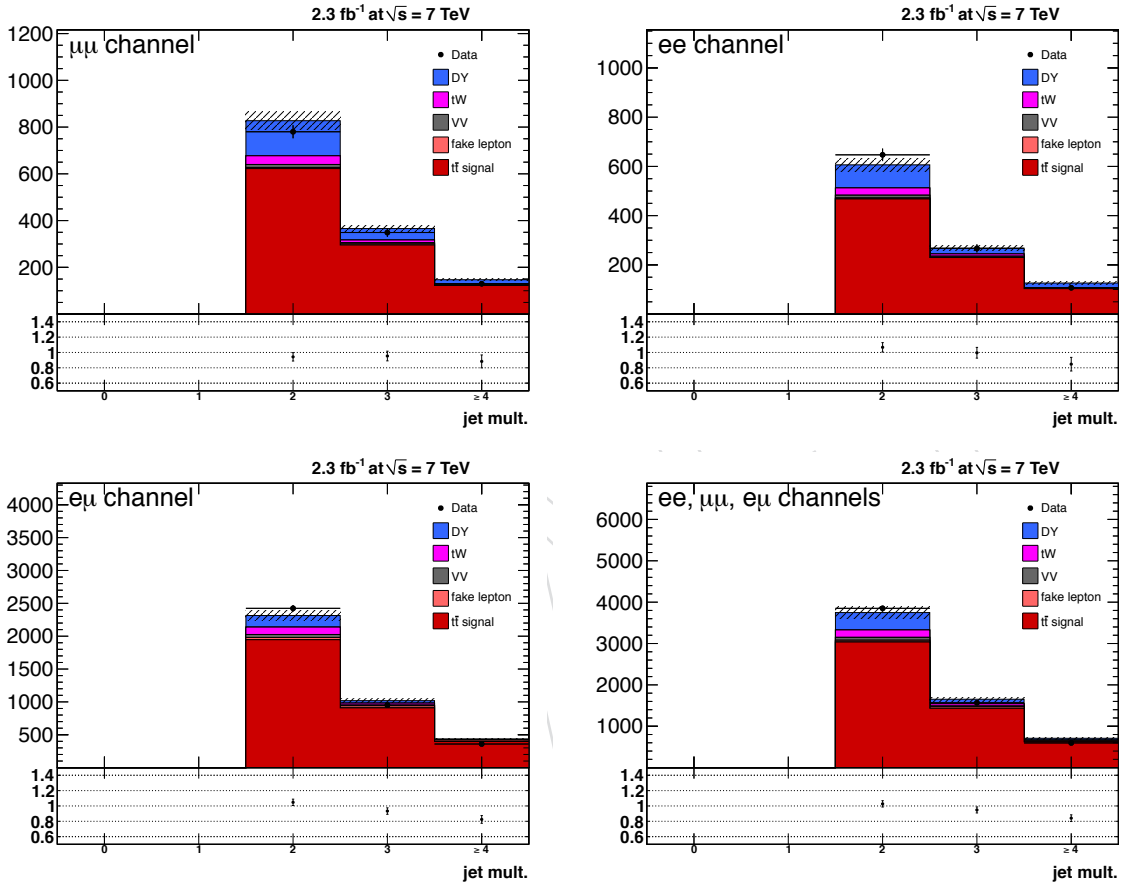

Figure 32: Jet multiplicity distributions in the three lepton-lepton channels, and for the overall combination after cutting on the missing E_T. Scale factors for trigger, lepton selection, $\not{E}_T$ and data driven background estimate are used. The hatched area corresponds to the SF uncertainties summer with an uncertainty of 4.5% on the luminosity.

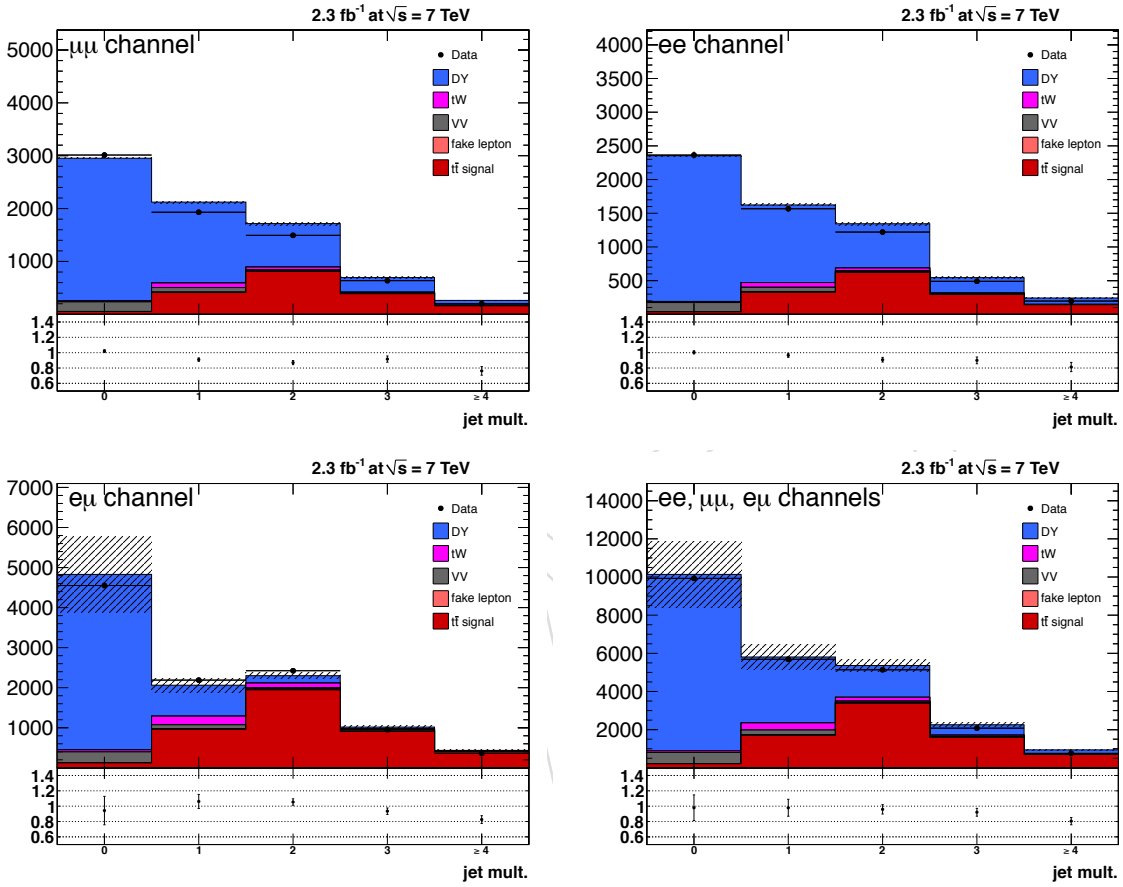

Figure 33: Jet multiplicity distributions in the three lepton-lepton channels, and for the overall combination after cutting in the missing E_T but without cutting on the jet multiplicity. Scale factors for trigger, lepton selection, $\not{E}_T$ and data driven background estimate are used. For DY, the same SF are used for the whole jet multiplicity range : 2.1 for ee, 1.9 for $\mu\mu$ and 1.3 for $e\mu$. The hatched area corresponds to the SF uncertainties summed with an uncertainty of 4.5% on the luminosity.

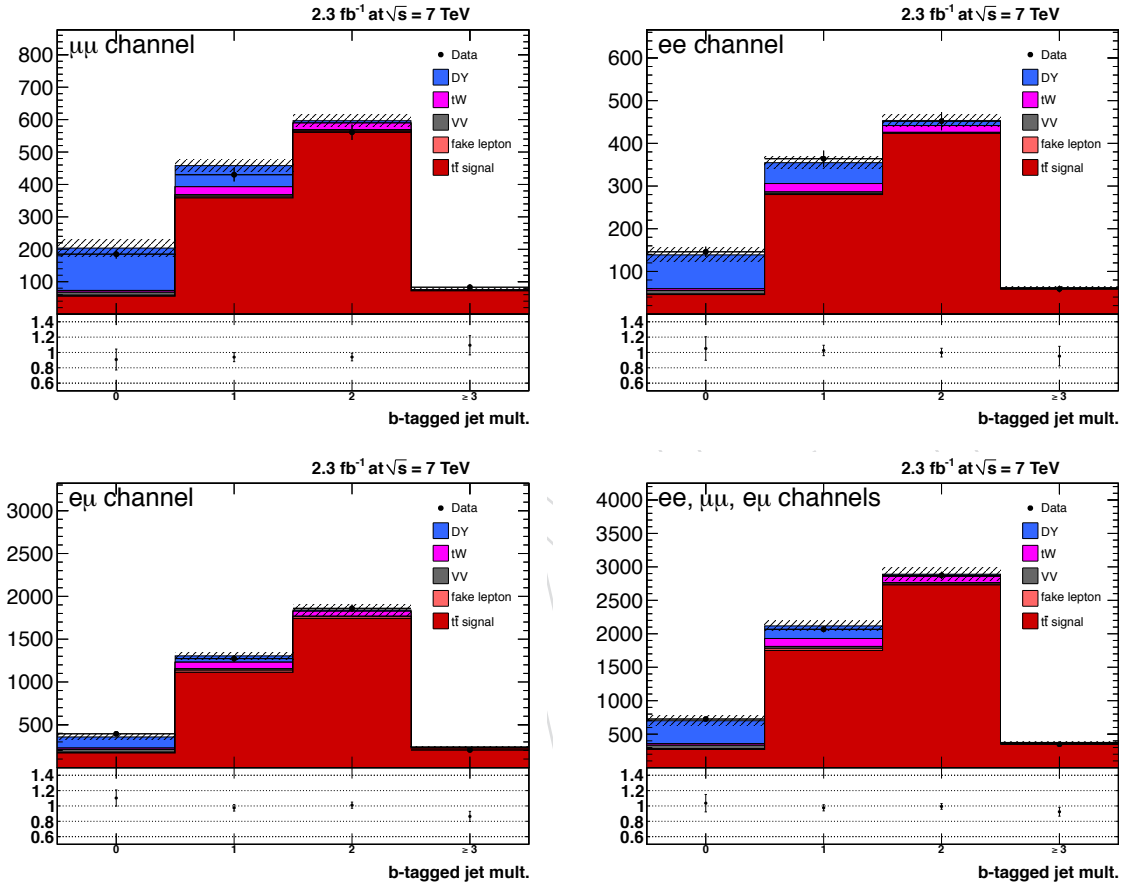

Figure 34: b-jet multiplicity distributions in the three lepton-lepton channels, and for the overall combination after cutting in the missing E_T. Scale factors for trigger, lepton selection, $\not{E}_T$ and data driven background estimate are used as well as the btag modelling in MC.The hatched area corresponds to the SF uncertainties summer with an uncertainty of 4.5% on the luminosity.

Cut	DATA	Sum MC	TT signal	Total Background	S/B
ll pair, M(ll)>20 GeV/c^2 and VxP	882420.0 ± 939.4	863899.9 ± 22680.2	2428.3 ± 67.3	861471.7 ± 22680.1	0.0
M(ll) $\notin$ [76,106]	83091.0 ± 288.3	78003.3 ± 2001.5	1845.8 ± 51.9	76157.4 ± 2000.9	0.0
$E_T(jet1,2) > 30$ GeV	4501.0 ± 67.1	4793.0 ± 208.2	1373.7 ± 39.4	3419.3 ± 204.5	0.4
$\not\!\!E_T > 40$ GeV	1259.0 ± 35.5	1340.4 ± 54.7	1040.5 ± 30.6	300.1 ± 45.3	3.5
btag ($\geq$1)	1074.0 ± 32.8	1135.5 ± 36.1	990.6 ± 29.1	144.9 ± 21.4	6.8
btag ($\geq$2)	644.0 ± 25.4	672.5 ± 20.2	636.2 ± 19.0	36.3 ± 7.0	17.5

Cut	Fake Rate Backg	SingleTop	DY	Diboson
ll pair, M(ll)>20 GeV/c^2 and VxP	47.4 ± 22.2	243.4 ± 7.1	859416.3 ± 22680.0	1764.6 ± 47.0
M(ll) $\notin$ [76,106]	29.5 ± 13.9	188.8 ± 5.7	75380.8 ± 2000.8	558.3 ± 15.4
$E_T(jet1,2) > 30$ GeV	25.5 ± 11.9	69.7 ± 2.5	3276.5 ± 204.1	47.6 ± 1.6
$\not\!\!E_T > 40$ GeV	15.3 ± 7.1	52.5 ± 2.0	216.7 ± 44.7	15.5 ± 0.8
btag ($\geq$1)	10.0 ± 5.5	47.0 ± 1.8	81.7 ± 20.6	6.1 ± 0.4
btag ($\geq$2)	4.7 ± 2.6	22.7 ± 1.0	7.9 ± 6.5	1.1 ± 0.1

Table 27: Dimuon cut flow, including SF for trigger efficiency, lepton and $\not\!\!E_T$selection. For the $t\bar{t}$, diboson and single top samples, the uncertainties account for the uncertainty on the luminosity and the various selection efficiencies. The DY backgrounds is estimated from data.

Cut	DATA	Sum MC	TT signal	Total Background	S/B
ll pair, M(ll)>20 GeV/c^2 and VxP	672870.0 $\pm$ 820.3	660243.6 $\pm$ 18171.5	1913.5 $\pm$ 56.0	658330.1 $\pm$ 18171.4	0.0
M(ll) $\notin$ [76,106]	63175.0 $\pm$ 251.3	57954.7 $\pm$ 1557.8	1461.3 $\pm$ 43.4	56493.4 $\pm$ 1557.2	0.0
$E_T(jet1,2) > 30$ GeV	3650.0 $\pm$ 60.4	3588.4 $\pm$ 162.7	1072.8 $\pm$ 32.6	2515.6 $\pm$ 159.4	0.4
$\not\!\!E_T > 40$ GeV	1021.0 $\pm$ 32.0	1000.7 $\pm$ 38.8	801.1 $\pm$ 25.1	199.7 $\pm$ 29.6	4.0
btag ($\geq$1)	875.0 $\pm$ 29.6	866.7 $\pm$ 28.8	759.3 $\pm$ 23.7	107.1 $\pm$ 16.3	7.1
btag ($\geq$2)	511.0 $\pm$ 22.6	515.0 $\pm$ 16.8	482.2 $\pm$ 15.4	32.8 $\pm$ 6.9	14.7

Cut	Fake Rate Backg	SingleTop	DY	Diboson
ll pair, M(ll)>20 GeV/c^2 and VxP	18.5 $\pm$ 12.9	194.1 $\pm$ 6.0	656748.0 $\pm$ 18171.4	1369.5 $\pm$ 38.3
M(ll) $\notin$ [76,106]	13.6 $\pm$ 9.5	149.7 $\pm$ 4.8	55896.0 $\pm$ 1557.1	434.2 $\pm$ 12.7
$E_T(jet1,2) > 30$ GeV	11.0 $\pm$ 7.7	54.1 $\pm$ 2.1	2409.0 $\pm$ 159.2	41.4 $\pm$ 1.5
$\not\!\!E_T > 40$ GeV	8.5 $\pm$ 5.9	41.5 $\pm$ 1.7	135.6 $\pm$ 28.9	14.1 $\pm$ 0.8
btag ($\geq$1)	2.4 $\pm$ 4.8	37.5 $\pm$ 1.6	61.5 $\pm$ 15.5	5.7 $\pm$ 0.4
btag ($\geq$2)	1.5 $\pm$ 2.7	17.5 $\pm$ 0.8	12.7 $\pm$ 6.3	1.1 $\pm$ 0.1

Table 28: Dielectron cut flow, including SF for trigger efficiency, lepton and $\not\!\!E_T$selection. For the $t\bar{t}$, diboson and single top samples, the uncertainties account for the uncertainty on the luminosity and the various selection efficiencies. The DY backgrounds is estimated from data.

Cut	DATA	Sum MC	TT signal	Total Background	S/B
ll pair, M(ll)>12 GeV/c^2 and VxP	10476.0 ± 102.4	9799.4 ± 148.0	4334.0 ± 104.7	5465.4 ± 104.7	0.8
-	10476.0 ± 102.4	9799.4 ± 148.0	4334.0 ± 104.7	5465.4 ± 104.7	0.8
$E_T(jet1,2) > 30$ GeV	3734.0 ± 61.1	3768.8 ± 94.3	3252.6 ± 79.5	515.3 ± 50.8	6.3
-	3734.0 ± 61.1	3768.8 ± 94.3	3252.6 ± 79.5	515.3 ± 50.8	6.3
btag (≥1)	3339.0 ± 57.8	3384.4 ± 77.9	3082.2 ± 75.3	301.4 ± 19.9	10.2
btag (≥2)	2066.0 ± 45.5	2079.4 ± 49.5	1969.4 ± 48.5	110.0 ± 9.5	17.9

Cut	Fake Rate Backg	SingleTop	DY	Diboson
ll pair, M(ll)>12 GeV/c^2 and VxP	104.0 ± 24.6	421.9 ± 10.7	3875.8 ± 97.8	1063.7 ± 25.7
-	104.0 ± 24.6	421.9 ± 10.7	3875.8 ± 97.8	1063.7 ± 25.7
$E_T(jet1,2) > 30$ GeV	84.9 ± 20.3	155.9 ± 4.4	219.8 ± 46.3	54.7 ± 1.9
-	84.9 ± 20.3	155.9 ± 4.4	219.8 ± 46.3	54.7 ± 1.9
btag (≥1)	49.9 ± 15.1	139.9 ± 4.0	89.2 ± 18.8	22.3 ± 0.8
btag (≥2)	26.2 ± 7.9	65.1 ± 2.0	14.9 ± 9.0	3.8 ± 0.2

Table 29: ElectronMuon cut flow, including SF for trigger efficiency, lepton and $\not\!\!E_T$selection. For the $t\bar{t}$, diboson and single top samples, the uncertainties account for the uncertainty on the luminosity and the various selection efficiencies. The DY backgrounds is estimated from data.The DY backgrounds is estimated from data.

8 Systematic uncertainties

We consider the following systematic uncertainties in this measurement: from uncertainties on the detector performance, from presence of extra proton-proton collisions (pileup), from variations in the signal acceptance due to uncertain knowledge in the signal production effects, from background estimates, and from the absolute normalisation of the sample integrated luminosity.

First of all, the uncertainty on the luminosity is taken as 2.2%. The other sources of systematics are presented below.

8.1 Systematics from Detector effects

8.1.1 Trigger and Lepton Selection Efficiencies

The trigger efficiencies and their scale factors and uncertainties are treated in Section 4.1. The per channel trigger scale factors and their error were found to be:

- ee **channel :** SF^{ee}_{trig} =0.962 $\pm$ 0.016
- $e\mu$ **channel :** $SF^{e\mu}_{trig}$ =1.008 $\pm$ 0.009
- $\mu\mu$ **channel :** $SF^{\mu\mu}_{trig}$ =0.977 $\pm$ 0.015

We measure the identification and isolation efficiencies in data using the tag and probe method that is described in detail in Section 4.2. The estimated uncertainty and the overall inclusive SF per channels were found to be :

- ee **channel :** $SF^{ee}_{Iso,ID} = 0.995 \pm 0.003$
- $e\mu$ **channel :** $SF^{e\mu}_{Iso,ID} = 0.994 \pm 0.005$
- $\mu\mu$ **channel :** $SF^{\mu\mu}_{Iso,ID} = 0.997 \pm 0.005$

Finally, the uncertainty coming from the lepton energy scale (LES) is estimated by comparing the dilepton invariant mass in Z+jets events and data after the trigger and the dilepton selections. After the selection, the dilepton invariant mass is fitted by a Gaussian distribution around the Z mass peak $80 < m_{ll} < 100\,\mathrm{GeV/c^2}$ as described in section 4.3. The LES uncertainties are estimated to be of 0.3% in the $\mu\mu$, $e\mu$ and ee channels.

Accounting for trigger, isolation, identification efficiencies, the final scale factors became:

- ee **channel :** $SF^{ee}_{Tri,Iso,ID} = 0.957 \pm 0.016$
- $e\mu$ **channel :** $SF^{e\mu}_{Tri,Iso,ID} = 1.002 \pm 0.010$
- $\mu\mu$ **channel :** $SF^{\mu\mu}_{Tri,Iso,ID} = 0.974 \pm 0.016$

The dielectron and dimuon scale factors are not correlated. The electron-muon scale factor uncertainty is correlated to the dielectron and the dimuon one: the correlation coefficients can be more simply established from an approximate relationship $\sqrt{SF^{ee} \cdot SF^{\mu\mu}} \approx SF^{e\mu}$. The correlation coefficient of the electron-muon scale factor is 0.80 relative to the dielectron, and also to the dimuon scale factors.

8.1.2 Jet energy scale

We follow the prescription described in [31] to apply the NEW recommended jet energy corrections. An uncertainty in the jet energy scale (JES) affects all jets p_T distributions which results as a possible bias in the selection. This could also have a potential impact on the selection of

the missing transverse energy ($\not\!\!E_T$) if type I $\not\!\!E_T$ is used, since it is affected by the jet corrections. However, we use the raw $\not\!\!E_T$ information in the current analysis, thus the uncertainty in the selection of the missing transverse energy is not obtained doing the propagation from the jet energy scale but from data as described in next section.

The uncertainties for the signal and for the simulated backgrounds single top, and diboson (VV) in the ee, $\mu\mu$, and $e\mu$ channels and the combined ones are presented in Table 30.

	$t\bar{t}$	Single Top	VV
ee	2.06	3.12	8.33
$\mu\mu$	1.88	2.70	11.54
eμ	1.73	3.67	5.95
all	1.72	3.33	7.02

Table 30: Jet energy scale uncertainties (in %) on the event yields of $t\bar{t}$ signal, single top, and diboson (VV) after required at least one b-tagged jet in the ee, $\mu\mu$, and $e\mu$ channels and the combined ones.

8.1.3 Jet energy resolution

It appears as if the jet energy resolution (JER) is about 10% worse in data compared to MC. An uncertainty in the jet energy resolution affects all jets p_T distributions which results as a possible bias in the selection. This could also have a potential impact on the selection of the missing transverse energy ($\not\!\!E_T$) if type I $\not\!\!E_T$ is used, since it is affected by the jet corrections. However, we use the raw $\not\!\!E_T$ information in the current analysis, thus the uncertainty in the selection of the missing transverse energy is not obtained doing the propagation from the jet energy resolution but from data as described in next section.

The uncertainties for the signal and for the simulated backgrounds single top, and diboson (VV) in the ee, $\mu\mu$, and $e\mu$ channels and the combined ones are presented in Table 31.

	$t\bar{t}$	Single Top	VV
ee	0.19	0.28	2.04
$\mu\mu$	0.35	0.45	2.00
eμ	0.28	0.30	1.79
all	0.28	0.14	1.50

Table 31: Jet energy resolution uncertainties (in %) on the event yields of $t\bar{t}$ signal, single top, and diboson (VV) after required at least one b-tagged jet in the ee, $\mu\mu$, and $e\mu$ channels and the combined ones.

8.1.4 B-tagging

The effect of the variations of SF_b (i.e. also SF_c) and SF_l have been estimated independently on the $t\bar{t}$ MC samples and on the simulated background samples (single top, and diboson).

Tables 32, 34, 36 give the systematics associated to SF_b, SF_c and SF_l varied separately for the signal and the simulated background in the ee, $\mu\mu$, and eμ channel respectively. To compute these systematics uncertainties the BTV-11-01 results were used [26]. These are the uncertainties propagated to the cross section measurement in v2 of the AN, kept in this version for comparison.

Tables 33, 35, 37 give the systematics associated to SF_b, SF_c and SF_l varied separately for the signal and the simulated background in the ee, $\mu\mu$, and eμ channel respectively following the new BTV POG recomendation [32, 33] published on Feb. 8th, 2012. SF_b is given now as a function of jet pT, from muon-jet data, SF_c remains equal to SF_b with twice the quoted uncertainty and SF_l as a function of jet pT for several eta bins. Average values of these quantities already show a improvement on the systematic uncertainties, it is huge of the SF_b, SF_c:

- SF_b = 0.984 $\pm$ 0.016 (BTV-11-01: SF_b = 1.00 $\pm$ 0.10)
- SF_c = 0.984 $\pm$ 0.032 (BTV-11-01: SF_c = 1.00 $\pm$ 0.20)
- SF_l = 1.08 $\pm$ 0.09 (BTV-11-01: SF_l = 1.07 $\pm$ 0.11)

The change in the SF_l does not induce any change in the event yields after the one b-tag requirement. The change in the SF_b induces very small changes well within the systematic uncertainty. These new systematic uncertainties are obtained comparing the nominal event yields after the one b-tag jet requirement when the new scale factos are used with the ones after taking into account the corresponding variation. These variations in percatange (33, 35, 37) are propagated to the cross section measurement in next section.

	$t\bar{t}$	Single Top	VV
uncer. from SF$_b$ $\geq$ 1-btag	3.89	5.38	0.00
uncer. from SF$_c$ $\geq$ 1-btag	0.06	0.00	2.08
uncer. from SF$_l$ $\geq$ 1-btag	0.18	0.85	6.25

Table 32: Uncertainties (in %) on the event yields of $t\bar{t}$ signal, single top, and diboson in the ee channel related to the uncertainty on the b-tagging SF_b, SF_c and the mistag rate SF_l. **Uncertainty in SF$_b$ of 10%**.

	$t\bar{t}$	Single Top	VV
uncer. from SF$_b$ $\geq$ 1-btag	0.68	1.14	0.00
uncer. from SF$_c$ $\geq$ 1-btag	0.07	0.00	0.00
uncer. from SF$_l$ $\geq$ 1-btag	0.26	0.57	4.08

Table 33: Uncertainties (in %) on the event yields of $t\bar{t}$ signal, single top, diboson and Drell-Yan di-tau events in the ee channel related to the uncertainty on the b-tagging SF_b, SF_c and the mistag rate SF_l. **Uncertainty in SF$_b$ of 2.%**.

	$t\bar{t}$	Single Top	VV
uncer. from SF$_b$ $\geq$ 1-btag	3.63	6.29	1.92
uncer. from SF$_c$ $\geq$ 1-btag	0.05	0.00	5.77
uncer. from SF$_l$ $\geq$ 1-btag	0.20	0.22	13.46

Table 34: Uncertainties (in %) on the event yields of $t\bar{t}$ signal, single top, and diboson in the $\mu\mu$ channel relat ed to the uncertainty on the b-tagging SF_b, SF_c and the mistag rate SF_l. **Uncertainty in SF$_b$ of 10%**.

The largest combined variations of both SF_b, SF_c and SF_l are used to estimate the systematic uncertainty in the cross section due to the b-tagging.

	$t\bar{t}$	Single Top	VV
uncer. from $SF_b \geq$ 1-btag	0.71	0.68	1.82
uncer. from $SF_c \geq$ 1-btag	0.05	0.00	3.64
uncer. from $SF_l \geq$ 1-btag	0.22	0.45	9.09

Table 35: Uncertainties (in %) on the event yields of $t\bar{t}$ signal, single top, diboson and Drell-Yan di-tau events in the $\mu\mu$ channel related to the uncertainty on the b-tagging SF_b, SF_c and the mistag rate SF_l. **Uncertainty in SF_b of 2.%**.

	$t\bar{t}$	Single Top	VV
uncer. from $SF_b \geq$ 1-btag	4.00	5.16	0.54
uncer. from $SF_c \geq$ 1-btag	0.05	0.15	2.70
uncer. from $SF_l \geq$ 1-btag	0.15	0.52	7.57

Table 36: Uncertainties (in %) on the event yields of $t\bar{t}$ signal, single top, and diboson in the eμ channel related to the uncertainty on the b-tagging SF_b, SF_c and the mistag rate SF_l. **Uncertainty in SF_b of 10%**.

8.1.5 Pileup

As discussed in Section 3.4 the official 3D pileup reweighting is used to properly re-weight Monte Carlo events: the data pileup distribution produced assuming a minimum bias cross section of 73.5 mb (measured at TOTEM [29]) is used in this case. In order to compute the uncertainty on the pileup reweighting two additional data pileup distributions are used, there a variation of $\pm 8\%$ in the number of interactions is applied. This variation is the official recommendation and should be plenty to cover the uncertainties due to pileup modelling.

The uncertainties for the signal and for the simulated backgrounds single top, and diboson (VV) in the ee, $\mu\mu$, and $e\mu$ channels and the combined ones due to the pileup are presented in Table 38.

8.1.6 Summary of detector uncertainties

Table 39 summarises the detector uncertainties on the $t\bar{t}$ signal in the ee, $\mu\mu$ and eμ channels.

8.2 Systematics from Theory

We derive estimates on theoretical systematic uncertainties from samples generated with different theory settings for a range of parameters. The effects from PDF uncertainties are estimated in situ in the signal sample (from [2]) . Table 41 presents the theoretical systematic uncertainties considered in this analysis.

8.2.1 MC generators

Dedicated Summer11 samples (described in Table 2) were produced with varying parameters to estimate the modelling uncertainties. The list of these parameters is the following:

- the factorisation scale Q^2,
- the Matrix-Element/Parton-Shower matching threshold,
- the top mass.

	$t\bar{t}$	Single Top	VV
uncer. from $SF_b \geq$ 1-btag	0.68	0.90	0.00
uncer. from $SF_c \geq$ 1-btag	0.04	0.23	2.66
uncer. from $SF_l \geq$ 1-btag	0.12	0.38	6.38

Table 37: Uncertainties (in %) on the event yields of $t\bar{t}$ signal, single top, diboson and Drell-Yan di-tau events in the eμ channel related to the uncertainty on the b-tagging SF_b, SF_c and the mistag rate SF_l. **Uncertainty in SF_b of 2.%**.

	$t\bar{t}$	Single Top	VV
ee	0.33	0.85	2.08
$\mu\mu$	0.83	0.90	1.92
eμ	0.37	0.82	0.00
all	0.46	0.75	0.35

Table 38: Pileup uncertainties (in %) on the event yields of $t\bar{t}$ signal, single top, and diboson (VV) after required at least one b-tagged jet in the ee, $\mu\mu$, and $e\mu$ channels and the combined ones.

First, the branching fraction of W $\rightarrow$ lν decays used in the Madgraph samples is set to its leading order value 1/9. The current world average is 0.1080$\pm$0.0009. We apply a scale factor equal to $(0.108 \times 9)^2$ with a fractional uncertainty of 1.7%, which is added to the total systematic uncertainty, the same in all final states.

The uncertainty related to the top mass was estimated using $t\bar{t}$ Madgraph samples generated with different top masses as shown in Table 40. After applying the event selection on these samples, the observed shift in events yield compared to the nominal value of the top mass (which is 172.5GeV/c^2), rescaled to a conservative uncertainty of 2 GeV/c^2 on the top mass [34], was taken as the systematic uncertainty. For the current value of the cross-section, the uncertainties obtained for the top masses 163.5 and 181.5 GeV/c^2 were used. The uncertainties taken from this energy window give together with the 6 GeV/c^2 window the lowest systematic uncertainties taking into account the sum up of the three channels, however the choosen window also gives the lowest value for the sum up of the ee and $\mu\mu$ channels. **Should we take a different approach to treat this uncertainty?**.

8.2.2 PDF uncertainties

From [35], [2].

The effect on the acceptance of the PDF uncertainty was assessed in the madgraph signal sample. This effect has been estimated in the previous analysis. We quote that result here for completeness.

The intrinsic uncertainty on the acceptance with the default CTEQ6.1 PDF was calculated using the weights method at the generator level with the following selection:

- two leptons (electron or muon)
  - within $|\eta| < 2.5$
  - $p_T > 20.0$ GeV
- two generator level jets
  - within $|\eta| < 2.5$

Source	ee	$\mu\mu$	eμ	measurement	Correlation type (%)
Lepton Efficiencies (Trigger, ID/Iso)	1.7	1.7	1.0	1.7/1.7/1.0	(ee-eμ: 80, $\mu\mu$-eμ: 80, ee-$\mu\mu$: 0)
Lepton Energy Scale (LES)	0.3	0.3	0.3	0.3	100
Jet Energy Scale (JES)	2.1	1.9	1.7	1.9	100
Jet Energy Resolution (JER)	0.2	0.3	0.3	0.3	100
MET Efficiency	1.6	1.2	1.1	1.3	100
B-tagging	0.7	0.7	0.7	0.7	100
B-tagging	3.9	3.6	4.0		100
Pileup	0.3	0.8	0.4	0.5	100
Total Systematic	3.1	3.3	2.5	3.0/3.0/2.7	
Total Systematic	5.4	4.8	4.8		

Table 39: Uncertainties (in %) due to different systematic effects on the $t\bar{t}$ signal in the ee, $\mu\mu$ and eμ channels. Type represents how the uncertainty is treated in the cut & count method, the correlation is indicated in percetange. The numbers in the column *measurement* are used to stay consistent with the systematic treatment done in the PLR method, where the systematic uncertainty has to be the same in the three channels if they are 100% correlated. Those numbers result from giving a weight of 1 to the systematic uncertainties in the ee and $\mu\mu$ channels and a weight of 2 to the systematic uncertainties in the eμ channel. Values obtained using SF_b, SF_c, SF_l with the corresponding uncertainties from BTV-11-001 [26].

	$\mu\mu$	ee	$\mu\mu$ + ee	$e\mu$	All
using 2 from 11-12 GeV/c^2	3.14	2.32	2.55	1.81	2.05
using 2 from 9 GeV/c^2	3.00	2.70	2.46	1.82	1.79
using 2 from 6 GeV/c^2	3.85	2.70	3.12	1.51	1.77
using 2 from 3 GeV/c^2	4.91	1.83	3.43	3.05	1.95

Table 40: Uncertainties related to the top mass (in %) on the event yields of $t\bar{t}$ signal in the three different channels. Different pairs of MC were compared to the nominal one: 161.5-184.5 GeV/c^2 (window 11-12 GeV), 163.5-181.5 GeV/c^2 (window 9 GeV), 166.5-178.5 GeV/c^2 (window 6 GeV), 169.5-175.5 GeV/c^2 (window 3 GeV), giving uncertainties per several GeV/c^2.

- $p_T > 30.0$ GeV
- dR to each lepton > 0.4

The relative uncertainty on the acceptance was found to be approximately 0.5%. Reweighting the central value of the acceptance to that predicted by the MSTW 2008 NLO (68% C.L.) and NNPDF_2.0_100 PDFs yielded a change of less than 0.1%. Reweighting using the CTEQ66 PDFs with maximal and minimal α_s values also yielded a change in acceptance of less than 0.1%. Due to the negligible variation in the acceptance when the PDF parameters were varied, we do not assign additional systematics.

8.2.3 Summary of theoretical uncertainties

Table 41 summarises the theoretical uncertainties.

8.3 Systematics from Backgrounds.

Uncertainties from data-driven background determination are presented in sections 5 and 6. The uncertainties on the remaining backgrounds are estimated through simulation. The uncertainties on the diboson (VV), and single top backgrounds arise from the same sources as for the

Source	ee	$\mu\mu$	ee + $\mu\mu$	eμ	measurement	Correlation type (%)
Branching Ratio	1.7	1.7	1.7	1.7	1.7	100
Event Q^2 scale	4.7	2.7	3.3	1.7	1.4	100
Matching	4.6	4.1	4.2	1.4	1.1	100
Top Mass (using 2 GeV/c^2)	2.7	3.0	2.5	1.8	1.8	100
PDF	0.1	0.2	0.3	0.1	0.4	100
Total Systematic	7.3	6.0	6.1	3.3	3.1	

Table 41: Uncertainties (in %) due to different systematic effects on the $t\bar{t}$ signal in the ee, $\mu\mu$ and eμ channels. Type represents how the uncertainty is treated in the cut & count method, the correlation is indicated in percetange. The numbers in the column *measurement* are used to stay consistent with the systematic treatment done in the PLR method, where the systematic uncertainty has to be the same in the three channels if they are 100% correlated. Those numbers are the systematic uncertainty that results from taking into account the number of events from the three channels, ee, $\mu\mu$ and eμ.

$t\bar{t}$ signal. In addition, there is an uncertainty on each of the background production cross sections of 30%. This uncertainty is conservative with respect to the uncertainties on the inclusive production rate, and is expected to cover the uncertainties on the rate of these backgrounds in the phase space of the event selections used in this analysis. Uncertainties from data-driven backgrounds are decorrelated between channels, the ones estimated through simulation are 100% correlated.

9 Cross-Section measurement

9.1 Counting method

The signal production cross section σ_{data} can be measured using the following equation:

$$\sigma_{data} = \sigma_{theory} \frac{N - B}{SF \cdot S_{exp}} = \sigma_{theory} \frac{S_{obs}}{SF \cdot S_{exp}}, \tag{79}$$

where $\sigma_{theory} = 164.\ pb$ is the cross section used to normalise the expected number of signal events in the simulation, S_{exp}. It corresponds to the measured cross section in the $t\bar{t}$ lepton+jets channel [36]. The estimate of observed signal events, S_{obs}, is derived from the number of observed events, N, and the number of background events, B. Differences between real data and expectations are absorbed into the scale factor SF. The scale factor accounts for differences in the expectation normalisation due to the integrated luminosity estimate, differences in event selection, as well as differences in theoretical modelling of the fraction of events passing event selections. Each difference corresponds to a separate scale factor SF_i, which contribute to the total as $SF = \Pi SF_i$.

The definition in Eq. 79 can be trivially converted to a more common definition in terms of the total fraction of produced $t\bar{t}$ events expected to pass selections (A) and the total integrated luminosity ($\mathcal{L}$):

$$\sigma_{data} = \frac{S_{obs}}{SF \cdot \mathcal{L} \cdot A}. \tag{80}$$

The measurement of σ_{data} has statistical and other uncertainties taken into account as follows. In Eq. 79 only S_{obs} and SF have an uncertainty, all other values are treated as precise. The

statistical uncertainty on σ_{data} arises only from N:

$$\delta_{stat}(\sigma_{data}) = \sigma_{data}\frac{\sqrt{N}}{S_{obs}}. \quad (81)$$

The systematic uncertainty is a combination of uncertainties on the remaining estimators.

In a simplified form (Gaussian distributions without correlations), the systematic uncertainty on the cross section is given by:

$$\delta_{syst}(\sigma_{data}) = \sigma_{data}\sqrt{\left(\frac{\delta(B)}{S_{obs}}\right)^2 + \delta(Su)^2}, \quad (82)$$

where $\delta(Su)$ is a combination of uncertainties excluding the uncertainty on luminosity that is quoted separately.

Signal and background contributions compared to the number of events observed in data passing full signal selection with at least one b-tagged jet required and the resulting cross section measurement in separate event selection channels is shown in Table 42.

Source	$\mu\mu$	ee	$e\mu$
Dilepton $t\bar{t}$	990.6±48.2	759.3±37.2	3082.2±142.4
VV	6.1±2.0	5.7±1.9	22.3±7.3
Single top - tW	47.0±14.4	37.5±11.5	139.9±42.8
Drell-Yan	81.7±20.6	61.5±15.5	89.2±18.8
Non-W/Z leptons	10.0±5.5	2.4±4.8	49.9±15.1
Total background	144.9±25.5	107.1±19.9	301.4±49.7
Data	1074	875	3339

Source	$\mu\mu$	ee	$e\mu$
Cross section, pb	$153.8 \pm 5.4 \pm 7.8 \pm 3.4$	$165.9 \pm 6.4 \pm 8.2 \pm 3.6$	$161.6 \pm 3.1 \pm 7.0 \pm 3.6$
Cross section, %	$100.0 \pm 3.5 \pm 5.0 \pm 2.2$	$100.0 \pm 3.9 \pm 5.0 \pm 2.2$	$100.0 \pm 1.9 \pm 4.3 \pm 2.2$

Table 42: Expected signal and background contributions compared to the number of events observed in data passing full signal selection with at least one b-tagged jet required, and the resulting cross section measurements per channel. Drell-Yan and non-W/Z leptons from data-driven methods. The errors quoted for signal and MC backgrounds correspond to statistical, systematic and luminosity uncertainties. The uncertainties on the cross section include statistical, systematic, and luminosity normalisation uncertainties.

Systematic uncertainties coming from the lepton selection (trigger, identification and isolation lepton efficiency, lepton energy scale), jet energy scale, jet energy resolution, $\not{E}_T$selection, b-tagging, pile-up, and theory are included in the signal and simulated backgrounds systematic errors, and then, propagated to the cross section measurement. An additional 30% uncertainty on the total predicted cross section is taken into account for the purely MC backgrounds. When asymmetric uncertainties are obtained, the maximum value is taken in order to stay conservative.

A combination measurement is obtained using the BLUE method [37]:

$$\sigma_{t\bar{t}} = 161.0 \pm 2.6\ (\text{(stat.), } 1.6\%) \pm 6.9\ (\text{(syst.), } 4.3\%) \pm 3.5\ (\mathcal{L}, 2.2\%)\ \text{pb}$$

The considered systematic uncertainties are the same in the three channels if they are 100% correlated, in order to stay consistent with the PLR method.

A break-down of the statistical and systematic uncertainties contributing to the combined measurement is given in Table 43.

Source	Cont. to the $\sigma_{t\bar{t}}$(pb)	Cont. to the $\sigma_{t\bar{t}}$(%)
VV	0.4	0.2
Single top - tW	2.3	1.4
Drell-Yan	1.0	0.6
Non-W/Z leptons	0.6	0.4
Lepton efficiencies	1.7	1.1
LES	0.5	0.3
JES	2.8	1.8
JER	0.5	0.3
MET	1.9	1.2
B-tagging	1.1	0.7
Pile-up	0.7	0.4
Branching ratio	2.7	1.7
Event Q^2 scale	2.3	1.4
Matching	1.8	1.1
Top quark mass	2.9	1.8
Total Systematic	6.9	4.3
Luminosity	3.5	2.2
Statistics	2.6	1.6

Table 43: Break-down of the statistical and systematic uncertainties contributing to the combined cross section measurement given inclusively and in percentage.

9.2 Profile Likelihood Ratio method

A Profile Likelihood Ratio (PLR) Method (put references here) is used to estimate the signal cross section $\sigma_{t\bar{t}}$ of the top pair production in an individual dilepton channel ee,$\mu\mu$ or $e\mu$ as well as for their combination. The purpose of the PLR method is to test a hypothesized value of $\sigma_{t\bar{t}}$ by means of the following ratio constructed with the likelihood function L_{sys}:

$$PLR(\sigma_{t\bar{t}}) = \frac{L_{sys}(\sigma_{t\bar{t}}, \{\hat{\hat{U}}_i\})}{L_{sys}(\hat{\sigma}_{t\bar{t}}, \{\hat{U}_i\})} \tag{83}$$

where $\{U_i\}$ represents a set of nuisance parameters describing systematical effects. In the numerator, $\{\hat{\hat{U}}_i\}$ denotes the conditional maximum likelihood (ML) estimates of $\{U_i\}$ holding $\sigma_{t\bar{t}}$ fixed (and consequently is a function of $\sigma_{t\bar{t}}$). The denominator is the maximal unconditional likelihood function, i.e. $\hat{\sigma}_{t\bar{t}}$ and $\{\hat{U}_i\}$ are their ML estimators.The presence of the nuisance parameters broadens the profile likelihood as a function of $\sigma_{t\bar{t}}$ relative to what one would have if their values were fixed. This reflects the loss of information about $\sigma_{t\bar{t}}$ due to the systematic uncertainties.

In this note, the three channels ee, $e\mu$ and $\mu\mu$ are considered. These channels are statistically independent as they use orthogonal samples as described in section 3. We consider a likelihood

function defined as a binned likelihood built from a 2 dimensional distribution in (jet multiplicity (Njets) , Bjet multiplicity (NBjets)) space. This 2D distribution is provided by the event selection before any B-tagging cuts for a jet multiplicity ≥ 2. An example of such distribution transformed into one dimension for better visibility is given in Figure 35.

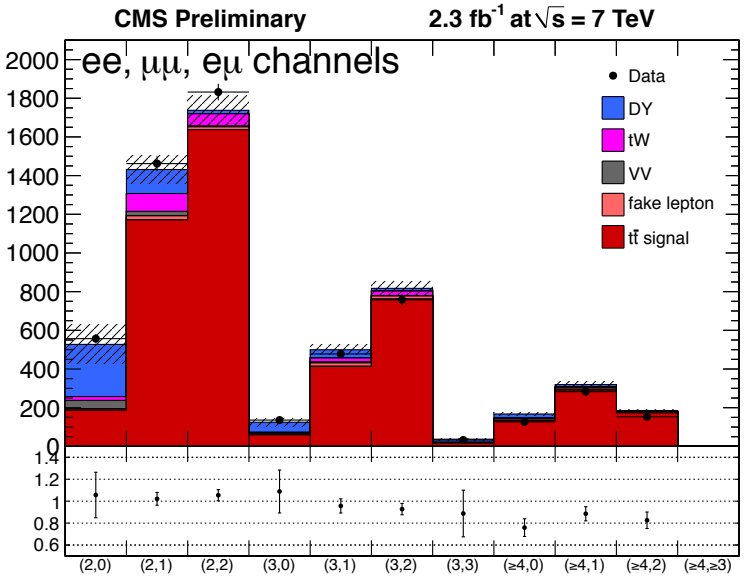

Figure 35: 2D (Njets,NBjets) distribution (transformed in a 1D view with X-axis representing (Njets,NBjets)) for Data and MC combining the 3 decay channels ee, $\mu\mu$ and $e\mu$. In the upper plot, error bars represent statistical uncertainty while in the lower plot, they include systematic uncertainties.

If no systematic uncertainty is considered and for a specific decay channel j, the bins being statistically independent, it can be written:

$$L_{stat}(\sigma_{t\bar{t}}) = \prod_{k\ bins} P(N^{obs}_{j,k}, \mu_{j,k}) = \prod_{k\ bins} \frac{\mu^{N^{obs}_{j,k}}_{j,k}}{N^{obs}_{j,k}!} e^{-\mu_{j,k}} \tag{84}$$

where $P(N^{obs}_{j,k}, \mu_{j,k})$ is the Poisson probability of expected $\mu_{j,k}$ signal-plus-background events in bin k:

$$\mu_{j,k} = N^{sig}_{j,k}(\sigma_{t\bar{t}}) + N^{bkg}_{j,k} \tag{85}$$

with $N^{sig}_{j}(\sigma_{t\bar{t}}) = \sum_k N^{sig}_{j,k}(\sigma_{t\bar{t}}) = \sigma_{t\bar{t}}\mathcal{L}\epsilon_j$

The number of background events $N^{bkg}_{j} = \sum_{k\ bins} N^{bkg}_{j,k}$ distributed in bins of the 2D (Njets,NBjets) templates is computed from three kind of processes:

1. the processes estimated by dedicated data-driven (DD) methods (QCD multi-jets, W+jets and DY - see sections 6, and 5),
2. the non-$t\bar{t}$ processes expected from the simulation (single-top and di-bosons) and
3. the contamination from the other $t\bar{t}$ decays which explicitly depends on the cross section $\sigma_{t\bar{t}}$.

928 The calculation of N_j^{bkg} is thus given by the following:

$$N_j^{bkg} = \sum_n N_n^{DD} + \sum_l N_l^{MC} + \sum_m N_m^{other\ t\bar{t}}(\sigma_j), \quad (86)$$

$$= \sum_n N_n^{DD} + \sum_l \sigma_l^{MC} BR_l^{MC} \mathcal{L}\epsilon_l^{MC} + \sum_m \sigma_{t\bar{t}} BR_m^{other\ t\bar{t}} \mathcal{L}\epsilon_m^{other\ t\bar{t}}. \quad (87)$$

929 The cross section $\sigma_{t\bar{t}}$ in each individual decay channel could be extracted by minimising the
930 negative log-likelihood function -$logL_{stat}(\sigma_{t\bar{t}})$. The statistical uncertainty on the cross section is
931 obtained by the usual procedure of varying the negative log-likelihood by half a unit above the
932 minimum.

933 In order to treat the systematic uncertainties coming from the detector knowledge, the theo-
934 retical calculations, the simulation or the estimation of the backgrounds, new parameters U_i
935 are introduced corresponding to the individual source of systematic uncertainty i. Additional
936 terms are then added in the definition of the likelihood with a model depending on the nature
937 of the systematics:
938 • The simplest model is corresponding to rate uncertainty which affects the normalisation of
939 the 2D template (signal and backgrounds) keeping its shape unaffected. In that case, the ML
940 function for a decay channel j can be extended as:

$$L_{sys}(\sigma_{t\bar{t}}, \{U_i\}) = P(N_j^{obs}, \mu_j(\{U_i\})) = \prod_{k\ bins} \frac{\mu_{j,k}(\{U_i\})^{N_{j,k}^{obs}}}{N_{j,k}^{obs}!} e^{-\mu_{j,k}(\{U_i\})} \times \prod_i Gauss(U_i, 0, 1). \quad (88)$$

941 where $Gauss(U_i, 0, 1))$ is a Gaussian distribution centered on 0 with width 1.

The number of expected events μ_j is now multiplicatively dependant on the uncertainty parameters U_i according to

$$\mu_{j,k}(\{U_i\}) = \mu_{j,k}(1 + \prod_i U_i \sigma_{U_i})$$

with σ_{U_i} the input uncertainty for nuisance parameter i.
The corresponding variations (reflecting efficiency variations) are expected to be uncorrelated within a decay channel. Background rate uncertainties, trigger effects , lepton efficiencies as well as theoretical uncertainties are treated on this way.
• It is possible that rate uncertainty doesn't suffice to describe the effect of the systematic uncertainty on the expected distribution in an observable because the whole template could be affected bin by bin (correlation effects). In order to include such source of systematics i, a morphing of the distribution is performed by means of an interpolation between the original 2D template (without uncertainty) and templates affected by ± 1 sigma deviations. Different schemes of interpolation can be considered, we used a linear one : the number of events passing the selection is obtained by varying the uncertainty parameter U_i by one standard deviation up ($+1\sigma$) and down (-1σ). The linear approximation is made to describe the variation of the number of selected events as function of the systematic parameters:

$$N^l(\{U_i\}) = N_{nom}^l \times \prod_i F^l(U_i) \quad (89)$$

942 where N_{nom}^l is the nominal number of events for the process l with all parameters U_i egal to
943 0. The correction factors $F(U_i)^l$ for each process l take the following values, depending on the

sign of U_i:

$$F^l(U_i) = (\frac{N^l_{+1\sigma}}{N^l_{nom}} - 1)U_i + 1 \text{ if } U_i \geq 0 \quad (90)$$

$$F^l(U_i) = (-\frac{N^l_{-1\sigma}}{N^l_{nom}} + 1)U_i + 1 \text{ if } U_i < 0, \quad (91)$$

where $N^l_{U_i^{nom}}$ and $N^l_{\pm 1\sigma}$ are respectively the number of selected events obtained in the nominal case, and when the source of systematics is varied by $\pm 1\sigma$. In that case, a reasonable prior distribution for U_i is a normal distribution with mean 0 and width 1.
An exponential interpolation has also been tested with a morphing on a distribution $T_{j,m}$ for a process m and a decay channel j according to:

$$T_{j,m}(U_i) = T_{j,m}\left(\frac{T(U_{\pm 1\sigma})}{T_{j,m}}\right)^{|U_i|}$$

with $T(U_{\pm 1\sigma})$ being the modified templates obtained for $U_i = \pm 1$ of the systematics i. The different interpolation approaches lead to very similar results.
For a given channel j, it is assumed that there are no correlations between the different source of systematics. Moreover the uncertainties are considered as Gaussian and in that case, the likelihood can be rewritten as:

$$L_{sys}(\sigma_{tt}, \{U_i\}) = \prod_{kbins} \frac{\mu_{j,k}^{N^{obs}_{j,k}}}{N^{obs}_{j,k}!} e^{-\mu_{j,k}(\{U_i\})} \times \prod_i Gauss(U_i, 0, 1). \quad (92)$$

This model allows to treat correlation effects between bins. Systematics considered with this rate and shape template morphing are JES, JER and B-tagging uncertainties.
• Special case for B-tagging uncertainties:
In that particular case, uncertainties are coming from B-tagging Scale Factor for heavy and light flavour, SFb and SFl respectively. These global Scale Factors are provided by the BTV-POG and correspond to the ratio of the Btagging efficiency determined with data to the MC Btagging efficiency. Because the 2D templates used in the PLR correspond to the selection without B-tagging cut, the B-tagging uncertainty is affecting only the template shape, the total number of B-tagged jets remaining unchanged. This shape morphing is analytically computed by determining the combinatorial probability of tagging NBjets in an event with Njets, knowing the flavour of the jets. As a consequence, the SFb and SFl dependencies for each k bin of the (Njets,NBjets) space are individually introduced by means of fitted correction functions $F^l(U_{SFb,SFl})$ for a process l according to :

$$N^l_k(U_{SFb,SFl}) = N^l_k \times F^l(U_{SFb,SFl}) \quad (93)$$

By construction, the normalisation is unchanged and bin migration is taken into account. An example of such correction functions is illustrated by Figure 36. For signal, the fitted function are parabolic while a linear dependence is used for background.

Therefore bin by bin correlation effects are naturally included into the model.

The minimisation of the negative log-likelihood with respect to $(\sigma_{t\bar{t}}, \{U_i\})$ leads to the determination of the Maximum Likelihood Estimates $(\hat{\sigma_{tt}}, \{\hat{U}_i\})$ of all the parameters.
The errors are then extracted using the Profile Likelihood Ratio (PLR) defined as by equation

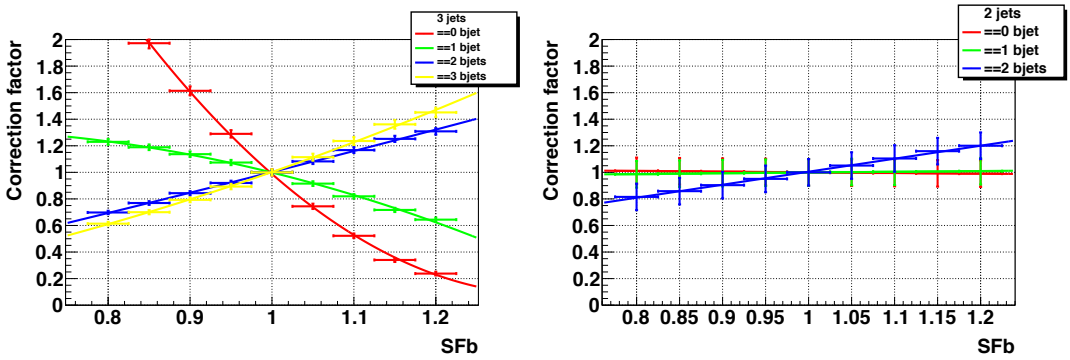

Figure 36: Examples of corrections functions for SFb applied for a (Njets,NBjets) bin. Right: for signal with 3 jets. Left: for DY background with 2 jets.

83: The PLR curve is used to derive the interval error at $\pm 1\sigma$ by changing $min(-logL_{sys})$ to $min(-logL_{sys}) + 0.5$ in order to get the Gaussian equivalence at 68% CL. The returned error is then the combination of the statistical error plus the one related to the considered systematic uncertainty. The minimisation of the negative log-likelihood is performed using the class TMinuit from ROOT with the use of the algorithm MINOS.
The technique described above for a given decay channel can be extended for the channel combination As the decay channels are statistically independent, the full likelihood function is expressed as the product of the individual likelihood functions :

$$L_{ch} = \prod_{ch} L_{ch}(\sigma_{tt}, \{N_{ch}^{obs}, \{U_i\}) \tag{94}$$

and the corresponding PLR function is derived from equation 83. Several U_i are shared between the channels (for example the Btagging scale factor), which explicitly introduces correlations between the channels.

The results obtained with the profile likelihood ratio method with 2.3 fb^{-1} of data are presented in the table 45. The systematic uncertainties include the uncertainties from the backgrounds estimation (from Data-Driven methods or MC expectations), from the lepton efficiencies, from the trigger efficiencies, from the jet energy scale and jet energy resolution, from B-tagging scale factors, from lepton energy scale and from theoretical uncertainties, see table 45.

9.2.1 Additional test for PLR

Two sorts of additional tests have been performed to test the PLR approach with MC:
• More than 4000 pseudo experiences have been realized mimicking the individual measurement with data. Due to the high number of nuisance parameters and the rather long time to do the test, it has been done on a single channel (emu) and for the 3 channels combined. The pull distribution, representing the fitted cross-section value minus the input cross-section value (164 pb) divided by the total cross-section measurement error, is displayed in the Figure 37 showing no important bias for the fitted value (mean compatible with 0) and for the total error (variance of the Gaussian fit compatible with 1). On the same Figure, the combined cross section measurement distribution for each pseudo-experiment is shown.

• Bias test and pull distribution

• Cross-section dependence with respect to m_{top}

Source	ee	$\mu\mu$	eμ	Type (input correlation%)
DY background	25	25	30	Rate(0)
SingleTop background	30	30	30	Rate(100)
Diboson background	30	30	30	Rate(100)
Fake lepton background	65	50	30	Rate(0)
Trigger	1.7	1.5	0.9	Rate(0)
Lepton Efficiency(ID,Iso)	0.3	0.5	0.5	Rate(0)
LES	0.3	0.3	0.3	Rate(100)
MET	1.4	1.4	1.4	Rate(100)
Jet Energy Scale (JES)	$\pm1\sigma(p_T,\eta)$	$\pm1\sigma(p_T,\eta)$	$\pm1\sigma(p_T,\eta)$	Shape(100)
Jet Energy Resolution (JER)	$\pm1\sigma(p_T,\eta)$	$\pm1\sigma(p_T,\eta)$	$\pm1\sigma(p_T,\eta)$	Rate and Shape(100)
B-tagging(SFb, SFl)	(4.0,9.0)	(4.0,9.0)	(4.0,9.0)	Shape(100)
Scale				
$(Q^2 = M(t)^2 + \sum p_t^2(jet))$	1.0	1.0	1.0	Rate(100)
Matching	1.0	1.0	1.0	Rate(100)
TopMass	1.8	1.8	1.8	Rate(100)
Branching ratio ($W \to l\nu$)	1.7	1.7	1.7	Rate(100)
Pileup	0.5	0.5	0.5	Rate(100)

Table 44: Uncertainties (in %) used for the PLR method in the ee, $\mu\mu$ and eμ channels.Type represents how the uncertainty is treated in the PLR. (correlation%) denotes if the uncertainty is fully correlated (100) or decorrelated(0) between the channels. .

Table 45: Estimation of the $t\bar{t}$ cross section with 2.3 fb^{-1} using the PLR method with (Njets,NBjets) distribution. The estimation are presented with their statistical and systematic errors (luminosity is presented separately). Cross-sections values correspond the the selection without b-tagging requirements.

Channels	Cross-section $\pm(stat)\ \pm(sys)\ \pm(lumi)$
$\mu\mu$	$157.8\pm5.55^{+8.1}_{-7.5}\pm3.5$
ee	$167.8\pm6.55^{+8.8}_{-8.2}\pm3.7$
$e\mu$	$161.7\pm3.1^{+7.0}_{-6.6}\pm3.6$
combi	$161.6\pm2.5^{+6.5}_{-6.2}\pm3.6$

• Linearity test:

The linearity of the measurement is tested using a toy MC carlo procedure. The PLR measurement is performed for different input top cross sections, varying from 150 to 175 pb. For each point, the $t\bar{t}$ sample is randomly split in 2 statistically independent sub-samples. One sub-sample is used as pseudo-data and rescaled to a given cross section, the other sub-sample is used as $t\bar{t}$ signal template to perform the PLR fit. The measured cross-section as a function of the input cross-section is shown on Figure 38. The linearity test is conclusive and no cross section bias of the measurement is found.

Different signal MC samples generated with different top mass were also used to show the mass dependence of measured top production cross-section. The reference top mass used in the hypothesis of PLR was $m_{top} = 172.5\ GeV$. Figure 39 describing $\sigma_{t\bar{t}}/\ \sigma_{t\bar{t},m_{top}=172.5\ GeV}$ illustrates the dependence which was fitted with a second order polynomial.

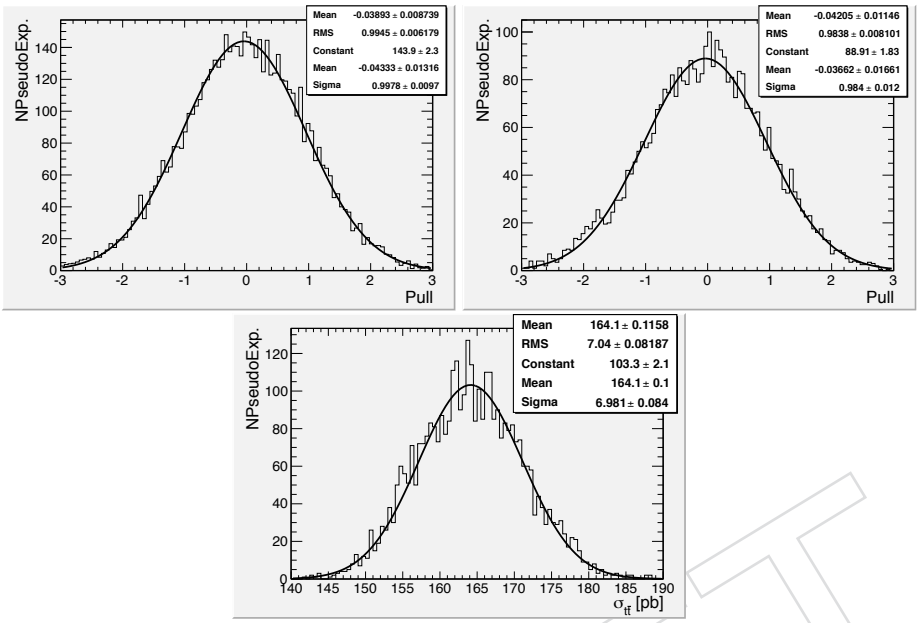

Figure 37: Pull distribution for about 4000 pseudo-experiences realized for the $e\mu$ channel (left plot) and for the 3 channels (right plot) combined. The lower plot shows the distribution of cross section measured for each pseudo-experiment, for the 3 channels combined.

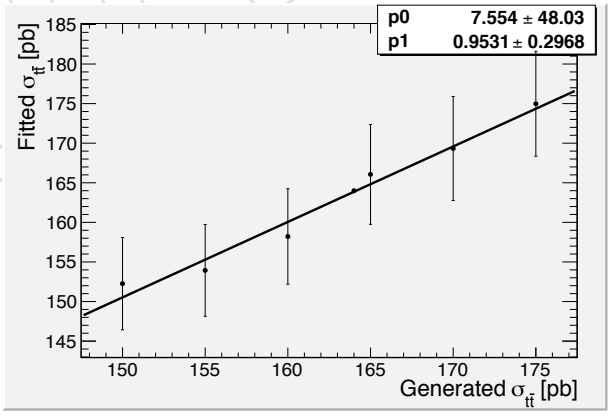

Figure 38: Fitted $t\bar{t}$ cross section as a function of the input cross section, fitted with a 1 order polynomial.

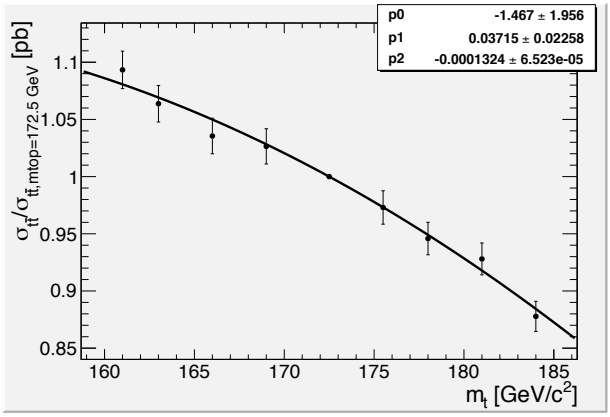

Figure 39: Ratio between the measured cross-section to the one obtained for $m_{top} = 172.5\ GeV$ as a function of m_{top} for the ee, $\mu\mu$ and $e\mu$ combined decay channels .

9.3 Comparison between cut&count and PLR measurements

Figure 40 shows the comparison between the cross section measurement obtained using the cut&count and the PLR methods, in the three different channels and for the combination.

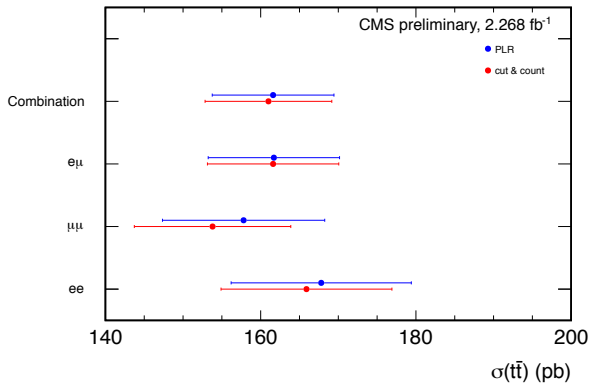

Figure 40: Comparison between the cross section measurement obtained using the cut&count and the PLR methods, in the three different channels and for the combination.

9.4 Results from LP2011 and JHEP 2010

The previous presented measurement can be compared with previous measurements from LP2011 [12], 1.14 fb^{-1} and with 2010 JHEP publication [2], 36 pb^{-1}, being them respectively:

$$\sigma_{t\bar{t}} = 169.9 \pm 3.9\ (\text{(stat.), } 2.3\%) \pm 16.3\ (\text{(syst.), } 9.6\%) \pm 7.6\ (\mathcal{L}, 4.5\%)\ \text{pb}$$

$$\sigma_{t\bar{t}} = 168.0 \pm 18.0\ (\text{(stat.), } 11\%) \pm 14.0\ (\text{(syst.), } 8\%) \pm 7.0\ (\mathcal{L}, 4\%)\ \text{pb}$$

A considerable reduction of the systematic uncertainty has been achieved, mainly by reducing the uncertainty on the pile-up, b-tagging and by removing the lepton selection model uncertainty. The treatment of the systematic uncertainties from theory was common at LP2011 and 2010 JHEP publication.

9.5 Normalisation to the Z cross section

As the luminosity is most probably underestimated, an additionnal check is done : knowing the Z cross section from EWK-10-005, the $t\bar{t}$ cross section measurement are given normalized using Z events. In this way, the uncertainty coming from luminosity is replaced by the uncertainy on the Z cross section, which is of about 4.5%. The tested luminosity is of 2.253 fb^{-1}

For this study, the trigger scale factors are assumed to be 1. Indeed, as there are no jet selection for this study, the isolation at trigger level is assumed to have a lesser impact and the trigger scale factors to be closer to 1.

To rescale events according to the Z cross section, the following procedure is followed :

- After the dilepton pair selection, events in the Z mass region $60 < M_{ll} < 120 GeV/c^2$ are selected. In this region, the Z cross section was found to be 968 ± 44 pb in the $\mu\mu$ channel and 992 ± 48 pb in the *ee* channel: page 15 of EWK-10-005 (PAS).
- the MC is rescaled to the inclusive Z cross section, including lepton scale factors,
- the fraction of Z events in the Z mass peak is estimated.
- from the previous numbers, the number of Z events in the Z mass peak N_Z^{Pred} is predicted using the Z cross section and the selection efficiency measured from tag&probe,
- N_Z^{Pred} is compared to N_Z^{Data} to determine the normalisation.

The number of Z events predicted using the Z cross section measured by EWK-10-005 is :

$$N_Z^{Pred} = \frac{N_{in\,Z\,peak}^{MC} \sigma_{Z\to\mu\mu/ee}^{EWK10005}}{\sigma_{Z\to ll}^{theor}(Br(Z\to\mu\mu/ee)/Br(Z\to ll))(N_{in\,Z\,peak}^{MC}/N_{Z\,tot}^{MC})} \quad (95)$$

The branching ratios $Br(Z \to \mu\mu/ee)$ are assumed to be $1/3$.

The $t\bar{t}$ cross section becomes :

$$\sigma_{ttbar} = \frac{N^{data} - N_{bck}^{data}}{\varepsilon_{ttbar} L^{CMS} (N_Z^{Data}/N_Z^{Pred})} \quad (96)$$

Using the $\mu\mu$ channel only, the correction factor N_Z^{Data}/N_Z^{Pred} was found to be 1.019 ± 0.046, while with the *ee* channel only, the correction factor is found to be 0.978 ± 0.047. These numbers are found to be well compatible with the luminosity calculation from lumiCalc2 (new normalisation).

10 Conclusions

The work discussed in this analysis note presents a measurement of the cross-section of the $t\bar{t}$ process in dilepton final state. The measurement have been obtained following two different methods: one of them is a counting method (using $t\bar{t}$ event candidates selected with b-tagging) and the other is based on the profile likelihood ratio method (without using the btag selection). The cross-section have been obtained exclusively in the ee, $\mu\mu$ and eμ channels. A combined measurement has also been provided.

The 2 different top cross section measurements are found to give very comparable results and precisions, with a slightly better precision from the PLR measurement.

A List of missing items

B Change since previous version

B.1 Changes since AN-11-477-v1

Everything up to v2, v1 is an empty version.

B.2 Changes since AN-11-477-v2

- Systematics: Update on the $\not\!\!E_T$ SFs and uncertainties: method has been improved.
- Systematics: Update on the LES uncertainty for 2.3 fb^{-1} .
- Systematics: Update on the b-tagging uncertainty taking into account the new BTV POG's prescriptions.
- Systematics: Include top mass uncertainties extracted from 11-12, 9, 6, and 3 GeV/c^2.
- Results: cut & count: propagation of the new $\not\!\!E_T$ SF and uncertainty, LES uncertainty, and new B-tagging uncertainty to the cross-section, combination, and breakdown of the systematics. Add results taking into account the correction of the luminosity (up 6%).
- Results: PLR: improve the description of the method, present results and cross-checks.
- Add section: Cross-Section dependence with the top mass.

References

[1] CMS Collaboration, "Measurement of b-tagging efficiency using ttbar events", *CMS PAS* **BTV-11-003** (2011).

[2] CMS Collaboration, "First Measurement of the Cross Section for Top-Quark Pair Production in Proton-Proton Collisions at sqrt(s)=7 TeV", *Phys. Lett.* **B695** (2011) 424, arXiv:1010.5994. doi:10.1016/j.physletb.2010.11.058.

[3] CMS Collaboration, "LHC Combination: Top mass", *CMS PAS* **TOP-12-001** (2011).

[4] CMS Collaboration, "W helicity in top pair events", *CMS PAS* **TOP-11-20** (2011).

[5] CMS Collaboration, "Search for FCNC in top pair events", *CMS PAS* **TOP-11-28** (2011).

[6] CMS Collaboration, "Measure of R by using top-pair events", *CMS PAS* **TOP-11-29** (2011).

[7] CMS Collaboration, "Measurement of the top quark charge", *CMS PAS* **TOP-11-31** (2011).

[8] N. Kidonakis, "Top quark pair and single top production at Tevatron and LHC energies", (2010). arXiv:1008.2460.

[9] N. Kidonakis, "Next-to-next-to-leading soft-gluon corrections for the top quark cross section and transverse momentum distribution", (2010). arXiv:1009.4935.

[10] N. Kidonakis and R. Vogt, "The Theoretical top quark cross section at the Tevatron and the LHC", *Phys. Rev.* **D78** (2008) 074005, arXiv:0805.3844. doi:10.1103/PhysRevD.78.074005.

[11] N. Kidonakis, "Higher-order corrections to top-antitop pair and single top quark production", (2009). arXiv:0909.0037.

[12] CMS Collaboration, "Top pair cross section in dileptons", *CMS PAS* **TOP-11-005** (2011).

[13] "https://twiki.cern.ch/twiki/bin/view/CMSPublic/SWGuidePAT",.

[14] "https://twiki.cern.ch/twiki/bin/view/CMSPublic/WorkBookPAT",.

[15] "CMS CR-2010/203 – PAT: the CMS Physics Analysis Toolkit",.

[16] "https://twiki.cern.ch/twiki/bin/view/CMSPublic/WorkBookPF2PAT",.

[17] "https://twiki.cern.ch/twiki/bin/view/CMSPublic/SWGuidePF2PAT",.

[18] J. Alwall, P. Demin, S. de Visscher, R. Frederix, M. Herquet, F. Maltoni, T. Plehn, D. L. Rainwater, T. Stelzer, "MadGraph/MadEvent v4: The New Web Generation", *JHEP* **0709** (2007) 028.

[19] CMS Collaboration, "Commissioning of the Particle-Flow reconstruction in Minimum-Bias and Jet Events from pp Collisions at 7 TeV", *CMS Physics Analysis Summary* **CMS-PAS-PFT-10-002** (2010).

[20] "Site: https://twiki.cern.ch/twiki/bin/view/CMS/TWikiTopRefEventSel",.

[21] "Site: https://twiki.cern.ch/twiki/bin/view/CMS/ConversionBackgroundRejection",.

[22] M. Mulders et al., "Muon Identification in CMS", *CMS AN 2008/098* (2008).

[23] A. Rizzi, F. Palla, G. Segneri, "Track impact parameter based b-tagging with CMS", *CMS NOTE* **2006/019**.

[24] CMS collaboration, "Commissioning of b-jet identification with pp collisions at sqrt(s) = 7TeV", *BTV-10-001* (2010).

[25] CMS collaboration, "Measurement of b-tagging efficiency using $t\bar{b}ar$ events", *BTV-11-003* (2011).

[26] CMS collaboration, "Performance of b-jet identification in CMS", *BTV-11-001* (2011).

[27] BTV performance group, "Recipes to use the b-tag and mistag scale factors", *https://twiki.cern.ch/twiki/bin/view/CMS/PasBTV11001#How_to_get_b_tag_and_mistag_Data* (2011).

[28] "Site: https://twiki.cern.ch/twiki/bin/view/CMS/PileupMCReweightingUtilities",.

[29] TOTEM Collaboration, "First measurement of the total proton-proton cross section at the LHC energy of $\sqrt{s} = 7$ TeV", *EPL* **96** (2011) 21002, arXiv:1110.1395.

[30] W.Andrews et al., "A method to measure the contribution of DY$-> ll$ to a dilepton + MET selection.", *CMS AN-2009/023* (2009).

[31] "Site: https://twiki.cern.ch/twiki/bin/view/CMSPublic/WorkBookJetEnergyCorrections",.

[32] BTV performance group, "Recipes to use the b-tag and mistag scale factors", *https://twiki.cern.ch/twiki/bin/viewauth/CMS/BtagPOG#Recommendation_for_b_c_tagging_a* (2012).

[33] CMS collaboration, "b-Jet Identification in the CMS Experiment", *BTV-11-004* (2012).

[34] Particle Data Group Collaboration, "Review of particle physics", *J. Phys.* **G37** (2010) 075021. doi:10.1088/0954-3899/37/7A/075021.

[35] L. Bauerdick, et al., "A measurement of top quark pair production cross section in dilepton final states in pp collisions at 7 TeV", *CMS AN 2010/410* (2010).

[36] CMS Collaboration, "Top pair cross section in lepton+jets", *CMS PAS* **TOP-11-003** (2011).

[37] D. G. L. Lyons and P. Clifford, "How to combine correlated estimates of a single physical quantity", *Nucl. Instrum. Meth.* **A270, 110** (1988) arXiv:10.1016/0168-9002(88)90018-6.